An Investigation into the Effects of Variable Lake Ice Properties on Passive and Active Microwave Measurements Over Tundra Lakes Near Inuvik, N.W.T.

by

Grant Gunn

A thesis
presented to the University of Waterloo
in fulfillment of the
thesis requirement for the degree of
Master of Science
in
Geography

Waterloo, Ontario, Canada, 2010

AUTHOR'S DECLARATION

I hereby declare that I am the sole author of this thesis. This is a true copy of the thesis, including any required final revisions, as accepted by my examiners.

I understand that my thesis may be made electronically available to the public.

Abstract

The accurate estimation of snow water equivalent (SWE) in the Canadian sub-arctic is integral to climate variability studies and water availability forecasts for economic considerations (drinking water, hydroelectric power generation). Common passive microwave (PM) snow water equivalent (SWE) algorithms that utilize the differences in brightness temperature (Tb) at 37 GHz – 19 GHz falter in lake-rich tundra environments because of the inclusion of lakes within PM pixels. The overarching goal of this research was to investigate the use of multiple platforms and methodologies to observe and quantify the effects of lake ice and sub-ice water on passive microwave emission for the purpose of improving snow water equivalent (SWE) retrieval algorithms.

Using *in situ* snow and ice measurements as input, the Helsinki University of Technology (HUT) multi-layer snow emission model was modified to include an ice layer below the snow layer. Emission for 6.9, 19, 37 and 89 GHz were simulated at horizontal and vertical polarizations, and were validated by high resolution airborne passive microwave measurements coincident with *in situ* sampling sites over two lakes near Inuvik, Northwest Territories (NWT). Overall, the general magnitude of brightness temperatures were estimated by the HUT model for 6.9 and 19 GHz H/V, however the variability was not. Simulations produced at 37 GHz exhibited the best agreement relative to observed temperatures. However, emission at 37 GHz does not interact with the radiometrically cold water, indicating that ice properties controlling microwave emission are not fully captured by the HUT model.

Alternatively, active microwave synthetic aperture radar (SAR) measurements can be used to identify ice properties that affect passive microwave emission. Dual polarized X-band SAR backscatter was utilized to identify ice types by the segmentation program MAGIC (MAp Guided Ice Classification). Airborne passive microwave transects were grouped by ice type classes and compared to backscatter measurements. In freshwater, where there were few areas of high bubble concentration at the ice/water interface Tbs exhibited positive correlations with cross-polarized backscatter, corresponding to ice types (from low to high emission/backscatter: clear ice, transition zone between clear and grey ice, grey ice and rafted ice). SWE algorithms were applied to emission within each ice type producing negative or near zero values in areas of low 19 GHz Tbs (clear ice,

transition zone), but also produced positive values that were closer to the range of *in situ* measurements in areas of high 19 GHz Tbs (grey and rafted ice). Therefore, cross-polarized X-band SAR measurements can be used as *a priori* ice type information for spaceborne PM algorithms, providing information on ice types and ice characteristics (floating, frozen to bed), integral to future tundra-specific SWE retrieval algorithms.

Acknowledgements

This thesis could not have been written without financial and academic support provided by Professor Claude Duguay. Thanks is also extended to all those who helped answer countless questions and provided useful insight, from faculty and staff at the University of Waterloo to research scientists at the Finnish Meteorological Institute where I spent three months as a research scientist. The collaboration with other researchers, namely Chris Derksen of Environment Canada, Juha Lemmetyinen of the Finnish Meteorological Institute and Professor David Clausi of the University of Waterloo has directly lead to the publication of the articles enclosed in this paper. The specific contributions of each research is outlined in the Preface.

Dedication

This thesis is the culmination of work that I would never have been able to accomplish had it not been for the support and encouragement of my parents, whose success and achievements have motivated me to follow my aspirations.

I would also like to thank all those who have offered me countless hours of guidance and support along the way. I will cherish all that I have learned from the travels, laughs and new memories I have made as a direct result of my time at the University of Waterloo.

Table of Contents

List of Figures

List of Tables

Preface

This thesis contains two journal articles that investigate microwave interaction in the presence of variable ice types for the purpose of improving SWE retrieval algorithms. The first paper, accepted in *Remote Sensing of Environment* discusses the efficacy of the HUT snow emission model when applied to sampling sites overlying floating lake ice. The second paper, prepared for submission to *Remote Sensing of Environment* discusses the relationships present between active and passive microwave remote sensing when coincident with variable ice types at the surface layer of floating ice. Collaboration with colleagues, whether direct or indirect, aided in the submission of these papers, and are credited below.

The first article (Chapter 3) is the result of direct collaboration with Professor Claude R. Duguay, Dr. Chris Derksen, Juha Lemmetyinen and Peter Toose. Prof. Duguay aided a great deal with the initial proposal of the article, and provided continuous advice and comments throughout the duration of the study. Dr. Chris Derksen also provided a great deal of significant support through comments and advice before submission and during reviews. Dr. Derksen's text contributions to the paper included the description of the passive microwave instruments, and the calibration procedures/receiver drift. Juha Lemmetyinen's contributions included running the HUT model using the *in situ* data as input, and the in-text description of the model. Airborne radiometer and *in situ* data were collected and provided by Environment Canada, with countless questions and concerns fielded by Dr. Chris Derksen and Peter Toose.

The second article (Chapter 4) is the result of collaboration with Professor Claude R. Duguay, Dr. Chris Derksen, Professor David Clausi, and Peter Toose. Prof. Duguay again provided a great deal of guidance and comments throughout the drafting of the article. Dr. Chris Derksen and Peter Toose of Environment Canada provided the datasets necessary for this study, including airborne passive microwave Tbs and *in situ* measurements. Active microwave X-band acquisitions from TerraSAR-X were also provided by Environment Canada, donated by the Deutsches Zentrum fűr Luft- und Raumfahrt (DLR), the German Aerospace Centre. The sea-ice segmentation program MAGIC was provided by Professor Clausi of the University of Waterloo, which was essential for this work.

Chapter 1
General Introduction

1.1 Introduction

Seasonal snow in arctic and subarctic environments represents a significant amount of annual water storage within the hydrological cycle. The accurate measurement of snow extent and snow properties such as depth, density and snow water equivalent (SWE) are important for hydroelectric power generation, and local or regional climate modeling (Marshall et al., 1992; Cohen and Entekhabi., 1999; Walker and Silis 2002; Derksen et al. 2003; Derksen and Walker 2004; Lemmetyinen et al., 2008a). The monitoring of snowpack properties is also essential for economic development in regions where snow melt is the dominant source of water. In the western United States, 70% of the annual water supply is derived by snowmelt, totaling an economic benefit of approximately $348 billion (Adams et al., 2004). Furthermore, the monitoring of snowpack properties can aid in disaster mitigation by forecasting areas most prone to flooding. The costs associated with flooding caused by snowmelt can total up to $4.7 billion in a single event, like the Red River flood of 1997 that affected the Midwestern United States (Adams et al., 2004). Snow also influences the development of lake ice, as its low thermal conductivity restricts heat transfer from the ice.

Lakes in arctic/subarctic environments represent a considerable heat sink for solar radiation, providing a time-lag of energy between the air and water, governed by the high thermal conductivity of water (Menard et al, 2002). Accurate lake ice condition datasets have been identified as necessary inputs for numerical weather prediction models, as their exclusion yields temperature anomalies of 5 - 10°C (Goodison et al., 1999; Winger and Brown, 2008 pers. comm)**.** Changes in lake ice phenology, primarily dates of initial freeze-up and break-up have also been identified as useful indicators of local and regional climate variability (Duguay, et al., 2003; Kouraev et al., 2007). Furthermore, many northern communities require information on ice conditions for survival (drinking water, coldwater fishing) and transportation (ice roads). Therefore, the need for accurate snow and lake ice property retrieval is of importance to both local communities and global climate modeling.

1.2 Remote Sensing of SWE

Typical measurements of snow and lake ice properties are collected through *in situ* snow courses; however the extreme variability of snow (on the order of hundreds of metres) biases the upscaling of measurements from local to regional scales. Snow courses are also intermittent and restricted to populated regions (Derksen et al., 2003). Therefore, a need for continuous remote measurements of snow and lake ice properties is present in northern communities, where *in situ* measurements are logistically cumbersome to collect. Passive and active microwave remote sensing have become an increasingly viable method of collecting snow and lake ice properties in northern latitudes, as their measurement methods are independent of solar radiation, and are largely unaffected by atmospheric conditions. Comprehensive overviews of passive and active microwave remote sensing are provided in Chapter 2.

Passive microwave SWE retrieval algorithms are derived using frequency differences between a shorter scattering wavelength and longer background wavelength, characteristically 37 and 10 or 19 GHz respectively. The basic theory behind the use of the frequency differences is that the 37 GHz channel is susceptible to volume scatter caused by physical properties of the snowpack (snow depth, density, SWE, grain size and the presence of ice lenses). Coefficients and constants for a linear equation are derived based on the differences between the two frequencies to produce SWE algorithms based on *in situ* measurements. Algorithms are either global (hemispheric) such as Chang et al (1987) and Kelly et al., (2003), or specific to homogeneous landcover types (Goodison and Walker, 1994; Gan, 1996; Goita et al., 2003; Derksen et al., 2005; Derksen et al., 2010), which are discussed in Section 2.5. Hemispheric algorithms (Chang et al., 1987) provide general agreement for the majority of sites investigated, although falter in regions that have unique emission characteristics. Regional algorithms investigate unique emission characteristics that are present in homogeneous land cover types, such as prairie (Goodison and Walker, 1994), boreal forest (Goita et al., 2003), and tundra environments (Gan, 1996, Derksen et al., 2005; Derksen et al., in press). SWE retrieval algorithms have been successfully developed and applied to prairie and boreal forest regions, as microwave emission dynamics are well understood. Tundra-specific algorithms characteristically applied to lake-rich areas underestimate SWE because of the inclusion of water beneath the lake ice in measured Tbs, affecting the background non-scattering frequency channel. The development of a Tb-evolution algorithm is presented in Derksen et al., (2010). However, it cannot be applied to passive microwave data acquired at single measurement periods, limiting its use to phenological

studies. Several studies have addressed the effect of the inclusion of lakes in passive microwave remote sensing, although the emission dynamics at the satellite scale are relatively poorly understood (Gan, 1996; Duguay et al 2005; Rees et al., 2006).

Active microwave SWE retrieval algorithms are not commonly utilized at the operational level because of the smaller image swath compared to that of passive microwave measurements. The basis of active microwave algorithms is that transmitted radiation will be scattered by snow grains that approximate the size of the incident wavelength, and is returned back to the sensor at a rate determined by the physical properties of the snowpack, discussed in section 2.6 (Ulaby and Stiles, 1980; Praks et al., 1998). These studies were performed over terrestrial snowpacks, where the influence of the underlying soil medium is negligible and well documented (Ulaby et al., 1982). In the case of a snowpack over a frozen lake, the underlying ice is a further scattering medium and serves to complicate backscatter measurements. Studies have successfully been able to infer physical characteristics of the ice cover itself (frozen to bed/free floating, ice thickness), but have not been able to quantify the effect of ice types or snowpack information on measured backscatter (Weeks et al., 1977; Weeks et al., 1978; Morris et al., 1995; Duguay et al., 2002; Duguay and Laleur, 2003).

There have been few studies examining the synergy between active and passive microwave remote sensing for the purpose of SWE retrieval, but have produced promising results (Nghiem and Tsai, 2001; Hallikainen et al., 2003; Tedesco and Miller, 2007). Studies utilizing active and passive measurements that have similar incidence angles and spatial resolutions have produced improved SWE retrievals for agricultural and boreal environments (Hallikainen et al., 2003). While the effects of sub-snow lake ice has been acknowledged for both passive and active microwave measurements, there have been no studies that have examined the scattering matrices evident in both datasets, and the relationship that exists between them.

1.3 Research Objectives

The overall objectives of this research are to utilize passive and active microwave measurements to identify the dominant sources of scatter over subarctic lake ice in a tundra environment, and quantify (the existence of) any relationships between brightness temperatures (Tbs) and sigma nought backscatter (σ°) to identify areas of improvement within existing SWE retrieval algorithms.

The data for this study were collected during an intensive field campaign conducted by Environment Canada in April of 2008 over several lake systems northeast of the Mackenzie Delta Region. The collection of field measurements included: snow pits (snow depth, density, SWE, grain size, stratigraphy and ice thickness), 30 snow depth and SWE measurements, and 5 ice type and thickness measurements, totaling 25 sites located on Sitidgi and Husky Lakes approximately 50 km northeast of Inuvik, Northwest Territories. High resolution airborne passive microwave Tbs at 6.9, 19, 37 and 89 GHz were collected coincident to the ice sampling sites at a resolution of 80 x 100 metres. TerraSAR-X X-band (9.65 GHz) backscatter measurements were acquired in Stripmap mode (3 x 3 m resolution) over Sitidgi and Husky Lakes at co- (VV) and cross-polarizations (VH).

To identify the main dominant scattering sources, the study was divided into two components: 1) evaluation of a modified Helsinki University of Technology (HUT) (Pulliainen et al., 1999) microwave snow emission model when applied to snow on lake ice and 2) segmentation of TerraSAR-X imagery for the purpose of investigating relationships that may exist between active and passive measurements, and to define the sources of scatter from observations over lake ice.

1.3.1 Evaluation of the Modified HUT Microwave Snow Emission Model

To identify passive microwave emission characteristics over lake ice, the modified HUT snow emission model was applied to lake ice sites over Sitidgi and Husky Lakes. The physical properties of the lake ice and snowpack were compared to simulated and airborne Tbs to identify not only the efficacy of the model, but also the *in situ* properties that could have produced erroneous results noticed in model outputs.

1.3.2 Evaluation of the Effect of Ice Types on Microwave Interaction

The objective of using the segmentation software MAGIC (Clausi et al., 2010) was to investigate the sources of scatter within the ice and define unique areas of similar backscatter, which was compared to low-frequency airborne passive microwave Tbs. Studies have theorized that fluctuations in backscatter are caused by the incorporation of bubbles near the ice/water interface (Weeks et al., 1977; Duguay et al., 2003), but have not quantified the effect of variable ice type on Tbs/backscatter.

Therefore, one objective was to identify unique ice types at the surface from *in situ* measurements and relate them to variations in Tb and backscatter.

1.4 Thesis Outline

In Chapter 2, an extensive overview of background information is provided examining the physical properties of tundra snow on lake ice and the process of lake ice development. Passive/active microwave remote sensing and the synergy between the two is also be examined, as well as microwave emission models. Finally, the physical properties of a snowpack and lake ice that affect microwave interaction is examined, forming the basis for this work. Chapter 3 is the first appended paper, entitled "Evaluation of the Helsinki University of Technology's Modified Snow Emission Model Over Lake Ice Using Airborne Passive Microwave Measurements". Chapter 4 is the second appended paper, entitled "Investigating the Influence of Variable Ice Types on Passive and Active Microwave Measurements over Tundra Lakes". Chapter 5 outlines the conclusions derived from both papers, identifies the limitations of the study, and lists recommendations for future studies utilizing active and passive measurements.

Chapter 2
Background

This chapter is divided into three main components designed to provide a sufficient base of knowledge before presenting results within the appended papers. Firstly, the physical properties and formation/sublimation processes of snow and lake ice in Arctic and Subarctic environments are provided, followed by the remote sensing measurement methods that are used to obtain information of *in situ* conditions. An extensive introduction into the passive and active microwave remote sensing of high-latitude tundra environments is provided, discussing how relevant snow and ice properties affect microwave measurements at various frequencies. Finally, a brief introduction of snow emission models and the synergy between passive and active microwave remote sensing is presented to provide the research context for the appended papers in Chapter 3 and 4.

2.1 Physical properties of Snow and Lake Ice in Subarctic Environments

2.1.1 Arctic/Subarctic Snow

Regional climate conditions in arctic and subarctic tundra environments create unique snow characteristics, as described by Sturm et al. (1995). Tundra snowpacks are on average relatively thin with a depth range of 10 – 75cm, a bulk density of 0.38g cm^{-3}, and contain a large fraction of depth hoar overlaid by multiple wind slab layers. Snow distribution in tundra environments is a function of land cover type and topography. Tundra environments are characterized by short, low lying vegetation such as small shrubs and boreal trees that act as catchments for wind-redistributed snow (Pomeroy et al., 1997). Accumulation drifts can also form based on terrain topography, with wind depositing snow on leeward sides of hills or in concave areas in hummocky terrain (Liston and Sturm, 1998). Land cover in tundra environments is also dominated by lakes, typically on the order of 20% and as much as 40% (Duguay et al., 2005). Snow cover on arctic lakes exhibit considerable differences compared to snow on land in the surrounding tundra. According to Sturm and Liston (2003) and Derksen et al. (2009), snow on lake ice is thinner, denser and contains less SWE than the surrounding land measurements as a result of wind redistribution. The flat ice surface on lakes allows for a characteristic accumulation of deep snow at shorelines as a result of shoreline vegetation acting as a catchment trough (Sturm and Liston, 2003). Snow on lakes also exhibits fewer stratigraphic

layers than land, and a more pronounced slab-to-hoar percentage (Derksen et al., 2009). The marked differences between terrestrial and lake snow are reflected in its thermal properties; lake snow has less than half the thermal insulation capacity than terrestrial snow, influencing lake ice development (Sturm and Liston, 2003).

2.1.2 Lake Ice Development

Ice Formation (Congelation/Black Ice): When surface water cools as a result of low air temperatures, a negative temperature gradient is formed causing a deficit of heat in the atmosphere and initializes a heat flux from open water to the air (Bengtsson, 1986). The denser, cooler surface water sinks and displaces warmer water to the surface, a process referred to as "lake-mixing" until the full volume of the lake reaches its maximum density at 4°C. Surface water becomes less dense at the cold air/water interface as it cools further, and drops to freezing levels. Congelation ice forms downward from the surface, with crystals vertically oriented at the C-axis (column-like). The crystal orientation causes the ice to possess very little light reflective properties, allowing most light to transmit to the water below, and appears "black" (Figure 2-1). Black ice grows fastest in the early portion of the winter season, as its surface is free of any insulating medium (snow or white ice). Bengtsson (1986) noted that un-insulated black ice can grow at a rate of two times more than that of similar black ice with considerable surface layers of white ice. In high-latitude regions, low annual precipitation coupled with polar darkness can facilitate the growth of black ice to potentially exceed depths of 3 metres (Adams, 1976; Woo et al., 1989; Kouraev et al., 2007). Although black ice is largely inclusion free, certain factors can increase air bubble concentration levels.

Figure 2-1: Congelation/Black Ice in Inuvik, NWT.
Note that the drill hole can be seen through the clear ice.
Source: Toose, P., Inuvik Field Campaign, (2008).

Freezing congelation ice generally expels gas from the ice/water interface during periods of growth. However, when rapid ice growth is not impeded by an insulating surface (snow) the rapid freezing rate lowers the efficiency of gas expulsion, causing an increase in air bubble inclusion (Adams, 1976; Roulet et al., 1986; Mullen et al., 1988). Another factor that can cause an increase in air bubble concentration is the level of gas saturation within the water medium. When the process of ice growth can no longer expel gases, tubular bubbles are formed within the encroaching ice layer (Morris et al. 1995). Figure 2-2 depicts tubular bubbles within congelation ice, which are often restricted to the bottom layers of the ice.

Figure 2-2: Black Ice with Tubular Bubbles in Churchill, MB (Source: Duguay et al, 2002).

Effects of Snow Cover on Lake Ice Development: Other than air temperature, snow overlying ice is one of the most significant factors affecting lake ice development. Snow possesses a low thermal conductivity, causing it to act as an insulator for lake ice from sub-freezing air temperatures (Adams, 1976; Adams and Roulet, 1980; Bengtsson, 1986; Woo, 1989). When the ice/air thermal gradient is insulated by snow, the temperature gradient at the ice/snow interface becomes warmer, effectively slowing the growth of congelation ice (Adams and Roulet, 1980). The magnitude at which the snow cover affects development of lake ice depends on the depth and density of the snowpack (Adams, 1976; Duguay et al., 2002; Duguay et al., 2003; Jeffries et al., 2005). Redistribution by wind can affect both of these variables. Wind either strips snow from the surface or compacts it. Compacted snow possesses a higher thermal conductivity, allowing for a greater amount of heat loss at the snow/ice interface and increased congelation ice growth (Bengtsson, 1986). Wind-blown snow accumulation zones can also cause localized variations in ice thickness as a result of the variable insulation properties imposed on the ice (Adams 1976).

White/Snow Ice Formation: As snow accumulates over congelation ice throughout the winter, it begins to weigh on the ice and can depress it below the hydrostatic water level, causing cracking. If the ice is depressed, water will either flood from the edges of the ice cover (Adams, 1976; Adams and Roulet, 1980), or rise up through the cracks to the hydrostatic water level (Adams, 1976; Adams and Roulet, 1980; Bengtsson, 1986). The flooding of the snow will cause slush to form, and upon freezing will form snow or "white" ice (Figure 2-3). White ice generally forms rapidly as the thick layer of snowcover insulating the ice has become rather thin, and thus possesses a higher thermal conductivity (Adams, 1976; Adams and Roulet., 1980). The process of slushing/white ice formation can occur multiple times during the winter season, as long as the snowcover is adequate to depress the ice cover below the hydrostatic water line. A thicker concentration of white ice is generally found near shorelines as they are the first to be flooded when an entire ice cover is depressed (Adams and Roulet., 1980, Bengtsson, 1986). Solely white ice can be formed if a snow precipitation event occurs at the same time of initial ice freeze-up, caused by the incorporation of snow crystals into congelation ice (Bengtsson, 1986; Mullen et al., 1988). Another method in which white ice can be formed is if liquid precipitation (rain/sleet) percolates through the snow to the snow/ice interface and subsequently freezes (Bengtsson, 1986).

Figure 2-3: White Ice north of Inuvik, NWT. Source: Toose, P., Inuvik Field Campaign, 2008.

2.2 The Need for Microwave Remote Sensing

Conventional measurements of snow and lake ice properties (snow depth, density, SWE) are obtained through *in situ* snow courses. Unfortunately, the high variability of snow in tundra environments biases the upscaling of *in situ* measurements to regional scales, as most snow courses are restricted to populated regions, and are lacking in northern environments (Derksen et al. 2003). *in situ* snow courses are also temporally intermittent and therefore limit phenological studies due to the high spatial and temporal variability of snow and lake ice (Lemmetyinen et al., 2008; Walker and Goodison, 2000). Also, it is logistically cumbersome to monitor the spatial variability of lake ice thickness throughout the winter seasons in arctic areas, where lakes can occupy a significant portion of the landscape. The number of manual lake ice observations including freeze-up/breakup dates and ice thickness measurements has drastically declined since the 1990s, with almost no conventional observations in Canada (Lenormand et al., 2002).

Alternatively, satellite remote sensing has become a viable method of observing various snowpack properties to provide snow extent, depth and SWE measurements globally. Polar orbiting satellites allow for measurements at coincident ground swaths with frequent revisit times. Optical and infrared sensors such as Landsat Multispectral Scanner and Thematic Mapper, the National Ocean and

Atmospheric Administration's (NOAA) Advanced Very High Resolution Radiometer (AVHRR) and NASA's Moderate-Resolution Imaging Spectroradiometer (MODIS) have been successfully utilized to estimate snow extent (Hall and Riggs, 2007; Helfrich et al., 2007). However they cannot be used to accurately derive other snowpack properties such as snow depth, density, and SWE. Optical sensors also experience imaging restrictions caused by low solar illumination and poor weather conditions. Sensors that measure the reflectance of radiation in the visible portion of the electromagnetic spectrum are dependent on the reflection of incoming solar radiation from the surface to record measurements. Areas of interest to snow and lake ice studies in the high arctic or subarctic regions experience prolonged periods of darkness during the winter season (Woo, 1989). Cloud cover also effectively restricts the use of visible and infrared sensors, as water vapour contributes to non-selective scattering of the visible portion of the electromagnetic spectrum. Alternatively, microwave remote sensing provides measurements that are independent of reflected solar radiation.

2.3 Passive Microwave Remote Sensing

Measurements from passive microwave sensors are independent of solar radiation, and experience minimal atmospheric interference compared to optical imaging sensors. The use of passive microwave sensors for the remote sensing of SWE began with the launch of the Electrically Scanning Microwave Radiometer (ESMR) onboard NASA's Nimbus 5 and 6 satellites in 1972 as a precursor to the Scanning Multichannel Microwave Radiometer (SMMR) on board NASA's Nimbus 7 in 1978, followed by the Special Sensor Microwave Imager (SSM/I) onboard DSMP-F8 through DSMP-F15 (excluding F9 and F14) in 1987, and the Advanced Microwave Scanning Radiometer (AMSR-E) onboard NASA's Earth Observing System (EOS) in 2002. Table 2-1 displays an instrument overview of all spaceborne microwave sensors. While the ESMR and SMMR sensors are decommissioned, the SSM/I and AMSR-E sensors are continuing to collect measurements, adding to the 30-plus year time record of passive microwave measurements.

Table 2-1: Spaceborne passive microwave instrument overview.

Satellite	Sensor	Sensor Type	Channels	Frequency (GHz)	Swath Width (km)	Polarization	Inc Angle (deg)	Field of View
Nimbus - 5 Nimbus - 6	ESMR	Electrically Scanning Phased Array	1 1	19.35 37	3000 1300	Horizontal Dual	50	25 x 25km up to 160 x 45km at downtrack
Nimbus - 7	SMMR	Horn Antenna	10	6.6 10.7 18 22 37	800	Dual	50	95 x 148 70 x 109 43 x 68 36 x 56 18 x 27
DSMP-F8 to F-15 (excluding F9 & F14)	SSM/I	Horn Antenna	7	19.35 22.2 37 85.5	1400	Dual	53.1	45 x 70 40 x 60 30 x 38 14 x 16
Earth Observing System Aqua	AMSR-E	Conical Scanner	12	6.925 10.65 18.7 23.8 36.5 89	1445	Dual	55	73 x 43 51 x 30 27 x 16 31 x 18 14 x 8 6 x 4

Passive microwave sensors measure naturally emitted radiation from its target source, in this case, the Earth's surface. The Earth acts as a gray body emitter, as it absorbs electromagnetic radiation and emits a fraction of the initial incident radiation at a lower dominant frequency (based on the Rayleigh-Jeans law). The magnitude of emission in the microwave portion of the electromagnetic spectrum is much lower than that of optical remote sensing. Therefore, the Instantaneous-Field-of-View (IFOV) for spaceborne measurements cover a large portion of Earth's surface. In the microwave region shorter wavelengths are emitted at higher frequencies, thereby increasing the spatial resolution of the IFOV as a greater amount of microwave emission is collected at the sensor (see Table 2-1). Microwave emission is measured using the calibrated antenna temperature, otherwise referred to as brightness temperature (Tb), which can be expressed by:

$$T_b(f,\theta) = e(f,\theta)T \quad \textbf{(1)}$$

where *e* is the emissivity of the surface/target relative to the frequency (*f*) and incidence angle (*θ)* examined, and T is the physical temperature of the medium in Kelvin (K). Fluctuations in emissivity are affected by the dielectric constant and surface roughness of the medium. Microwave emission is also affected by scatter caused by objects approximating the size of the frequency wavelength, thereby lowering Tbs. In lake-rich high-latitude environments various factors influence the land surface brightness temperature including the physical parameters of snow (depth, dielectric constant/density, grain size, stratigraphy, wetness), vegetation, and the properties of the underlying mediums (soil, lake ice).

2.4 Factors that Affect Microwave Emission from the Snowpack

2.4.1 Snow Depth

As wavelengths begin to approximate the size of dry snow grains (20 GHz and higher), emitted microwaves are scattered in all directions at a rate proportional to the depth and SWE content of the snowpack (Hall et al., 1978; Goita et al., 2003; Duguay et al., 2005; Kelly, 2009). Deeper snowpacks scatter emitted microwaves more efficiently thereby allowing less radiation to reach the radiometer, resulting in lower Tbs (Mätzler et al., 1982; Hall et al., 1991; Kelly 2009). Figure 2-4 displays the characteristic drop of airborne Tbs at 37 GHz (wavelength (λ) = 0.8 cm) when measured over a mature snowpack, while Tbs with frequencies lower than 20GHz (λ = 1.5 cm) remain relatively constant over terrestrial snow. This relationship forms the basis of most SWE retrieval algorithms, discussed in Section 2.5.

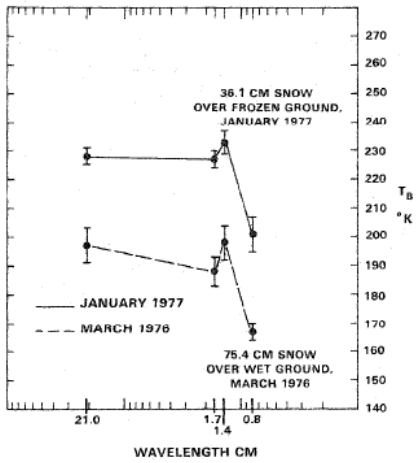

Figure 2-4: Brightness Temperature relative to snow depth (Hall et al. 1978).

As SWE increases during the winter season, the scattering relationship at 37 GHz may reverse as the snowpack itself begins to contribute to microwave emission (Figure 2-5) (Mätzler et al. 1982; Derksen et al., 2010). In this scenario, SWE algorithms that exploit the differences between the 19 and 37GHz channels tend to systematically underestimate SWE levels above 120 mm.

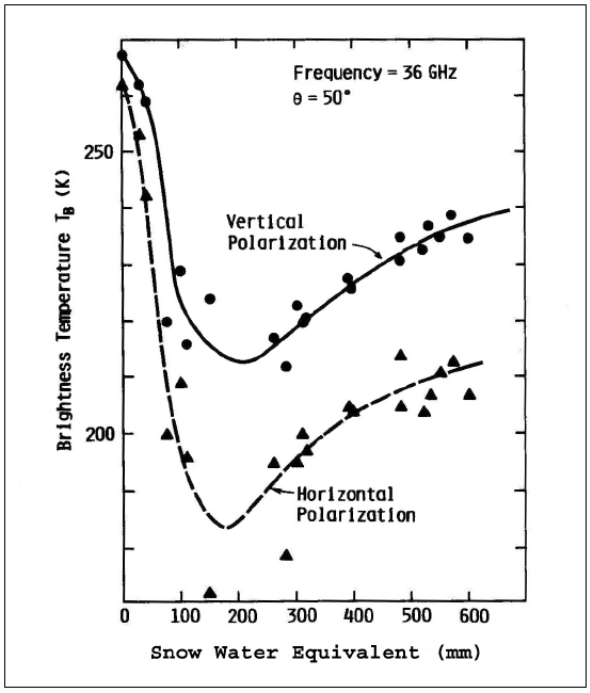

Figure 2-5: 37GHz rebound as SWE exceeds 100mm, according to Mätzler et al. (1982).

2.4.2 Dielectric Constant/ Snow Density

The complex dielectric constant of snow is given by the following equation:

$$\epsilon^* = \epsilon_{ds}' + j\epsilon_{ds}'', \quad \textbf{(2)}$$

where ϵ_{ds}' is the real part of the dielectric constant, and ϵ_{ds}'' is the imaginary lossy portion.
When interpreting dielectric constant properties, the constituents in the snow must be examined. Snow (as a homogeneous medium) contains a mixture of ice crystals and pockets of air (Hallikainen et al., 1986; Stogryn, 1986; Ulaby et al., 1982). Components of snow that may affect the dielectric constant are: frequency, temperature, volumetric water content and density (Ulaby et al., 1982). The imaginary part of the dielectric constant of snow (ϵ_{ds}") is very small in the microwave region and considered largely ineffective (0.001 at 5.3GHz) (Rott et al., 2004). When acquiring measurements in the microwave region, the real part of the dielectric constant of snow (ϵ_{ds}') is independent of temperature and frequency, as long as the temperature is such that no melting occurs in the snowpack (Hallikainen et al., 1986; Ulaby et al., 1982). Therefore, the dielectric constant (ϵ_{ds}') of dry snow is predominantly dependent on snow density (Hallikainen et al. 1986), as displayed in Figure 2-6. In common snowpacks, the dielectric constant of dry snow ranges from 1.4 – 2, and rarely exceeds 3 when snow contains some water in liquid form (Ulaby et al., 1982). Therefore, low density snow (typical of freshly fallen layers) has the weakest sensitivity to microwaves, thereby lowering the efficiency of microwave scatter (Mätzler et al., 1982). Snow on lake ice tends to be denser than the surrounding tundra landscape, as observed by Sturm and Liston (2003). Denser snow raises the dielectric constant, thereby lowering microwave emission at a proportional rate.

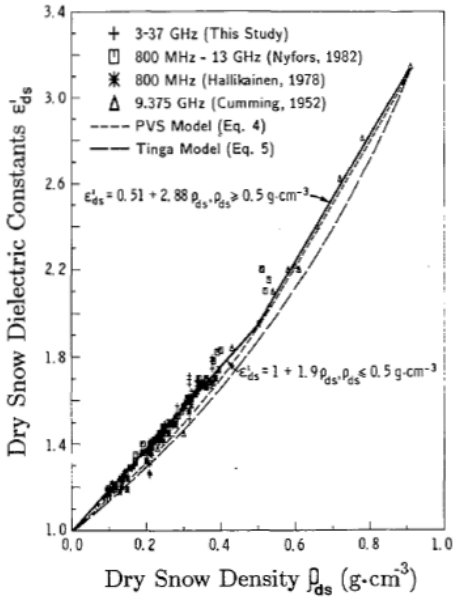

Figure 2-6: Dielectric Constant of snowpacks with varying densities. Source: Hallikainen (1986).

2.4.3 Grain Size

During the winter season, snow exposed to cold temperatures and wind effects is subject to metamorphism. According to Sturm and Liston (1995), snowpacks in tundra environments possess few ice lenses and large amounts of depth hoar. The increase in snow grain size in the bottom layers of the snowpack better approximates the size of the 37 GHz wavelengths used in SWE retrieval algorithms, such that an increase in grain size scatters microwave more efficiently, lowering brightness temperatures received at the sensor (Hall et al., 1986; Derksen et al., 2005). Growth in snow grain size is directly proportional to the amount of potential scattering, and can lower brightness temperature by as much as 20 K with no change in SWE (Hall et al., 1986; Chang and Hall., 1987; Hall et al., 1991; Armstrong et al., 1993). SWE algorithms using frequency differences from one scattering channel and one background channel coincident with considerable depth hoar can therefore overestimate SWE as a result of enhanced scatter at 37 GHz (Hallikainen et al., 1986; Roy et al., 2004; Duguay et al,. 2005).

2.4.4 Stratigraphy

Throughout the winter season, the metamorphosis of a snowpack causes an increase in grain size close to the bottom of the pack as a result of vapour transfer along a temperature gradient, while snow at the surface is metamorphosed by wind action, splintering and separating snow grains (Sommerfeld and LaChappelle, 1970). The result is a layered snowpack with varying densities and dielectric constants that affects the resultant Tb measured at the sensor (Colbeck, 1991). While microwave emission is not affected when a single snow slab is compacted, (Edgerton et al., 1971), the most notable stratigraphic influence is ice lenses, causing a difference of up to 40K at 19 GHz and 33K at 37 GHz in horizontally polarized emission, as horizontally polarized emission is most susceptible to horizontal layering (Rees et al., 2010).

2.4.5 Snow Melt

Due to its high dielectric constant (~80), liquid water in snow increases Tbs of all microwave frequencies, effectively hindering accurate measurements of snow parameters (i.e. SWE, depth and extent) (Hall et al., 1978; Gan 1996; Chang et al., 1997). The emissivity of a snowpack with liquid water inclusions is higher than that of a dry snowpack (e = 0.957 and 0.7 respectively), causing higher measured Tbs (Hewison and English, 1999). Therefore, when melt is present in snowpacks, historical algorithms designed to retrieve its physical properties falter because they cannot account for water within the snow. However, temporal snow melt algorithms for both passive and active microwave studies use the significant change in dielectrics to apply Tb thresholds for the purpose of mapping regional snowmelt (Forster et al., 2001; Tedesco, 2007; Ramage et al., 2007).

2.4.6 Lake Ice

Classic empirical algorithms that derive information about snowpacks using brightness temperature differences are consistently confounded by the presence of within-pixel lake ice, as the magnitude of microwave emission at low frequencies is directly proportional to ice thickness (Hall et al., 1981: Duguay et al., 2005: Lemmetyinen et al., 2008; Derksen et al. 2009). Frequencies that are emitted from depths greater than the snowpack thickness interact with underlying lake ice and water mediums. Table 2-2 lists the depths at which common spaceborne passive microwave radiometer frequencies are emanated from for ice without impurities.

Table 2-2: Depths from microwaves are emitted for pure ice at frequencies used onboard spaceborne sensors at various temperatures (incidence angle of 50^0). Source: Surdyk (2002).

	6.6 GHz (m)	10.7 GHz (m)	18 GHz (m)	37 GHz (m)
190 K	58	20	6.6	1.4
230 K	34	12	4.5	0.9
265 K	19	8	2.8	0.7

Low frequency microwaves (6, 10.7, 18 GHz) are emitted from deep within the snowpack or ice, as a function of the longer wavelengths. Depending on snow depth/ice thickness, low frequency emission can interact with liquid water beneath floating ice, contributing to the measured brightness temperature. The high dielectric constant (ϵ^* ~80) and low emissivity (e = 0.504 at 24 GHz) of water results in lower brightness temperatures than that of soil (ϵ^* ~3) (Ulaby et al., 1982; Hewison and English, 1999). Toose (2007) observed that 19 GHz airborne passive microwave Tbs drop considerably when measured over free floating lake ice; but once a lake has frozen to bed emission is similar to that of snow on land. As a result, algorithms that utilize longer wavelengths (10, 19 GHz) as background frequencies often produce negative SWE in lake-rich environments in which lakes have not frozen to bed (Derksen et al., 2005, Duguay et al., 2005).

Further problems exist when examining within-pixel lake ice, as issues of scale and variable ice phenology also affect microwave emission. Throughout the course of the winter season, ice cover can change (caused by deformation features; i.e. cracks, rafting), become thicker (possibly freezing to the bed for shallow lakes), incorporate gas bubbles, or form white ice; all of which can potentially affect emission (Rees et al., 2006). The use of spaceborne radiometers also presents a problem of scale. The high density of small ponds and lakes that are characteristic of tundra environments cannot be resolved in one 25 x 25km Equal-Area Scaleable Earth (EASE) grid cell. Based on a number of microclimate factors (i.e. air temperature, size/depth of the lake, snow mass), multiple lakes at varying stages of freezing/thawing evolution can also be included within one pixel, further complicating SWE retrieval algorithms (Duguay et al., 2005).

2.5 Passive Microwave SWE Retrieval Algorithms

SWE algorithms have been proposed for various spatial domains, from regional to hemispheric. It has become apparent that errors in hemispheric algorithms are the result of the over-simplification of scattering mechanisms that vary with different land cover and snowpack types. This section will briefly review previous SWE retrieval algorithms and their applicability to tundra environments.

The most common form of SWE retrieval algorithms empirically utilize a scattering channel and background channel to isolate emission scatter caused by a snowpack, (37 and 19 GHz, respectively), proposed by Chang et al., (1987), followed by Rott and Aschbacher (1989). The assumptions made when applying this model are that the Tb frequency differences (ΔT_B) can be modeled using a linear equation, and that atmospheric effects on measurements will be minimized by using the difference between two frequencies, while retaining sensitivity to snowpack properties (Wang & Tedesco, 2007).

Using this approach, Chang attempted to derive a global snow model by linearly fitting the difference between 18 GHz (background) and 37 GHz (scattering) to *in situ* snow depth measurements that were less than 30cm **(3)** (Chang et al., 1997). As a global snow model, physical snowpack variables within the algorithm were simplified (mean grain size = 0.3 mm, density = 300 kg m^{-3}). However, the simplification of snowpack properties causes the algorithm to falter in areas of variable terrain and extreme snow depth.

$$SWE = 4.8 * (Tb18H - Tb37H)\ mm \quad \textbf{(3)}$$

To increase SWE retrieval accuracy, airborne passive microwave measurements coupled with ground observations were utilized by Goodison and Walker (1994) in an effort to produce spring water availability forecasts for Prairie farmers in Canada. The algorithm showed good agreement (+/- 10mm) with dry snowpacks in Prairie regions but did not transfer well to other landcover types, leading to the development of landcover-specific algorithms (Goita et al,. 2003; Derksen et al., 2005) This suite of algorithms now utilized by Environment Canada (EC) incorporates specific equations to be applied to unique landcover types, determined by the International Geosphere-Biosphere Programme (IGBP) 1km global land use classification (Derksen et al., 2005).

$$SWE = F_D SWE_D + F_C SWE_C + F_S SWE_S + F_O SWE_O \quad \textbf{(4)}$$

$$F_D SWE_D = 33.5 - 1.97(37V - 19V)$$

$$F_C SWE_C = 16.81 - 1.96(37V - 19V)$$

$$F_S SWE_S = -1.95 - 2.28(37V - 19V)$$

$$F_O SWE_O = -20.7 - 2.59(37V - 19V)$$

where F_D is the fraction of deciduous forest, F_C is the fraction of coniferous forest, F_S is the fraction of sparse forest, and F_O is the fraction of open area within an SSM/I pixel. This algorithm performs well for the unique landcover types each equation was designed for, however, fails to address the fractional influence of lakes on microwave emission from tundra environments. When the open area algorithm was applied to SSM/I pixels over tundra zones a total of 70% of sites exhibited SWE underestimation, with 50% of sites on the order of -30 to -50mm (Derksen et al., 2005).

In another study, the EC algorithms were applied to the Mackenzie GEWEX (MAGS) study site to validate models designed for fractional open and forested areas. In areas of the Mackenzie River basin where small, sub-pixel lakes dominate the landscape, the open environment algorithm consistently underestimated true SWE levels as frozen lakes possessed markedly differing microwave emission characteristics (Walker and Silis, 2002). Depth hoar metamorphism is also a prevalent feature of snow in tundra environments both on and off lakes, and is not accounted for in these algorithms (Sturm and Liston, 2003; Derksen et al., 2003).

In an effort to include the unique emission characteristics of fractional tundra and lake areas within spaceborne measurements, Gan (1996) derived the following equation,

$$SWE = K_5(AREA_{Tundra})(18H - 37H) + K_6(AREA_{Water})(Temp + 273) + K_7 \quad \textbf{(5)}$$

where $AREA_{Tundra}$ and $AREA_{Water}$ are the fraction of tundra and water within a pixel, (Temp + 273) is the physical temperature of the lake ice and K_5, K6 and K_7 are variable coefficients to be fitted to *in situ* measurements. This is the first conceptual framework derived for tundra environments that account for within-pixel water fraction. While the equation variably accounts for fractional land cover, it essentially approximates Rott and Aschbacher's linear model to provide a best-fit to *in situ* measurements. It assumes that microwaves are emitted from a lake as a function of its physical temperature, however the equation does not account for the effects of liquid water beneath the ice, as well as volume scattering caused by snow overlying the ice (Gan 1996). Therefore, the AREAWater function within the model provides an offset for the linear model but does not account for the physical

properties of the lake influencing microwave emission, ultimately underestimating SWE retrievals relative to *in situ* measurements.

A promising algorithm for lake-rich tundra environments was recently published by Derksen et al. (2010), whereby the traditional scattering and background frequency difference has been abandoned to examine a single, scattering frequency (37 GHz). The algorithm utilizes the cumulative difference between monthly averages of AMSR-E 37 GHz pentad footprints that are independent of lake ice fraction, and account for the characteristic slope change of Tbs when SWE levels exceed 120mm, as displayed in **(6).**

$$\Delta 37V_{month} = \left| 37V_{month\ i} - 37V_{month\ i-1} \right| \quad \textbf{(6)}$$

The results of this algorithm have been promising when cumulative monthly AMRS-E differences were compared to *in situ* SWE measurements (r^2 = 0.77). The basis of this algorithm assumes that the thickness of lake ice included in the sensor footprint is such that microwaves are emitted from within the ice pack. According to Table 2-2, as long as ice thicknesses are greater than ~1 metre, 37 GHz will emanate from the ice. If not, radiometrically cold water will still be included into the signal, and confound SWE retrievals.

Semi-empirical approach

Studies have also examined non-empirical approaches to estimate SWE using passive microwave data. For example, Pulliainen (2006) and Durand and Marguilis (2007) propose data assimilation between spaceborne and *in situ* measurements. Pulliainen (2006) uses the HUT snow emission model to produce simulated brightness temperatures, then assimilates weather station, grain size and spaceborne AMSR-E measurements to derive SWE. The assimilation performs better than average Tb difference algorithms, but requires continuous adjusting of the input grain size parameter, as the HUT model is quite sensitive to grain size fluctuations. Durand and Marguilis (2007) assimilate simulated and multi-scale (passive microwave, MODIS) measurements with a land surface model (derived by weather station, topographic and vegetation data using an ensemble Kalman filter). In areas where common frequency-difference algorithms are unable to quantify SWE levels SWE was accurately estimated with an RMSE of approximately 2cm.

Both Pulliainen (2006) and Durand and Marguilis (2007) effectively estimate SWE in regions that common algorithms falter, however non-empirical algorithms require *in situ* data as drivers, and can

therefore only estimate SWE in regions where snow property information is known. Also, non-empirical algorithms characteristically exhibit better agreement for point-based features, but are not appropriate when regionalized to areas where input data changes both spatially and temporally (Pulliainen, 2006).

2.6 Active Microwave Remote Sensing

As opposed to passive microwave remote sensing, active microwave radar is a self-luminescent system whereby the source of illumination is at the sensor, and the measurement of the medium is the returned signal. The most commonly utilized radar in spaceborne applications is a monostatic synthetic aperture radar (SAR) system whereby the antenna is used for both transmitting and receiving purposes (Ulaby et al., 1982). A synthetic aperture radar system largely functions similar to a real aperture system. SAR systems are designed to transmit and receive either co-polarized (vertical send/vertical return (VV), horizontal send/horizontal return (HH)) or cross-polarized (vertical send/horizontal return (VH), horizontal send/vertical return (HV) backscatter returns at specific microwave frequencies. The most common of these frequencies and some selected satellites that utilize them for previous and current snow and ice studies are listed in Table 2-3**.** Note that QuikSCAT is not a SAR but is included because of the amount of cryospheric studies that utilized the Ku-band scatterometer.

2.6.1 Synthetic Aperture Radar

The basic theory of SAR technology is that the antenna transmits a radio frequency pulse or "chirp" linearly over a certain frequency range (bandwidth), called frequency modulation (FM) (McCandless and Jackson, 2004). The "up-chirp" interacts with the ground media, and the synthetic aperture antenna measures the returned energy and processes it on a time delay as a function of frequency; the frequency transmitted first is delayed the longest, to form a de-chirped waveform of a desired bandwidth (10 to 40 MHz on most SAR systems), as displayed in Figure 2-7 (McCandless and Jackson, 2004; Ulaby et al., 1982).

Table 2-3: Overview of spaceborne active microwave sensors that are commonly used for cryospheric studies.

Frequency	Satellite	Year Launched	Band	Frequency (GHz)	Incidence Angle (deg)	Polarization	Beam Mode	Resolution (m)	Swath Width (km)
C-band (4 - 8 GHz)	ERS-1/2	1991/1992	C-band	5.25	23	VV	Standard beam mode	30	100
	RADARSAT-1	1995	C-band	5.3	37 - 47	HH	Fine beam mode	8	45
					20 - 49		Standard beam mode	30	100
					20 - 45		Wide beam mode	30	150
					20 - 49		ScanSAR narrow beam	50	300
					20 - 49		ScanSAR wide beam	50	500
	ENVISAT	2002	C-band	5.25	15 - 45	VV, HH, VV/HH, HV/HH, VH/VV	Image, Wave & Alternating Pol Wide Swath Global Monitoring Mode	30 150 1000	Image/Wave - 100 Wave - 5 Wide/Global - 400+
	RADARSAT-2	2008	C-band	5.25	20 - 49	HH/HV	Standard beam mode	28 x 28	100
					20 - 45	HH/HV	Wide beam mode	25 x 28	150
					30 - 50	HH/HV	Fine	10 x 9	50
					20 - 49	HH/HV	ScanSAR Wide	100 x 100	500
					20 - 47	HH/HV	ScanSAR Narrow	50 x 50	500
					20 - 41	HHVV/HHVH	Standard qual pol	25 x 28	300
					20 - 41	HHVV/HHVH	Fine Qual Pol	11 x 9	25
					30 - 50	HHVV/HHVH	Multi look fine	11 x 9	50
					30 - 40	HHVV/HHVH	Ultrafine	3 x 3	20
X-band (8 - 12 GHz)	TerraSAR-X	2007	X-band	9.65	20 - 55	Single: HH/VV, HH/VH, VV/HV or Dual: HH/VV	High Resolution Spotlight	1m single, dual 2m	10
					20 - 55		Spotlight	2m single, dual 4	10
					20 - 45		StripMap	3m single, dual 6	up to 3000
					20 - 45		ScanSAR	16 x 16m	100
Ku-band (12 - 18 GHz)	QuikSCAT Scatterometer	1999	Ku-band	13.4	46	HH	Horizontal Pol	22.5 km egg	1800
					54	VV	Vertical Pol	11.125km slices	

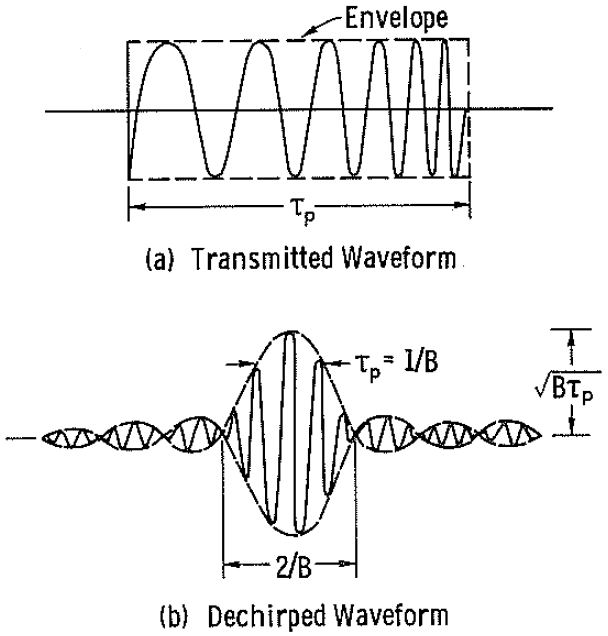

Figure 2-7: Frequency Modulation technique used to form a "dechirped waveform" (Ulaby et al., 1982).

The variables measured by the SAR antenna are the phase shift and intensity. The phase shift can be used for interferometric analyses, and the more commonly used intensity (power) is the magnitude of radiation "backscattered" towards the receiving antenna (Ulaby et al., 1982). The amount of energy backscattered by objects that are in the propagation path of the transmitted waveform is measured as a ratio between the between the transmitted and backscattered radiation, expressed as

$$\frac{P_t G^2 \lambda^2 \sigma}{(4\pi)^3 R^4} \quad \textbf{(7)}$$

where P_t is the transmitted power, $G$is the antenna gain, λ is the wavelength, σ is the radar scattering cross-section, and R is the range between the antenna and the target (Ulaby et al., 1982). The magnitude of the scattering cross-section varies for individual sub-targets viewed by the SAR as a result of the differential gain experienced by variability in of the target direction from the radar. Therefore, the *differential backscattering coefficient* or *backscattering coefficient* is defined as the average scattering cross-section per unit area, as expressed by (Ulaby et al., 1982)

$$\sigma^0 = \frac{\sigma_i}{\Delta A_i} \quad \textbf{(8)}$$

where ΔA_i is the area of the target. The backscattering coefficient (σ^0) is most commonly expressed in studies using a logarithmic scale, ranging between -30dB to +5dB. On most SAR systems, a $\sigma^0$of lower than -30dB is considered to be influenced by the noise floor of the sensor (Ulaby et al., 1982).

Active microwave SAR systems are widely utilized for their fine spatial resolution. For example, TerraSAR-X measurements can range from up to 1m resolution in SpotLight mode and 3m resolution in StripMap. The method by which the fine spatial resolution is achieved is briefly discussed. Range resolution (perpendicular from the sensor azimuth) is achieved through pulse compression of the backscattered signal, as detailed above. Azimuth resolution (a.k.a. along tack resolution) is determined by use of the synthetic aperture, where resolution is a function of the Doppler bandwidth of the received signal at any specific target (McCandless and Jackson, 2004). Displayed in Figure 2-8, the beam width of the SAR observes object *A* in all three measurements, with the distance *B* equaling the Doppler bandwidth. The phase shifts of all returned pulses of *A* that are within the Doppler bandwidth are saved, processed and summed to produce one coherent target (*A*) (Woodhouse, 2006). The resulting spatial resolution of the single look (all pulses processed) is equivalent to one half of the along track distance *B*, providing a synthesis to a real aperture radar system but with a much smaller antenna (McCandless and Jackson, 2004; Woodhouse, 2006).

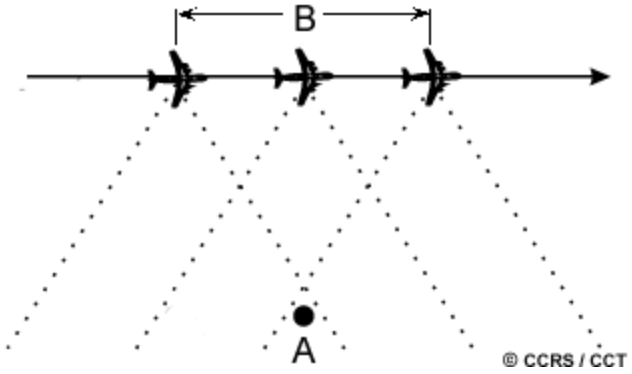

Figure 2-8: Illustration of the Doppler effect used by SAR to obtain high resolution.
Source: http://www.ccrs.nrcan.gc.ca

2.6.2 TerraSAR-X

Many studies have utilized spaceborne SAR for cryospheric applications, using mostly C-band (5.3 GHz) measurements from RADARSAT-1 or ERS 1 or 2 (Kozlenko and Jeffries, 2000; Duguay et al., 2002; Duguay and Lafleur, 2003; Nghiem and Leshkevich, 2007). The efficacy of spaceborne X-band measurements for snowpack property retrieval has become apparent through NASA space shuttle missions (Shi and Dozier, 2000; Shi 2004). With the launch of TerraSAR-X by DLR (German Aerospace Centre) in June of 2007, a time series of spaceborne X-band SAR measurements is available for the first time. Tandem-X, DLR's sister satellite to TerraSAR-X was launched in June of 2010 for the purpose of creating a global DEM that meets the criteria outlined by the emerging HRTI level 3 standard (Krieger et al., 2005), allowing for the potential of a unique interferometric dataset during the winter season.

TerraSAR-X operates at X-band at a dominant frequency of 9.65 GHz on a sun synchronous polar orbit at an average altitude of 514km. It is a commercial-based satellite with 3 beam modes at various spatial resolutions; SpotLight mode has a spatial resolution of up to 1m and a swath of 5 x 10km, Stripmap mode has a spatial resolution of 3m and a swath of 30 x 50km and ScanSAR mode has a spatial resolution of up to 18m, with a swath of 100 x 150km (Werninghaus et al., 2003).

TerraSAR-X orbits the Earth at a polar dawn-dusk repeat cycle, at an 11 day repetition cycle, meaning that the satellite repeat orbit with imaging swaths at the same ground placement every 11 days. Despite the 11 day repeat cycle, swath overlap allows for the average revisit time (albeit with a difference incident angle and position within the swath) to be 2.5 days (Werninghaus et al., 2003).

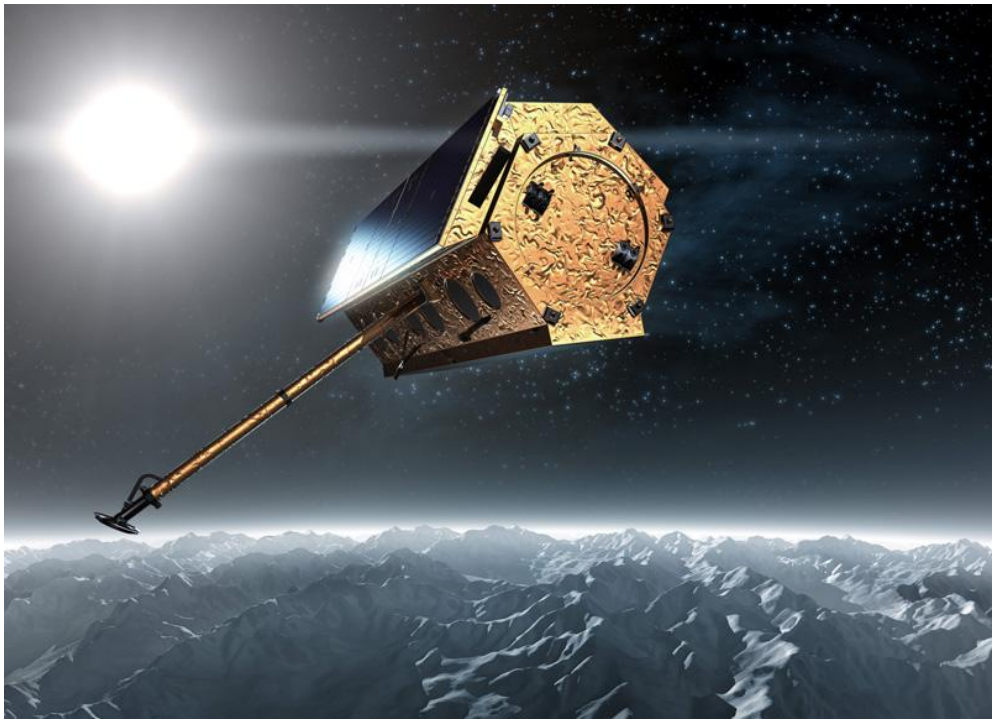

Figure 2-9: Artistic conception of TerraSAR-X ©*EADS* Astrium GmbH

2.7 Factors that Affect Microwave Backscatter

Backscatter measured at the receiving antenna is a summation of the scatter caused by all targets that are encompassed by the scene swath. The magnitude of scatter depends on the surface roughness and dielectric constant of the medium, and can be a result of any of the following sources: surface, volume or sub-surface scatter.

If the transmitted wavelength is such that there is no transmission through the surface of the incident media, surface scatter will be dependent on two factors: dielectric constant, and surface roughness. The dielectric constant of the media essentially governs the magnitude of specular reflection of the incident wave, as a media with an increased dielectric constant absorbs more radiation. In the case of the remote sensing of snow, an increase in volumetric water content will reduce surface scatter (Ulaby et al., 1982). Also, increased surface roughness will provide more scattering targets for incident microwaves to interact with whereas a smooth surface will cause specular reflection of the signal, thereby reducing backscatter (Ulaby et al., 1982).

Volume scatter occurs when the propagated signal penetrates sufficiently through the surface and encounters an inhomogeneous media made up of variable dielectric constants that approximate the size of the incident wavelength. Snow is an inhomogeneous media, predominantly comprised of ice crystals of various size, shape and orientation surrounded by air pockets. Variable amounts of volume scatter can occur, dependent largely on the wavelength of the incident signal, surface roughness of the media and the density of the potential scatterers (Ulaby et al., 1982).

Sub-surface scatter denotes the scattering that takes place at the bottom layer of the media examined, such as the ice surface of a lake underneath a snowpack. The scattering mechanisms in this case are consistent with previous surface scatter considerations, however the total magnitude of the signal may be less after penetrating through the previous layer (Ulaby et al., 1982). When considering backscatter return for snow on lake ice, three major parameters must be considered: the sensor utilized, the physical characteristics of the snowpack, and the physical properties of the subsurface media, such as ice and water.

Sensor parameters: The return measured from a snowpack is dependent on the frequency of the measurement. Synonymous with passive microwave remote sensing, the shorter the wavelength used in observation, the more likely that it will interact with individual ice crystals present in the snowpack and produce backscatter. Studies using frequencies below 8 – 10 GHz have not noticed considerable fluctuations in backscatter as a result of changes in snow depth, as these wavelengths transmit through the snowpack with negligible scatter and interact with sea ice or freshwater ice beneath (Ulaby et al., 1984; Nghiem and Tsai, 2001). However, select studies using C-band (5.3 GHz) have observed increases in backscatter with an increase in snow depth (Praks et al., 1998) or density (Shi and Dozier, 2000), while studies examining the use of L-band (1 GHz) have not yielded significant results (Praks et al., 1998). Frequencies higher than 8 GHz like X- (9.65 GHz) and Ku-band (17 GHz) have been identified as being sensitive to fluctuations in snowpack parameters as the shorter wavelength is more likely to be scattered by individual ice crystals (Praks et al., 1998).

Snowpack parameters: Many snowpack parameters affect an incident microwave signal, causing surface, volume, double-bounce, or subsurface scattering. These factors include: depth, density, SWE, liquid water content, surface roughness, stratification and snow grain size (Ulaby et al., 1984),

however, the latter two have not been investigated extensively. Backscatter increases as a result of snow depth, density and SWE have been noticed by studies using C- (5 GHz), X- (9.6 GHz) and Ku-band (13 – 17GHz). Ulaby and Stiles (1980) noticed steady increases in backscatter at X-band with increases in snow depth and SWE as a result of increased volumetric scattering, illustrated in Figure 2-10.

The presence of liquid water within the snowpack during the spring melt or freeze/thaw periods late in the season causes backscatter to drop abruptly at all frequencies studied due the absorptive properties of water (Nghiem and Tsai, 2001; Yueh et al., 2009). The sharp drop in backscatter aids in snow melt detection discussed later in this section. Sharp backscatter fluctuations have been noticed in tandem with diurnal melt/freeze cycles leading up to the spring thaw (Hallikainen et al., 2004). During melt cycles, backscatter fluctuations are also dependent on surface roughness and dielectric constant, as smooth surfaces can cause specular reflection of the signal, while the high dielectric constant of water absorbs it. Both interactions will cause a significant decrease in backscatter (Ulaby et al., 1982).

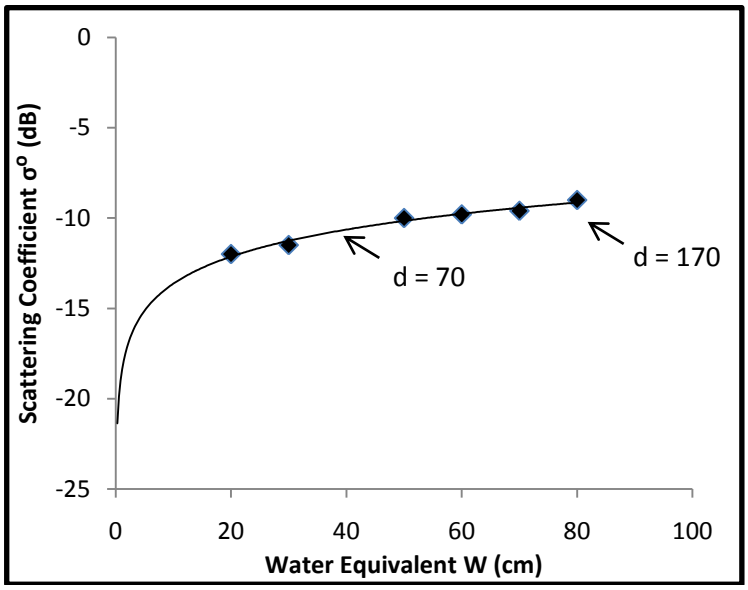

Figure 2-10: X-band HH scatter as a result of increases in SWE (d = snow depth (cm)). Source: Modified from Ulaby et al., 1980.

Subsurface Parameters: Subsurface parameters affect backscatter based on the dielectric properties of the surface, as well as the presence of liquid water (Ulaby et al., 1982; Shi and Dozer 2000). Figure 2-11 illustrates the scattering mechanisms within an average snowpack. The underlying medium directly affects the magnitude of four of the five scattering mechanisms.

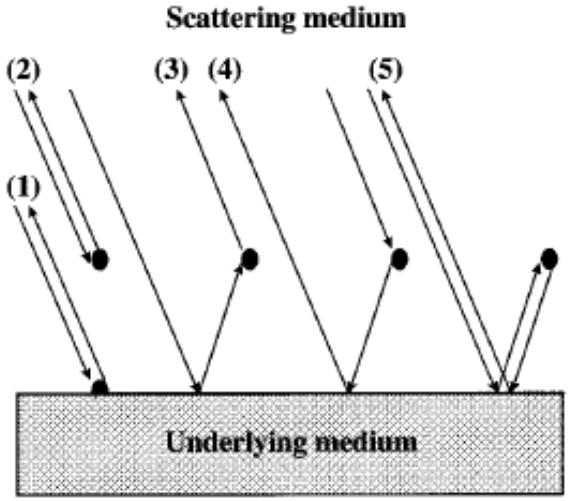

Figure 2-11: Sources of scatter in a snowpack (1) Direct scatter from a rough surface, (2) volumetric scattering, (3&4) double-bounce effect of scattered signal and (5) double-bounce. Source: Nghiem and Tsai, 2001.

If the incident microwave possesses a penetration depth sufficient to reach the underlying medium, the surface roughness and dielectric constant of either frozen soil or lake/sea ice controls the scattering characteristics. Figure 2-12 identifies the dominant scattering mechanisms present for microwave incident on a lake that is partially frozen to bed. The refractive index of snow, ice, and water are heavily dependent on the dielectric permittivity of the medium, with values similar to their respective dielectric constants (Sadiku, 1985). Ice has a higher dielectric constant than snow and thus, a higher relative permittivity, as snow is comprised low density ice crystals and air pockets. Therefore, the effective incidence angle of transmitted microwave radiation is increased when propagating through the snow/ice interface, however, the signal is reflected at the ice/water interface as a result of the sharp dielectric contrast between water ($\epsilon^* \sim 80$) and ice ($\epsilon^* \sim 3$). Inclusions within the ice such as deformation features (cracks, ridges) and elongated bubbles can act as scatterers, providing a double bounce effect because of the reflection at the ice/water interface (Duguay et al., 2003). If a lake is frozen to bed, the signal transmits through the ice medium and interacts with the

ground surface. Therefore, the resulting backscatter of snow on top of clear ice that is frozen to bed is characteristic to snow on land (Duguay et al., 2003).

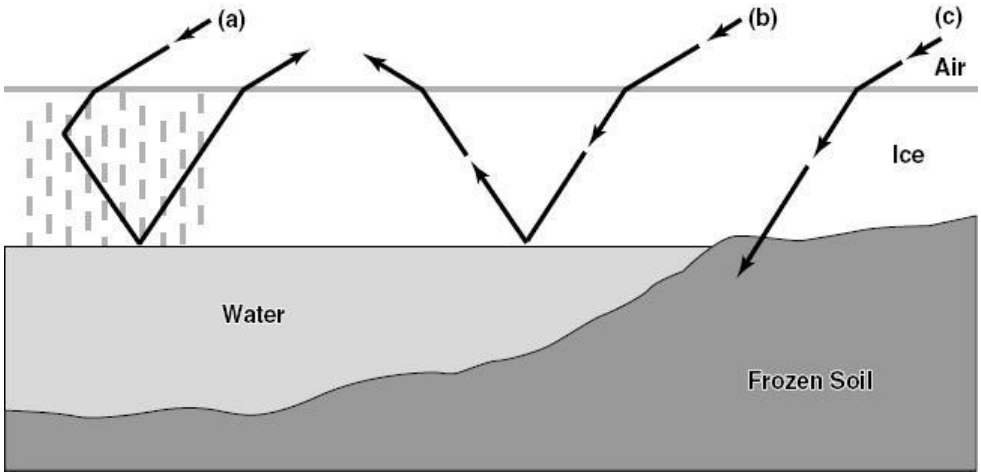

Figure 2-12: Microwave interaction in the presence of: (a) vertically oriented bubbles, (b) ice/water interface, (c) ice frozen to bed (Duguay et al. 2002).

2.8 Microwave Snow Emission Models

Microwave snow emission models serve to enhance our understanding of the physical dynamics of microwave emission and scatter caused by various snowpack properties. The justification for the use of snow emission models is if Tbs can be simulated accurately based on the use of *in situ* snow properties as input, the model can be inverted to retrieve those properties from spaceborne measurements. Microwave snow emission models simulate the magnitude of emission measured by spaceborne radiometers as a function of the amount of scatter and attenuation caused by the snowpack. The transmitted radiation is calculated using radiative transfer theory, whereby media (snow grains) are either treated as discrete scatterers or continuous scattering media.

2.8.1. Theoretical Models

Discrete Scatterers: When snow grains are treated as discrete scatterers, the magnitude of emission is based on the assumption that each particle within the media is an independent scatterer. Each particle is treated as a spherical Rayleigh or Mie scatterer, or as various non-spherical shapes (discs,

columns). Snowpacks are often treated as a dense medium, where several discrete scatterers are present within the propagation path of emitted microwaves. This representation of snow is known as the dense media radiative transfer (DMRT) theory (Kuga et al., 1990). Using a quasicrystalline approximation (QCA), the DMRT model has been successfully applied to snow emission modeling (Tsang et al., 2000). The major components of the model are the extinction coefficient (absorption + scattering coefficients), the phase matrix (used for higher-order multiple-scatter considerations) and the media albedo (scattering / extinction coefficients) (Tsang et al., 2000). These inputs are derived from the physical parameters of the snowpack, such as dielectric constant, snow grain size or sizes, orientation, and stratigraphy (Tsang et al., 1987). A more comprehensive overview of the DMRT snow emission model is given in Tsang et al. (2000).

Continuous Scatterers: When snow grains are treated as a continuous scattering media, the snowpack is characterized as a layer of variable effective permittivity as derived by its random correlation function. The effective permittivity controls the magnitude of emission scatter during transmission through the medium (Jin, 1989). The magnitude of emission (scattering coefficient) of a medium can then be calculated using either the weak or strong fluctuation theory for the purpose of solving the radiative transfer equation (Tsang et al., 1985). The use of the strong fluctuation theory has been successfully applied to the simulation of Tbs for 18 GHz with limited input parameters (snowpack temperature, density and grain size) (Stogryn, 1986). However, the sensitivity of 37 GHz Tbs to snowpack layering requires the inclusion of extra parameters including snow stratigraphy, ice layers, density and grain size gradients (Stogryn, 1986). A more comprehensive overview of the strong fluctuation theory is provided by Jin (1989).

2.8.2 Semi-Empirical Models

For the purpose of operational SWE monitoring using passive microwave remote sensing, theoretical methods can be too computationally expensive and require too many inputs. Alternatively, semi-empirical models like HUT's snow emission model (Pulliainen et al., 1999) or the Microwave Emission Model of Layer Snowpacks (MEMLS) (Wiesmann and Maztler, 1999a; Wiesmann and Maztler, 1999b) provide a more straightforward algorithm that can be inverted with satellite Tbs. This study investigates the use of the HUT model for emission from a snowpack on top of lake ice, as described below.

2.8.3. HUT Snow Emission Model

The HUT model estimates Tb emission by treating the snowpack as a single layer, with a basic assumption that the transmitted radiation propagating through the medium is scattered mostly in the forward direction (Pulliainen et al., 1999). The components used to solve the Delta-eddington approximation of the radiative transfer equation (absorption and extinction coefficients) are derived using the snow grain size and complex dielectric constant of dry snow (Lemmetyinen et al., 2008). Unlike the previous models, the scattering coefficient denotes the amount of radiation that is scattered towards the sensor, and is given by a constant, *q*. In Pulliainen et al. (1999), $q = 0.96$ as derived by fitting simulations to measured Tbs in previous studies, and is applied to simulations for frequencies between 5 – 90 GHz. The effects of soil and subsurface roughness on Tb emission are also incorporated into the model, using empirical and semi-empirical equations (Pulliainen et al., 1999). Further modifications have been made to the HUT model with the consideration of multiple layers for snowpacks with considerable depth hoar or wind slab layers, as well as for the incorporation of subsurface lake ice (Kontu et al., 2008a; Kontu et al., 2008b). The modified HUT model also incorporates interlayer reflection and transmission coefficients to simulate microwave interaction between interfaces (Lemmetyinen et al., 2010).

The HUT snow emission model has been successfully implemented in Finnish boreal forest environments, effectively reducing Tb and SWE retrieval errors compared to previous algorithms (Pulliainen et al., 1999; Tedesco et al., 2004; Pulliainen, 2006). Correlations of simulated Tbs for 18.7 and 37 GHz were consistently reported to be above 0.7, however 6.9 GHz exhibited poor R^2 values close to 0.0 (Kontu et al., 2007). Roy et al. (2004) also successfully utilized the HUT model to simulate microwave emission in Canadian boreal forests after modifying the extinction coefficient to account for the inclusion of larger grains found in depth hoar layers.

As a single layer snow emission model, the HUT model exhibits notable drawbacks when simulating snowpacks that include any of the following: wet snow, extremely deep snow, mixed pixels, snow metamorphism (depth hoar) and multilayered snowpacks (Pulliainen et al., 1999; Tedesco et al., 2004; Roy et al., 2004; Butt and Kelly, 2008). To address the errors produced by multiple layered snowpacks, the HUT model has been updated to incorporate multiple layers, as well as interlayer reflection and transmission considerations at the interface between the two layers (Lemmetyinen et al., 2010). As the empirical scattering coefficient *q* can be customized to

characterize different scattering media, the modified HUT model can simulate emission from both lake ice and snowpack layers. Initial results for Finnish lakes indicate that Tb simulation accuracy improved for higher frequencies (37 GHz) and deteriorated for lower frequencies (18 GHz) that are influenced by subsurface lake ice (Lemmetyinen et al., 2009).

2.9 Synergy of Passive and Active Microwave Data

There have been few studies that have combined the use of passive and active microwave remote sensing for the purpose of snow property retrieval (Hallikainen et al., 2003; Tedesco and Miller, 2007). However, there has been a trend towards the use of current and historical snow products encompassing multiple sensors and satellites for the purpose of generating accurate global-scale data products (Derksen et al., 2003; Kouraev et al., 2008; Tang et al., 2009). Studies have already assessed the benefit of added supplementary data that has close to, if not the same spatial resolution and incident angle arrays using either NSCAT or QuikSCAT backscatter coupled with coincident SSM/I Tbs (Nghiem and Tsai, 2001; Tedesco and Miller, 2007). Accuracy is also increased when measurements are multi-frequency, multi-satellite or utilize an increased amount of *in situ* measurements (Hallikainen et al., 2004).

2.9.1 SWE Retrievals Using Synergistic Active and Passive Acquisitions

Hallikainen et al. (2003) identify the use of algorithms combining SSM/I (19, 37 GHz) and QuikSCAT (Ku-band) measurements for the purpose of SWE retrieval over boreal forest and agricultural land. A model was developed based on in situ measurements that utilized linear relationships noticed between individual sensor measurements and SWE values, based on the dynamic ranges of passive Tb and active σ^0 measured at zero and maximum SWE levels:

$$SWE = A * Tb + B * \sigma^0 + C \quad \textbf{(9)}$$

where Tb is the brightness temperature function (not shown), and σ^0 is the backscatter, while *A*, *B* and *C* are coefficients determined by linearly fitting the equation to in situ measurements (Hallikainen et al., 2003). Correlation coefficients showed improvement when using the combined active/passive equation relative to using solely active or passive measurements. The best result is obtained when an algorithm is applied that incorporates the gradient ratio between 37 and 19 GHz onboard SSM/I, divided by Ku-band (13.4 GHz) backscatter from QuikSCAT (Table 2-4**).**

Table 2-4: Correlation coefficients for passive, active and synergistic SWE retrieval methods. Source: Modified from Hallikainen et al., 2003.

Input Data	**Channel**	**Correlation Coefficient**		
		1999 – 2000	**2000 – 2001**	**2001 – 2002**
SSM/I Descending Orbit (7 – 9 am)	37V – 19V	-0.73	-0.91	-0.56
QuikSCAT Asc Orbit (6 am)	13.4 H	0.49	0.55	0.54
Combined SSM/I and QuikSCAT Data	37V – 19V / 13.4H	-0.81	-0.92	-0.67

For high latitude monitoring of SWE, synergistic studies must examine the effects of subsurface lake ice and water mediums on previously proposed algorithms. While the effect of lake ice has been investigated using passive and active microwave measurements separately, its presence has not been quantified in synergistic studies to date. The synergistic algorithm proposed by Hallikainen et al. (2003) incorporates both slope and offset variables *A. B* and *C* **(9)** to be fit to in situ measurements, making its use quite viable for lake-rich environments.

Based on the preceding research context provided, the following two appended papers focus on the effect of various ice properties on passive and active microwave interaction. The first paper focuses on the evaluation of the incorporation of lake ice emission in the HUT snow emission model for lakes in Northwest Territories; comparing simulations to airborne passive microwave footprints. The second paper provides an examination of the relationships that exist between active and passive microwave measurements over tundra lakes, focusing on the potential application of active/passive synergy to derive information on lake ice properties.

Chapter 3

Evaluation of the Helsinki University of Technology's Modified Snow Emission Model Over Lake Ice Using Airborne Passive Microwave Measurements

OVERVIEW

Algorithms designed to estimate snow water equivalent (SWE) using passive microwave measurements falter in lake-rich high latitude environments due to the emission properties of ice covered lakes on low frequency measurements. Microwave emission models have been used to simulate brightness temperatures (Tbs) for snowpack characteristics in terrestrial environments but cannot be applied to snow on lakes because of the differing subsurface emissivities and scattering matrices present in ice. This paper examines the performance of a modified version of the Helsinki University of Technology (HUT) snow emission model that incorporates microwave emission from lake ice and sub-ice water. Inputs to the HUT model include measurements collected over brackish and freshwater lakes north of Inuvik, Northwest Territories, Canada in April 2008, consisting of snowpack (depth, density, snow water equivalent) and lake ice (thickness, ice type). Coincident airborne radiometer measurements at a resolution of 80 x 100 metres were used as ground-truth to evaluate the simulations.

Results indicate that subsurface media are simulated best when utilizing a modeled effective grain size and a 1mm root mean square (RMS) surface roughness at the ice/water interface compared to using measured grain size and a flat Fresnel reflective surface as input. Simulations at 37 GHz (vertical polarization) produce the best results compared to airborne Tbs, with a root mean square error (RMSE) of 6.2 K and 7.9 K, as well as mean bias errors (MBE) of -8.4 K and -8.8 K for brackish and freshwater sites respectively. Freshwater simulations at 6.9 and 19 GHz H exhibited low RMSE (10.53 and 6.15 K respectively) and MBE (-5.37 and 8.36 K respectively) but did not accurately simulate Tb variability (R = -0.15 and 0.01 respectively). Over brackish water, 6.9 GHz simulations had poor agreement with airborne Tbs, while 19 GHz V exhibited a low RMSE (6.15 K), MBE (-4.52 K) and improved relative agreement to airborne measurements (R = 0.47). Salinity considerations reduced 6.9 GHz errors substantially, with a drop in RMSE from 51.48 K and 57.18 K for H and V polarizations respectively, to 26.2 K and 31.6 K, although Tb variability was not well

simulated. With best results at 37 GHz, HUT simulations exhibit the potential to track Tb evolution, and therefore SWE through the winter season.

3.1 Introduction

Snow cover in high-latitude environments is a source of water storage for six to eight months of the year, impacting the circulation of water within the hydrological cycle. The accurate measurement of snow properties (i.e. snow extent, density, depth and snow water equivalent (SWE)) is important for hydroelectric power generation, local and regional climate modelling, and can provide a good indication of future water supplies (Marshall et al., 1992; Cohen, J. and Entekhabi, D., 1999; Walker and Silis 2002; Derksen et al. 2003; Derksen and Walker 2004; Lemmetyinen et al., 2008a). A long term time series of snow cover extent can also serve as an indicator to be utilized in global climate change research (Kelly et al. 2003).

In lake-rich high-latitude environments both climate and topographic features affect snow and lake ice phenology. Tundra environments with consistently cold winter temperatures and a lack of vegetation have shallow snowpacks with infrequent ice lenses and a high percentage of depth hoar. However, snow on lakes tends to be thinner, denser and comprised of less SWE than snow on land. It also exhibits fewer layers and has a more pronounced slab-to-hoar fraction near the ice surface as a result of the low thermal conductivity of snow (Sturm et al., 1995). The presence of an insulating snowpack on lake ice also hinders the transfer of heat from the water column to the atmosphere at a rate dependent on the snowpack's depth and density, effectively slowing the downward development of congelation ice, while also promoting ice growth in the event of slushing events, creating variable ice types (for example, white, grey, and clear ice) (Adams and Roulet, 1980).

Accurate measurements of snow properties are obtained through in situ snow courses, however, the high variability of snow properties in tundra environments (typically on the order of hundreds of metres) biases the upscaling of in situ measurements to regional scales, as most snow courses are restricted to populated areas (Derksen et al., 2003). Snow courses are also typically intermittent, limiting phenological studies due to the high spatial and temporal variability of snow depth and density in tundra environments (Lemmetyinen et al., 2008a; Walker and Goodison 2000). Satellite remote sensing is useful to improve the temporal resolution of snow observations and measurements.

Optical and infrared sensors, such as Landsat Multispectral Scanner and Thematic Mapper, and the National Oceanic and Atmospheric Administration's (NOAA) Advanced Very High Resolution Radiometer (AVHRR) have been successfully utilized to estimate snow extent, albedo and physical temperature, however they cannot be used to accurately derive other snowpack properties. Alternatively, passive microwave remote sensing measurements have long been used to derive snow depth and SWE (Chang et al., 1997; Hall et al., 1991). A common basis for snow retrieval algorithms is to empirically relate the difference between a scattering and non-scattering frequency channel based on changes in snowpack properties (Gan, 1996; Walker and Goodison, 2000; Goita et al., 2003; Derksen et al., 2005; Brown et al., 2007). Uncertainties in how fluctuations of independent snow parameters (such as grain size) affect the emissivity of the snowpack, however, warrant the use of microwave emission models as a component of SWE retrieval algorithms (i.e. Pulliainen et al., 1999).

Microwave emission models utilize known factors that affect the emissivity of snowpacks to simulate brightness temperatures using in situ measurements as variable inputs. The models attempt to emulate how variability within various snowpack properties can cause either reduced or increased microwave emission. Simulations have been successful when applied to snow on land in terrestrial environments (including prairie, boreal, and tundra regions) for frequencies over 18GHz (Pulliainen et al., 1999; Roy et al., 2004; Kontu et al., 2008b; Rees et al., 2010). However, when microwave emission models are applied to lake-rich high-latitude environments the influence of water underneath lake ice can cause pronounced uncertainty in model simulations (Kontu et al., 2008a). The presence of the variable dielectric constants of water compared to ice and added scattering interfaces (water/ice, ice/snow) further confound brightness temperature simulations (Kontu et al., 2008a).

This study investigates the influence of ice covered lakes on microwave emission and examines the performance of a modified Helsinki University of Technology (HUT) snow emission model tailored to simulate emission over lake ice. Biases within the HUT snow emission model are investigated through a comparison of simulated and airborne measured brightness temperatures, utilizing in situ snow measurements as ancillary data. These parameters include: snow depth, density, SWE, snow grain size, and lake ice thickness.

3.2 Factors that Affect Microwave Emission in Tundra Environments

3.2.1 Components of Snow

Tbs observed by passive microwave radiometers can be expressed as:

$$T_b(f,\theta) = e(f,\theta)T \quad \textbf{(10)}$$

where e is the emissivity of the surface/target relative to the frequency (f) and incidence angle (θ) examined, and T is the physical temperature of the medium in Kelvin (K). Fluctuations in emissivity are affected by the dielectric constant and surface roughness of the medium. Microwave emission is also affected by scattering from objects approximately the size (or larger) of the frequency's wavelength, thereby lowering Tbs. In lake-rich high-latitude environments various physical properties of snow and ice contribute to brightness temperature fluctuations.

As wavelengths begin to approximate the size of dry snow grains at frequencies 20 GHz and higher, emitted microwaves are scattered in all directions at a rate proportional to the SWE of the snowpack (Goita et al., 2003; Duguay et al., 2005; Kelly, 2009). Deeper snowpacks scatter emitted microwaves more efficiently thereby allowing less radiation to reach the radiometer, resulting in lower Tbs. At a critical threshold, microwave emission from snowpacks with SWE over 100 to 150 mm has been observed in boreal and tundra environments, increasing the total emission (Ulaby et al., 1982; Matzler et al., 1982; Sturm et al., 1993). Other factors that contribute to scatter in dry snow conditions include increases in snow grain size and snow density (Kelly, 2009). Snow density affects the emissivity of a snowpack by modifying the dielectric constant. The complex dielectric constant (ϵ^*) of dry snow is given by:

$$\epsilon^* = \epsilon_{ds}' + j\epsilon_{ds}'', \quad \textbf{(11)}$$

where ϵ_{ds}' is the real part of the dielectric constant, and ϵ_{ds}'' is the imaginary lossy portion. Components of snow that affect the dielectric constant relative to the HUT snow emission model are frequency, temperature, volumetric water content, snow grain size and density (Ulaby et al., 1982; Hallikainen et al., 1987; Stogryn, 1986). In the microwave region of the electromagnetic spectrum, the real part of the dielectric constant of snow (ϵ_{ds}') is independent of temperature and frequency, so long as no melting occurs within the snowpack (Ulaby et al., 1982; Hallikainen et al., 1986). In wet snow conditions, the high dielectric constant of water ($\epsilon^* \sim 80$) acts as an emitter and raises microwave emission, hindering accurate measurements of snow parameters (Hall et al., 1978; Chang et al., 1997; Gan 1996). Therefore, the real part of the dielectric constant (ϵ_{ds}') of dry snow is

predominantly dependent on snow density (Hallikainen et al., 1986). In common snowpacks, the dielectric constant of dry snow ranges from 1.4 – 2, and rarely exceeds 3 when snow contains some water in liquid form (Ulaby et al., 1982). Snowpacks on lake ice tend to be denser and contain proportionately more depth hoar than the surrounding tundra landscape, thereby raising the extinction coefficient and lowering the emissivity of the snowpack (Hallikainen et al., 1986; Sturm and Liston, 2003).

3.2.2 Lake Ice

Empirical passive microwave algorithms that derive snowpack parameters utilizing frequency differences are consistently confounded by the inclusion of within-pixel lake ice, as the magnitude of microwave emission at low frequencies is directly proportional to ice thickness (Hall et al., 1981; Duguay et al., 2005; Derksen et al. 2005; Lemmetyinen et al., 2008a). Frequencies that emanate from depths greater than the snowpack thickness interact with underlying lake ice and water. Table 1 lists the depths at which common spaceborne passive microwave radiometer frequencies are emanated from ice (assuming no impurities).

Table 3-1: Depths at which microwaves are emitted for pure ice at frequencies commonly used onboard spaceborne sensors at (incidence angle of 50^0). Source: Surdyk (2002).

	6.6 GHz (m)	10.7 GHz (m)	18 GHz (m)	37 GHz (m)
190 K	58	20	6.6	1.4
230 K	34	12	4.5	0.9
265 K	19	8	2.8	0.7

Low frequency microwaves (6, 10.7, 19 GHz) are emitted from deep within the snowpack or ice volume, as a function of the longer wavelengths emanating through the medium. Depending on snow depth/ice thickness, low frequency emission can interact with liquid water beneath floating ice. The high dielectric constant ($\epsilon^* \sim 80$) and low emissivity ($e = 0.504$ at 24 GHz) of water results in lower brightness temperatures than that of soil ($\epsilon^* \sim 3$) (Ulaby et al., 1982; Hewison and English, 1999). Toose (2007) observed a drop in 19 GHz airborne passive microwave Tbs when measured over free floating lake ice. However, once a lake has frozen to bed, emission is similar to that of snow on land. As a result, algorithms that utilize longer wavelengths (10, 19 GHz) as background frequencies can

actually produce negative SWE values for tundra environments in which lakes have not frozen to bed (Derksen et al., 2005, Duguay et al., 2005).

Further problems exist when examining within-pixel lake ice, as issues of scale and variable ice phenology also affect microwave emission. Throughout the course of the winter season, ice cover can change (caused by deformation features; i.e. cracks, rafts), become thicker (possibly freezing to the bed), incorporate gas bubbles, or form white ice; all of which can potentially affect microwave emission (Rees et al., 2006). The use of spaceborne radiometers also presents a problem of scale. The high spatial density of small ponds and lakes that are characteristic of tundra environments cannot be resolved at the scale of satellite passive microwave measurements (typically 25 km). Based on a number of microclimate factors (i.e. air temperature, size/depth of the lake, snow mass), multiple lakes at varying stages of freezing/thawing evolution can be included within one pixel, further complicating SWE retrieval algorithms (Duguay et al., 2005).

3.3 Study Area

Snow course surveys were conducted over three major lake systems (Sitidgi, Husky, and Lakes A and B) adjacent to the Mackenzie River Delta, approximately 45 km northeast of Inuvik, Northwest Territories (NWT) (Figure 3-1). The area is characterized by a tundra landscape, set in the transition zone between the boreal forest and shrub vegetation (Marsh et al., 2008). The climate is characterized by cold winters and short mild summers, with a low amount of annual precipitation predominantly falling as snow. Based on Inuvik's 1971 – 2000 climate normal retrieved from the National Climate Data and Information Archive <http://www.climate.weatheroffice.ec.gc.ca>, average temperatures from October to May (ranging from 0° to -30° C) are sufficient for lake ice formation, with peak snow depths observed between February and April.

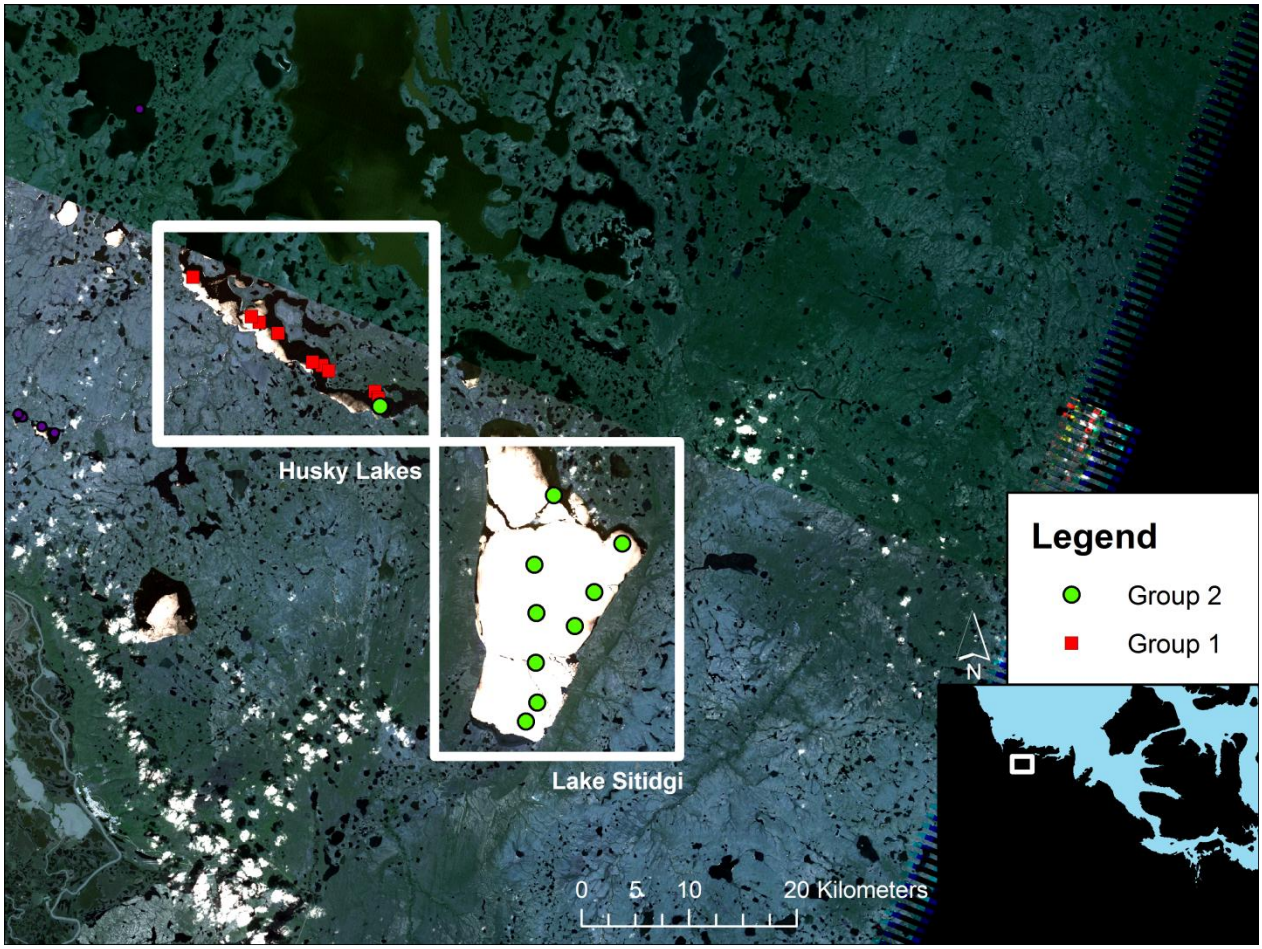

Figure 3-1: Extent of study area, northeast of Inuvik, Northwest Territories, Canada.

3.4 Data and Methods

The measurement of in situ snow and lake ice properties at 38 sample points was conducted along transects from April 6th to 15th, 2008. At each sampling point, 5 ice-auger holes were drilled by establishing a central point and spacing 4 auger holes 15 metres from the centre at 90° intervals. Lake ice measurements at each auger hole consisted of ice thickness, type (clear, grey/white surface or rafted ice) and bubble inclusion. Snow properties (density, SWE and grain size) were measured at each site, with 30 extra snow depth measurements collected at random throughout the sampling area to account for local scale variability. A snow pit was dug at the central point of each sampling site to assess the stratigraphy and document the type of layers within the snowpack. These snow parameters

were collected to provide ancillary data to brightness temperature variability that cannot otherwise be explained by ice parameters.

Airborne passive microwave measurements were made using dual-polarized radiometers (V, H) at 6.9, 19, 37 and 89 GHz mounted onboard the National Research Council of Canada's Twin Otter aircraft at a 53° incidence angle to simulate incidence angles of spaceborne platforms (Table 2). The airborne radiometers (parameters for the 19 and 37 GHz radiometers used in this study are provided in Table 3-2) were calibrated pre- and post each flight using warm (ambient temperature microwave absorber) and cold (liquid nitrogen) targets. Estimates of inter-calibration receiver drift were made by examining the pre- and post-flight calibration target brightness temperatures. The drift was approximately +/- 2K at 19 and 37 GHz, and +/- 4K at 89 GHz. Uncertainty in the 6.9 GHz measurements was higher (+/- 5K for 6.9H; +/- 10K for 6.9V) due to episodic radio frequency interference at the Inuvik airport, and a reduced gain between the cold and warm point measurements noted at the 6.9V channel. Airborne measurements were collected to provide benchmark microwave emission from pure lake ice footprints (80 x 100 metres) across the region of in situ sampling.

Table 3-2: Summary of flights conducted over study lakes

Flight Date	Flight Name	Lakes Visited	Flight Altitudes
April 8 2008	Tundra Lake Ice Flight	Sitidgi, Husky, Noel Lakes	Low - 916ft
April 8 2008	Trail Valley Creek Flight	Lakes A, B, & Noel	Low - 916ft
April 10 2008	Trail Valley Creek Flight	Lakes A, B, & Noel	Low - 916ft
April 112008	Sitidgi Lake Flight	Sitidgi Lake	Low - 916ft High 9156ft

Using in situ snow and lake ice measurements, microwave emission was simulated using a multiple layer adaptation of the HUT snow emission model, presented by Lemmetyinen et al., (2010). The original model by Pulliainen et al. (1999) described the microwave emission of frozen ground covered by a single layer snowpack, characterized by depth, density, snow grain size, temperature and moisture content. The modification by Lemmetyinen et al. (2010) allows the separation of the previously homogeneous snow layer into an indefinite number of separate planar layers, each characterized by their distinctive parameters. The layers can be described also as a non-scattering layer of clear ice.

For snow layers, the model applies the delta-Eddington approximation to the radiative transfer equation, considering most of the scattered radiation intensity to be concentrated in the forward direction. Then, as described by Pulliainen et al. (1999), the emission of a medium with thickness d_0 can be obtained from:

$$\begin{aligned} T_{SNOW} &= T_0 \frac{\kappa_a}{\kappa_e - q\kappa_s}\left(1 - \frac{1}{L}\right) \\ &= T_{phys} \frac{\kappa_a}{\kappa_e - q\kappa_s}\left(1 - \exp\left(\left(-\kappa_e + q\kappa_s\right)\cdot d_0 \cdot \sec\theta\right)\right) \end{aligned}, \tag{12}$$

where T_{phys} is the physical temperature, $1/L$ is the attenuation, κ_a the absorption coefficient, κ_s the scattering coefficient, κ_e the extinction coefficient, θ the incidence angle off nadir and q an empirical constant defining the total forward scattered incoherent intensity in the snowpack.

The absorption coefficient κ_a is determined from the complex dielectric constant following Mätzler (1987) and Hallikainen et al., (1986). Empirical equations defined by Hallikainen et al (1987) are used to relate the snow extinction coefficient κ_e to frequency and snow grain size. For frequencies 1 to 60 GHz Hallikainen et al. (1986) give

$$\kappa_e = 0.0018 f^{2.8} D_{obs}^2, \tag{13}$$

where f is the frequency in GHz and D_{obs} is the observed scattering particle (snow grain) diameter in millimetres. Equation (13) is the main source of the HUT model's high sensitivity to snow grain size. Optional formulations for (13) have been proposed by Roy et al. (2004). The empirical parameter q in (12) has been defined as $q = 0.96$ for snow, by fitting the HUT model to experimental snow slab emission data (see Pulliainen et al., 1999). For emission from a layer consisting of pure ice, it is assumed that q=1, corresponding to a non-scattering layer. This simplifies eq. (12) to

$$T_{ICE} = T_{phys}\left(1 - \exp\left(\left(-\kappa_a\right)\cdot d_0 \cdot \sec\theta\right)\right). \tag{14}$$

Emission from the medium under the stacked snow (or ice) layers is calculated based on the estimated dielectric constant of the medium and the roughness of its surface. The original model applied an empirical model for rough soil surfaces, derived by Wegmüller and Mätzler (1999). This is not directly applicable to the ice/water interface studied here, so the empirical modifications to Fresnel reflection coefficients proposed by Wegmüller and Mätzler (1999) are replaced by a simple consideration of modifying the coherent reflectivity component. Following Choudhury et al., (1979),

$$\left|r_p\right|^2 = \left|r_{p.Fresnel}\right|^2 \exp\left(-4k^2h^2\cos^2\theta\right), \tag{15}$$

where $r_{p.Fresnel}$ is the Fresnel reflection coefficient for polarization *p*, *k* is the wave number, *h* the height variation (RMS) of the rough surface and θ the incidence angle. This approach is applicable when surface roughness variations are small compared to the wavelength, i.e. incoherent effects from large scale variations in surface height do not arise. The magnitude of the height variations should satisfy $kh<<1$ (Kazumori et al., 2008), where *k* is the wave number. Although (15) was originally derived for ground surfaces, it has been applied also for sea surface emission (e.g. Guissard & Sobieski, 1987). In this study, this is considered applicable as information of large scale variations of the ice/water interface is extremely difficult to obtain, as for example, wave functions derived from wind speed used in ocean science cannot be applied here due to the static situation presented by ice. It should be noted, however, that in the case of severe ice deformation the above equation is insufficient. Furthermore, Ulaby et al., (1982) notes the limited accuracy of (15) in terms of relating the actual value of *h* to variations in reflectivity. However, since *h* is not measured in this case, it can be considered an empirical fitting parameter.

The multiple layer adaptation by Lemmetyinen et al. (2010) takes into account the effect of multiple reflections between layer interfaces following the incoherent approach used in the original model. Transmission, reflection and refraction at each layer interface are calculated following Fresnel's law. The omission of coherent components in multiple reflections introduces a source of error, when layer thicknesses are comparable to the wavelength (see Rees et al., 2010). However, this

does not affect simulations presented in this study as the thickness of all simulated layers far exceed the longest wavelength.

Four runs of the HUT emission model are investigated, whereby modifications are applied to two input parameters: snow grain size and roughness of the ice/water interface. The HUT model is extremely sensitive to fluctuations in snow grain size through (13), such that small variations or overestimation can significantly influence simulated emission. As a result, a logarithmic equation is applied to in situ measurements following Kontu and Pulliainen (2010) that derives effective grain size, minimizing the impact of uncertainty in grain size estimation on the simulations. The model is run separately with measured and effective grain size as inputs for the snow grain size, with two modifications to the ice/water interface for each. The ice/water interface is modeled using two treatments as input: a flat Fresnel coefficient based interface simulating a smooth surface that transmits microwave emission according to Fresnel's law, and a 1mm RMS surface roughness that simulates 1mm height variations, designed to emulate rougher surfaces at the ice/water interface.

3.5 Results

3.5.1 In situ Measurements vs. Airborne Tbs

Ice thickness is expected to correlate positively with low frequency emission (i.e. 6.9 GHz), as Tb is expected to increase with thicker ice as a result of less radiometrically cold water influencing the signal. When examining the Tb at horizontal (H) and vertical (V) polarizations at 19 GHz at all study sites relative to ice thickness, a negative association is noticed. However, there are noticeable groupings within the data at 6.9 and 19 GHz. Figure 3-2 displays the groupings at 19 GHz H within airborne Tbs. The groups are also spatially coherent, with sampling sites within group 1 clustered in the Husky lakes, and those within group 2 in Lakes A, B, and Sitidgi. Data provided by the Department of Fisheries and Oceans (DFO) indicate that backflow of saline water normally infiltrates upriver from the Arctic Ccean into the Husky Lakes via Liverpool Bay throughout the year, with salinity levels diminishing at the outflow point of Sitidgi Lake (Perrin, 2007). All study sites situated within the Husky Lakes exhibited similar associations between ice thickness and brightness temperature except for Husky-9, which was included as an outlier in group 2. According to DFO data collected from 2001-05, salinity concentrations reach zero levels approaching Sitidgi Lake, indicating

that Husky-9 was situated in a transition zone between the brackish (group 1) and fresh water (group 2) groups. Based on Hewison and English (1999), the presence of brine inclusion within ice raises the emissivity of the medium. In the presented results, with the exception of section 5.3, brine inclusions are not considered in the model simulations.

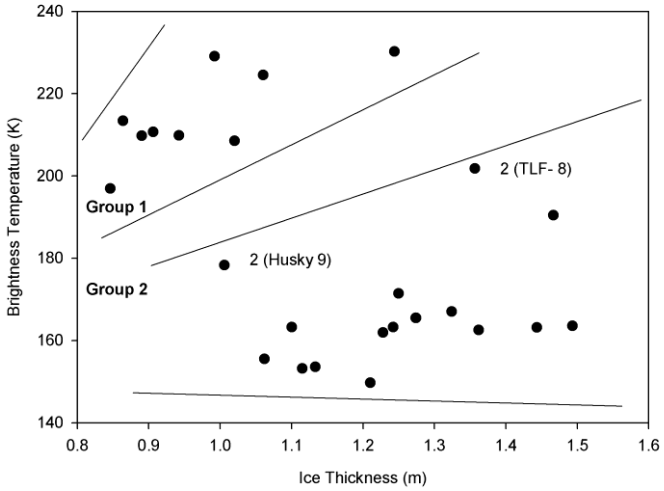

Figure 3-2: Delineation of brackish and freshwater sites by grouping similar 19 GHz H brightness temperature patterns. Husky 9 and TLF 8 are considered outliers due to small concentrations of salinity and ice rafting, respectively.

Based on the two spatially coherent brackish and freshwater groups, fluctuations in airborne measurements relative to snow and lake ice properties are examined. The stratigraphy of the snowpacks at both sites is consistent with high slab-to-hoar and depth hoar fractions noticed in tundra snowpacks over lake ice, as characterized by Sturm and Liston (2003). Site summaries of average snow depth, density, SWE, ice thickness and dominant ice type are presented in Table 3-3.

Table 3-3: Site Summaries of in situ measurements for fresh and brackish water groups

Freshwater

Site	Air Temp (C°)	Avg Snow Depth (cm)	Avg SWE (mm)	Avg Density (g/cm3)	Avg Grain Size (mm)	Avg Ice Thickness (m)	Dominant Ice Type
A-1	-13.4	22	73	0.315	1.6	1.21	Clear with Bubbles
A-2	-13.4	26	78	0.306	1.5	1.13	Grey Surface
B-1	-14.4	38	107	0.279	1.5	1.06	Grey Surface
B-4	-14.4	31	90	0.294	1.5	1.12	White-Grey
Husky-9	-11.0	31	82	0.257	2.5	1.01	Clear Ice
Sitidgi-1	-15.0	29	105	0.355	2.3	1.27	Grey Surface
Sitidgi-2	-15.0	30	93	0.310	2.3	1.24	Variable
Sitidgi-3	-15.0	27	77	0.281	2.3	1.23	Clear Ice
Sitidgi-4	-15.0	35	100	0.284	2.3	1.10	Grey Surface
TLF-01	-7.1	35	105	0.298	1.5	1.47	Rough-Rafted surface
TLF-02	-7.1	25	85	0.335	1.3	1.49	Clear Ice
TLF-03	-7.1	32	111	0.337	1.8	1.25	Rough-Rafted Grey
TLF-04	-7.1	23	68	0.300	2.4	1.44	Clear Ice
TLF-12	-7.1	30	95	0.320	2.4	1.32	Grey Surface
TLF-02.1	-15.0	27	87	0.314	2.3	1.36	Clear Ice

Brackish Water

Site	Air Temp (C°)	Avg Snow Depth (cm)	Avg SWE (mm)	Avg Density (g/cm3)	Avg Grain Size (mm)	Avg Ice Thickness (m)	Dominant Ice Type
Husky-1	-11.0	30	79	0.252	1.5	1.06	Clear Ice
Husky-2	-11.0	37	103	0.271	2.4	1.02	Clear Ice
Husky-3	-11.0	40	117	0.286	3.2	0.89	Clear Ice
Husky-4	-11.0	36	84	0.232	2.7	0.85	Clear Ice
Husky-7	-11.0	36	80	0.225	3.1	0.86	Clear with Bubbles
Husky-8	-11.0	36	91	0.247	2.5	0.91	Grey Surface
TLF-07	-7.1	31	90	0.283	2.4	0.94	Rough-Rafted surface
TLF-08	-7.1	25	84	0.315	2.4	1.36	Clear Ice
TLF-09	-7.1	31	95	0.311	2.4	0.99	Clear Ice
TLF-10	-7.1	21	68	0.322	2.4	1.24	Clear Ice

Sub-site variability of lake ice type was consistent for both brackish and freshwater groups, with approximately 50% of sites containing two distinct ice types, and approximately 20% of sites

containing either one or three ice types. Ice types do not appear to have a distinct effect on microwave emission except for the southern most portion of Sitidgi Lake, where rafted ice at fresh water site TLF-01 (see Figure 3-3) lowered emission at both 19 and 37 GHz. Lowered emission at 19 GHz is likely caused by scattering of the signal by the surface roughness of the ice, while at 37 GHz the influence of large grain sizes was a likely influence.

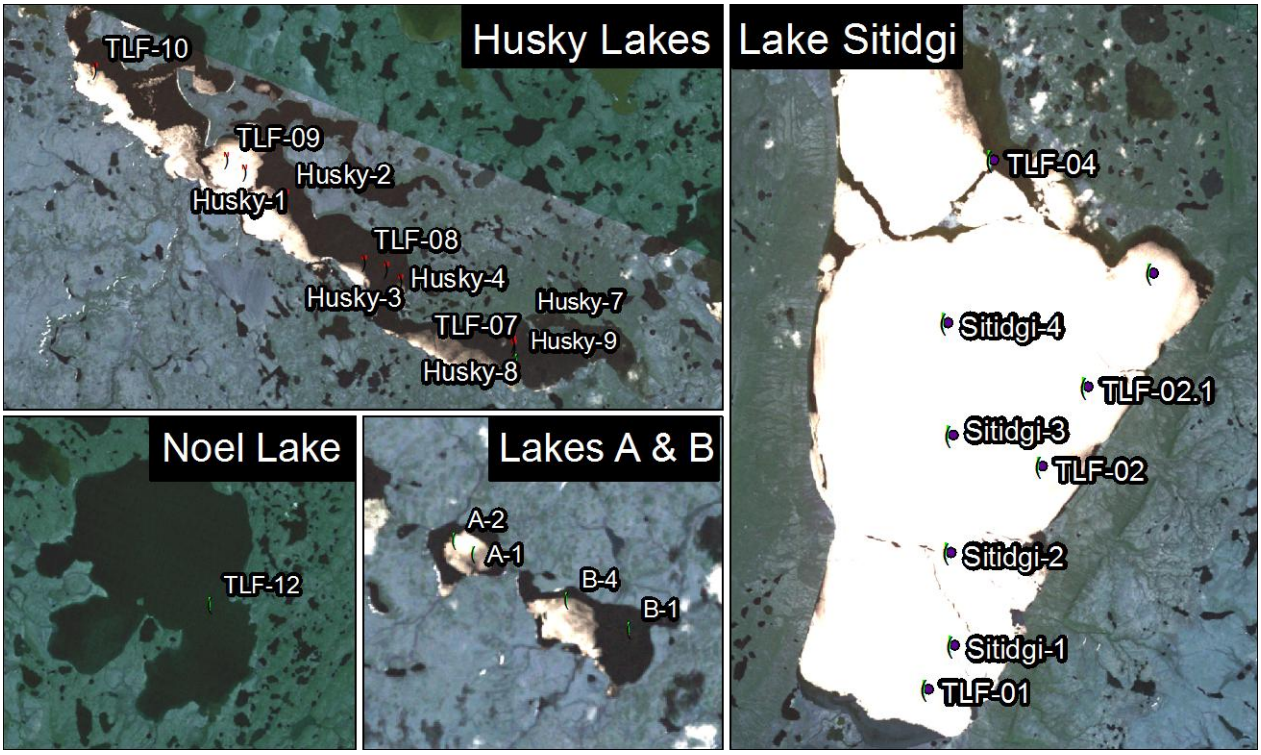

Figure 3-3: Location of survey sites within study area, Inuvik, NWT.

Lake ice thickness measurements exhibit a negative relationship with snow depth in both the brackish and fresh water groups; whereby lower snow depths permit a greater amount of thermal diffusion from the water column during ice development, resulting in thicker ice (not shown). Higher R values exist when consistent ice types are used for both brackish water (clear ice, R = 0.79) and fresh water (gray ice, R = 0.9) instead of all ice types, as processes of variable ice type development influence both ice thickness and snow depth/stratigraphy (Adams, 1976). As a result, both 19 and 37 GHz frequencies over brackish water exhibit negative associations with snow depth, and positive associations with lake ice thickness (not shown). Simulated emission at each survey site do not account for changes in snow stratigraphy or ice type, therefore sites with anomalous airborne emission such as TLF-01 may serve to confound RMSE and the overall agreement of the model.

3.5.2 Simulated Tbs vs. Airborne Measurements

Kontu et al., (2008b) reported satisfactory R values of 0.79 for the 36 – 18.7 GHz horizontally polarized frequency difference when comparing airborne measurements to simulated emission over lake ice. However, the general agreement of single frequencies was not examined. In this study, frequencies that are scattered by either snow or ice are examined separately to assess the efficacy of the modified HUT snow emission model for SWE retrieval. Model input values are derived for each sites from Table 3. Remaining parameters, which were not measured, are listed in Table 3-4.

.

Table 3-4: Constant values used in simulations for all target areas.

Parameter	Value
Ice density	0.916 g/cm^3
Snow moisture	0 %
Temperature of ice	-5 °C
Temperature of water	0 °C
Water salinity	0 (30*) psu
Ice salinity	0 (30*) psu

(*) parameters for brackish water sites in section 3.5.3

Table 3-5 shows RMS errors of brightness temperature simulations over brackish and fresh water lakes. RMS errors at 19 and 37 GHz at H and V polarizations are markedly lower when effective grain size is used as input, regardless of brackish or freshwater ice groups. The HUT model is very sensitive to fluctuations in grain size, often over-simulating scatter if an effective grain size equation is not applied to minimize variability. RMS errors for 37 GHz exhibit the greatest improvement when effective grain size is utilized, and fluctuate little when either of the ice/water surface roughness treatments are applied because emission at 37 GHz is not influenced by the ice/water interface (Table 3-1). RMS errors at 89 GHz also exhibit improvements similar to 37 GHz when effective grain size is utilized because both frequencies are sensitive to emission from above the ice/water interface, restricting signal interaction to the surface of the snowpack.

Table 3-5: RMSE (bold) and MBE (italics) for simulations relative to airborne measurements (K).

Group 1- Brackish Water	Horizontal Polarization				Vertical Polarization			
	6.9GHz	19GHz	37GHz	89GHz	6.9GHz	19GHz	37GHz	89GHz
Measured Grain Size/ 1mm RMS Surface Roughness	**67.55**	**40.62**	**21.15**	**22.66**	**75.48**	**45.68**	**22.17**	**28.05**
	-64.11	*-36.25*	*-18.24*	*12.55*	*-72.43*	*-41.56*	*-19.00*	*-19.58*
Effective Grain Size/ 1mm RMS Surface Roughness	**51.48**	**5.67**	**10.54**	**57.54**	**57.18**	**6.15**	**10.55**	**67.14**
	-48.65	*-2.46*	*-8.51*	*-57.05*	*-54.97*	*-4.53*	*-8.45*	*-66.63*
Measured Grain Size/ Fresnel Flat Surface	**77.22**	**56.95**	**22.90**	**22.66**	**84.71**	**61.22**	**23.74**	**28.05**
	-74.32	*-54.01*	*-20.10*	*-12.55*	*-82.08*	*-58.35*	*-20.67*	*-19.58*
Effective Grain Size/ Fresnel Flat Surface	**38.88**	**24.71**	**12.37**	**57.54**	**91.79**	**25.39**	**12.18**	**67.14**
	-59.96	*-23.74*	*-10.51*	*-57.05*	*-65.67*	*-24.79*	*-10.25*	*-66.63*
Group 2- Fresh water								
Measured Grain Size/ 1mm RMS Surface Roughness	**18.47**	**16.70**	**17.19**	**40.99**	**27.44**	**20.59**	**17.27**	**46.37**
	-13.35	*-9.46*	*-14.57*	*-22.40*	*-14.03*	*-12.34*	*-14.56*	*-28.94*
Effective Grain Size/ 1mm RMS Surface Roughness	**10.53**	**9.66**	**11.87**	**53.72**	**18.87**	**7.89**	**11.96**	**62.16**
	-5.37	*8.36*	*-9.27*	*-53.07*	*-5.09*	*7.12*	*-8.82*	*-61.50*
Measured Grain Size/ Fresnel Flat Surface	**26.89**	**29.30**	**18.25**	**40.99**	**33.34**	**32.19**	**18.22**	**46.37**
	-23.85	*-25.99*	*-15.66*	*-22.40*	*-23.96*	*-28.01*	*-15.54*	*-28.94*
Effective Grain Size/ Fresnel Flat Surface	**18.72**	**11.66**	**12.91**	**53.72**	**23.85**	**11.17**	**12.85**	**62.16**
	-16.40	*-9.65*	*-10.41*	*-53.07*	*-15.53*	*-10.03*	*-9.84*	*-61.50*

6.9 GHz

With average in situ air temperatures on the order of -12°C and ice thicknesses ranging from 0.85 to 1.5m during the measurement period, microwaves at 6.9 and 19 GHz are emitted from depths sufficient to interact with ice and water (Surdyk 2002). Based on the 6.9 GHz RMS errors listed in Table 3-5, the 1mm RMS surface best approximates measured Tbs. Figure 3-4 illustrates improved model agreement when using a 1mm RMS surface at the ice/water interface for brackish and

freshwater sites (RMSE = 51.48K and 10.53K respectively), however, the magnitude of RMSE noticed at brackish water sites is still very high. MBE values also indicate that model runs using a surface roughness of 1mm RMS at the ice/water interface produce the most optimized results at 6.9 GHz. Table 3-5 displays low MBE for 6.9 GHz when utilizing a 1mm RMS treatment for fresh water sites (5.37 K).

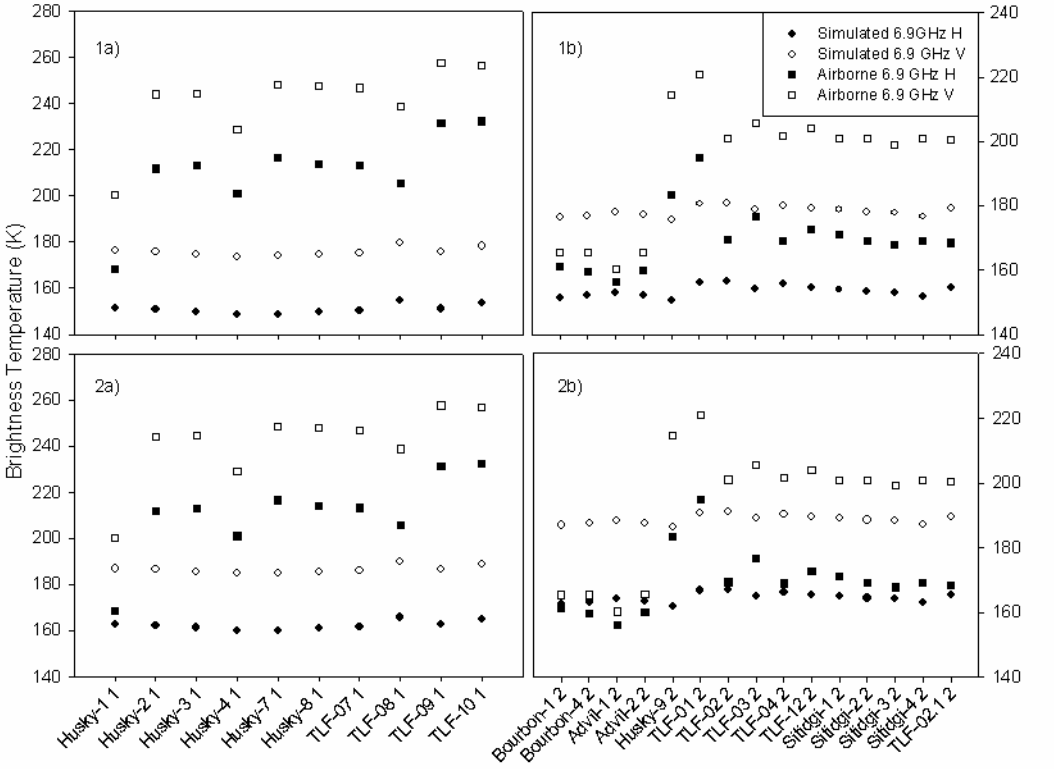

Figure 3-4: 6.9 GHz airborne and simulated brightness temperatures for: (1) Flat scattering surface and (2) 1mm RMS surface for (a) brackish and (b) fresh water groups.

As discussed in Hewison and English (1999), ice with brine inclusions has a higher emissivity than freshwater lake ice (*e* = 0.981 and 0.858 at 24 GHz respectively***)***, consistent with higher brightness temperatures noticed over the brackish Husky lakes compared to freshwater sites. Using a 1mm RMS surface simulates a high emissivity for the ice/water interface, resulting in high emission with ranges consistent with brightness temperatures over freshwater ice. Airborne Tbs over brackish water are generally higher possibly because of brine inclusions within the ice and the water underneath, which modify the dielectric constant of water and ice, and thus their microwave emission. These were not

addressed in the model simulations as measured values of the salinity content were not available; Section 3.5.3. presents simulation experiments using an estimated value for the salinity content. The use of a flat surface at the ice/water interface is based on transmission and reflection parameters following Fresnel's law, and consistently underestimates the transmissivity of the ice/water interface, producing a range of Tbs that are lower than the airborne measurements recorded over freshwater ice, consistent with results reported in Lemmetyinen et al., (2008b). Based on Table 3-5, the use of a flat surface that behaves with respect to Fresnel's reflection and refraction coefficients does not simulate realistic Tb variability for this study. From this point forward, all referenced measures of agreement (RMSE, MBE, and R) utilize a 1mm RMS ice/water interface.

Figure 3-4 illustrates that simulated brightness temperatures at 6.9 GHz do not capture the variability of airborne measurements for both groups, as simulated emission exhibits a range on the order of 5 K, whereas airborne measurements range up to 50 K. For wavelengths that only interact with water and ice (6.9 GHz), the modified HUT model simulates Tbs based on three input factors: water temperature, water interface roughness, and ice thickness. The small range of emission simulated by the HUT model indicates that other input factors are required to model emission from the water and ice mediums at 6.9 GHz.

19 GHz

As a result of the model sensitivity to snow grain size at 19 GHz, RMS errors are typically reduced for both the H and V polarizations when using effective grain size to simulate emission. Emission from both ice and snow serve to confound 19 GHz emission estimates, however low RMS errors are noticed when utilizing a 1mm RMS surface at the ice/water interface, consistent with patterns displayed at 6.9 GHz. When a 1mm RMS surface is used to model the ice/water interface, RMSE errors at H and V polarizations are 5.67 K and 6.15 K respectively for brackish water, and 9.66 K and 7.89 K for fresh water (Figure 3-5 & Figure 3-6). Despite having similar RMSE, simulations at 19 GHz for freshwater sites do not approximate Tb variability, with R values of -0.15 for H polarization and 0.01 for V polarization, as shown in Figure 3-6. Simulations for 19 GHz for brackish water sites provides a better agreement, with R values of 0.19 for H polarization and 0.47 for V polarization (shown in Figure 3-5).

37 GHz / 89 GHz

When comparing the 37 and 89 GHz frequencies, simulated emission is highly sensitive to the treatment of snow grain size. The use of measured and effective grain sizes account for a great deal of RMS error variability in the 37 and 89 GHz frequencies, although manipulation of the ice/water interface does not. As expected, 89 GHz RMS errors do not fluctuate at all when differing ice/water interfaces are modeled because of a lack of sensitivity at the depth of this interface. The lack of response from the higher frequencies (37, 89 GHz) to modifications at the ice/water interface indicates that the HUT emission model is effective at simulating the general characteristics of microwave emission at these frequencies.

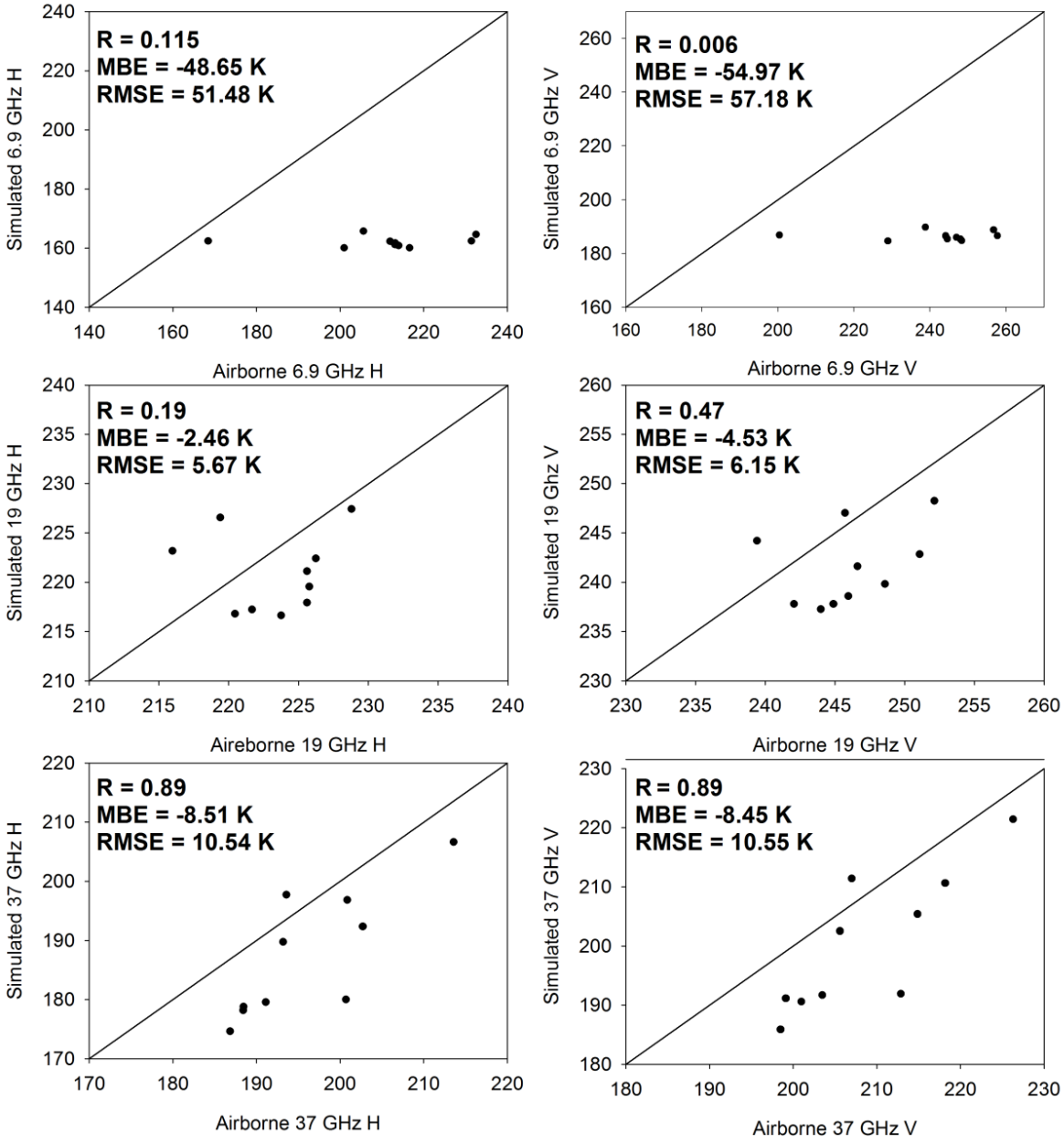

Figure 3-5: Agreement of simulated Tbs relative to airborne measurements over brackish water using effective grain size and a 1mm RMS ice/water interface as input.

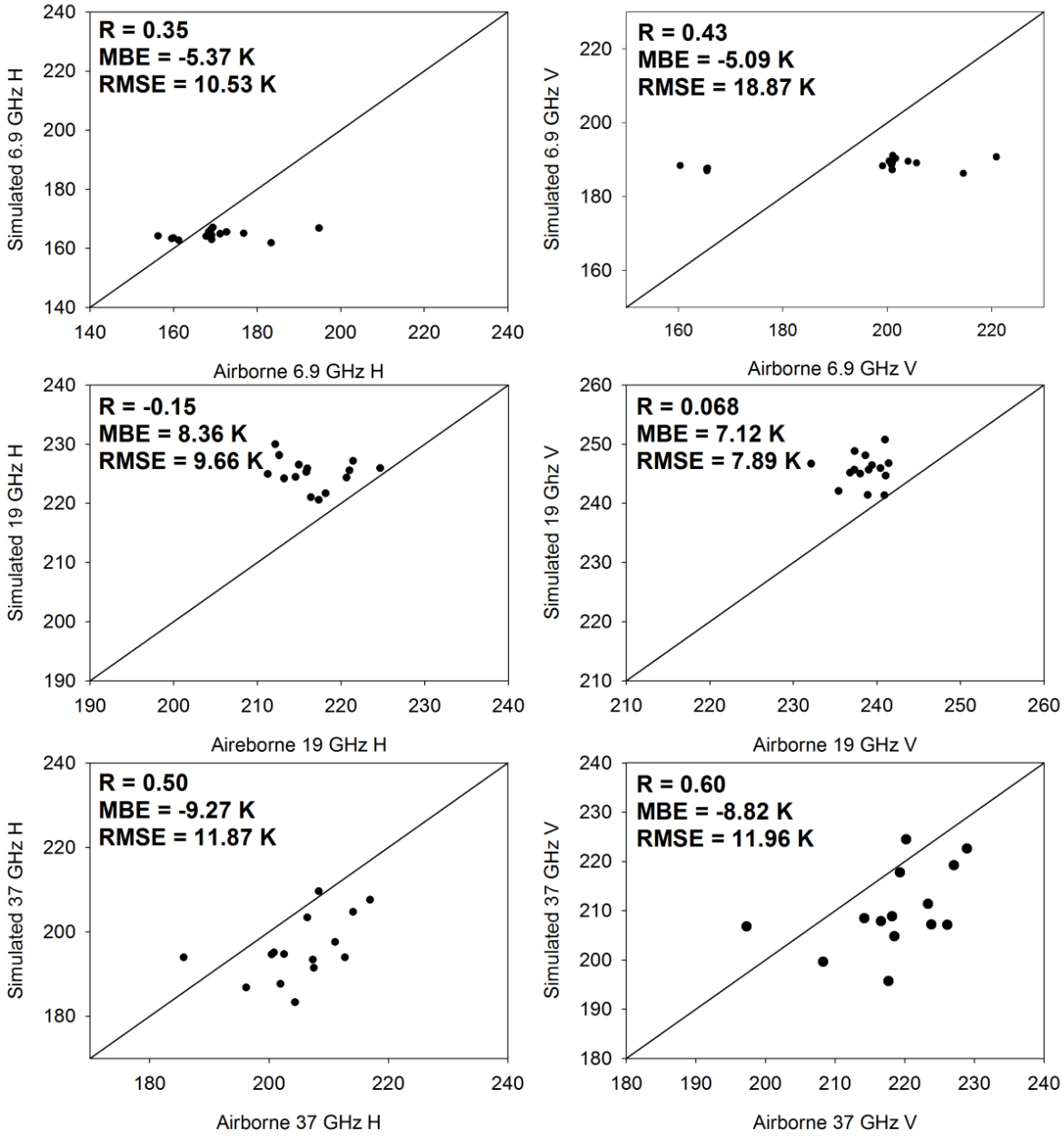

Figure 3-6: Agreement of simulated Tbs relative to airborne measurements over fresh water using effective grain size and a 1mm RMS interface as input.

3.5.3 Salinity Simulations vs. Airborne Measurements

RMSE, MBE and R values reported at 6.9 GHz for brackish sites in Table 3-6 indicate that an underestimation of airborne Tbs is occurring because of added emission caused by the inclusion of brackish water in both the water and ice media. RMSE and MBE values for 19 and 37 GHz H/V in the same simulation run (Effective Grain Size/1mm RMS, Table 3-6) indicates that the low agreement at 6.9GHz is the cause of a parameter that does not affect high frequencies, such as the inclusion of free water beneath the ice/water interface. The dielectric constant of saline water is calculated following Klein & Swift (1977) and Stogryn (1971). The salinity value for the brackish water sites was not measured; therefore, an arbitrary value of 30 ppt (parts per thousand) is used here for the water and ice media simulations at brackish water sites. The snow on top of the ice was not considered to include any residual brine.

Salinity considerations affect wavelengths that are emitted from depths at or below the ice/water interface (i.e. 6.9, 19 GHz). For 6.9 GHz H and V polarizations, the RMSE improves from 51.48 K and 57.18 K when utilizing effective grain size and a 1mm RMS surface to 26.2 K and 31.57 K respectively, as reported in Table 3-6. The addition of salinity did not improve 19 GHz RMSE or MBE, and had little to no effect on 37 and 89 GHz simulations.

Table 3-6: RMSE (bold) and MBE (italics) for simulations with salinity considerations (K)

	Horizontal Polarization				**Vertical Polarization**			
Group 1 - Brackish Water	**6.9GHz**	**19GHz**	**37GHz**	**89GHz**	**6.9GHz**	**19GHz**	**37GHz**	**89GHz**
Effective Grain Size/ 1mm RMS / 30 ppt Salinity	**26.20** *-16.40*	**8.57** *-9.65*	**10.97** *-10.41*	**57.54** *-53.07*	**31.57** *-15.53*	**6.00** *-10.03*	**11.02** *-9.84*	**67.14** *-61.50*

Despite the improved RMSE and MBE reported by 6.9 GHz, the simulation only improves the general magnitude of Tb, as displayed in Figure 3-7. Similar to previous model runs, the addition of salinity into the model simulates a variability of 5 K, while airborne Tbs have a variability on the order of 50 K. Therefore, 6.9 GHz exhibits poor R values of -0.04 and -0.02 for H and V polarizations, respectively. As overall trends in 19 and 37 GHz did not change with consideration of salinity, they are not shown.

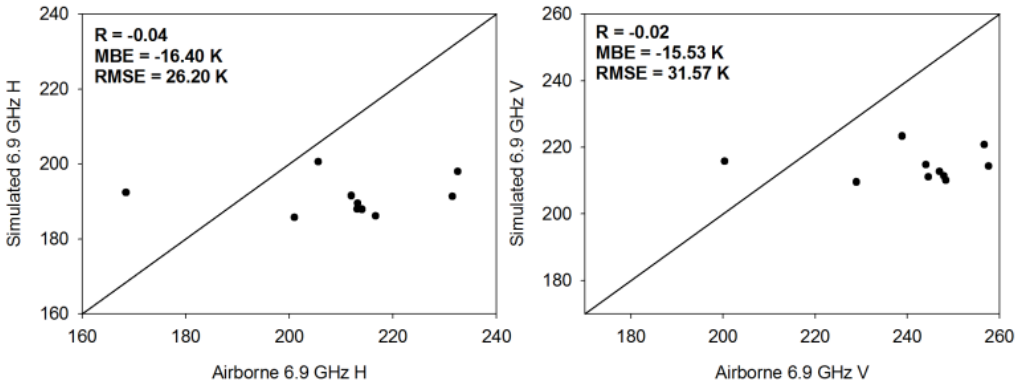

Figure 3-7: Agreement of 6.9 GHz simulated Tbs with salinity added relative to airborne Tbs over brackish water.

3.6 Discussion

Both brackish and fresh water simulations exhibit RMS errors below 10 K at 19 GHz; however freshwater simulations only emulate the general magnitude of measured Tbs. Fresh water simulations were clustered and overestimated brightness temperatures compared to airborne measurements, and may have been caused by an anomalous negative association noticed between 19 GHz airborne measurements and ice thickness depicted in Figure 8. Note that thicker ice lowers brightness temperatures (a), as opposed to simulated emission that have the expected relationship with ice thickness (b) (Kang et al., 2010). The inclusion of scattering interfaces in the ice medium (cracks, fractures, bubbles, grey/white ice) observed in the field, but not currently incorporated into the HUT model have been identified as a source of signal attenuation and scatter in synthetic aperture radar (SAR) investigations (Liston and Hall, 1995). These factors have also been suggested as a possible source of scatter for emitted microwaves (Hall et al., 1981), and provide a plausible explanation for the negative association observed in Figure 3-8.

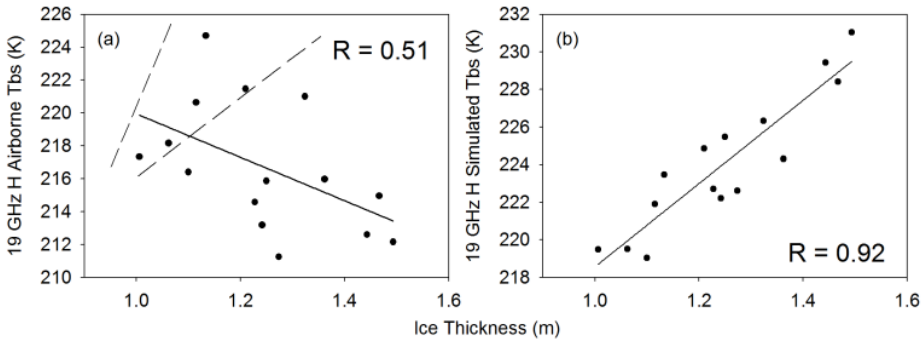

Figure 3-8: (a) Airborne 19 GHz measurements exhibit a negative association with ice thickness, differing from expected relationships exhibited in (b) simulated 19 GHz H Tbs. A grouping of sites on Lakes A and B (a) delineated by dashed lines appear to exhibit a positive association with ice thickness.

Examinations of various ice types (white, grey ice) and their effects on microwave emission yielded no cohesive relationship with measured 6.9 or 19 GHz Tbs (not shown), although there are not enough samples of unique ice types to identify significant microwave emission patterns. The substantial heterogeneity of ice types within the freshwater group (Table 3) indicates that emission from a combination of ice types could produce variable Tb characteristics, not encompassed within the framework of the presented HUT model, affecting emission that interacts with the ice medium (6.9, 19, 37 GHz).

Another factor that could have contributed to anomalous 19 GHz measurements relative to ice thickness is the inclusion of survey sites located on Lakes A and B into the freshwater group. Salinity measurements conducted by the DFO did not include survey sites on either of Lakes A or B, restricting their classification in this study to the fresh water group. Figure 3-8 displays the grouping of these sites along with a Husky Lake site (Husky 9) located in the transition zone between brackish and fresh water, exhibiting a possible positive association with ice thickness. However, the sample size of Lakes A and B is too small to conclude that they should form their own group.

Salinity considerations improved 6.9 GHz RMSE and MBE appreciably for brackish water sites, although did not improve RMSE or MBE values at 19, 37 or 89 GHz. All simulations of 6.9 GHz Tb exhibited poor estimation of airborne Tb variability, indicating that there are other factors controlling

microwave emission at 6.9 GHz. Deformation features, ice type, and bubble inclusions at the ice/water interface all have the potential to cause scatter, and were not considered in this study.

3.7 Conclusion

This study assessed the ability of a modified version of the HUT snow emission model for snow on lake ice to simulate brightness temperatures at 6.9, 19, 37 and 89 GHz frequencies. The ability to simulate Tbs in lake rich environments is important for the development and refinement of SWE retrievals at the satellite scale. Incorporating effective grain size and a 1mm RMS ice/water interface provided the lowest RMSE for the 6.9, 19 and 37 GHz frequencies for both brackish and freshwater survey sites, with brackish water sites requiring a salinity inclusion modification at 6.9 GHz. Based on the relatively poor R values of the model at 6.9 and 19 GHz, it is possible that input parameters used by the modified HUT model may not be adequate to simulate emission from lake ice at those frequencies for the lakes investigated. Within-site variability of lake ice types was prominent in the in situ measurements of both brackish and fresh water groups, with approximately 70% of sites exhibiting at least 2 different ice types with the local sampling area. Therefore, airborne radiometers with a spatial resolution of 80 x 100 m can produce mixed pixels regarding ice type, complicating brightness temperature measurements. The inclusion of input parameters such as average ice type, stratigraphy and salinity measurements across the simulated footprint could aid in further understanding emission patterns of lake ice, as consistent overestimation of emission at 19 GHz could indicate that a source of either enhanced emission or scatter has not been addressed.

The simulation of 37 GHz Tbs at H and V polarizations produced relatively low RMS errors (10.54 and 10.55 respectively) and high R values (0.89 and 0.89 respectively). During the period of maximum seasonal snow accumulation, the ice/water interface did not greatly influence emission, causing the emission dynamics to controlled by snow grain size and depth, similar to land-based snow at this frequency. Further testing of the presented HUT model for the incorporation of subsurface ice and water media should be applied to in situ measurements in the beginning or middle of the winter season, when snow parameters are such that 37 GHz emission can emanate from beneath the ice/water interface.

Despite the effective simulation of 37 GHz Tb over lake ice, errors in 19 GHz Tb simulations restrict the model's use for historical SWE algorithms because most algorithms utilize 19 GHz as a non-scattering frequency channel. However, Derksen et al., (in press) has demonstrated a single frequency, 37 GHz Tb evolution algorithm for the purpose of SWE monitoring in lake-rich tundra environments, but this approach is limited to the second half of the winter season when ice thickness is sufficient to reduce the influence of sub-ice water at 37 GHz. Based on the relative agreement of the presented HUT model with measured 37 GHz Tbs, simulations can be coupled with evolving 37 GHz Tbs to better comprehend emission dynamics through the water, ice and snow media for the improvement of tundra specific models.

3.8 Acknowledgments

This research was supported by a Government of Canada IPY grant (Variability and Change in the Canadian Cryosphere, Anne Walker, PI) and an NSERC Discovery Grant to C. Duguay. Thanks to Ken Asmus and Walter Strapp (Environment Canada) for support with radiometer measurements and processing, and Arvids Silis and Erin Thompson (Environment Canada) for contributing field measurements.

Chapter 4

Investigating the Influence of Variable Ice Types on Passive and Active Microwave Measurements over Tundra Lakes

OVERVIEW

Dual polarized airborne passive microwave (PM) brightness temperatures (Tbs) at 6.9, 19 and 37 GHz H/V and satellite X-band (9.65 GHz VV/VH) active microwave backscatter measurements were combined with coincident *in situ* measurements of snow and ice characteristics to examine emission/interaction caused by variable ice properties. Algorithms designed to estimate snow water equivalent (SWE) using the common Tb difference approach (37GHz – 19 GHz) continually underestimate *in situ* levels when applied to pure lake ice pixels in the Canadian subarctic. Ice thickness measurements were found to be positively correlated with 19 GHz vertically polarized passive microwave emission (R = 0.67), and negatively with 19 GHz horizontally polarized emission (R = -0.79), indicating that surface conditions at the ice/snow interface are affecting emission. This paper examines the effect of surface ice types on coincident passive and active microwave measurements for free-floating ice in two lakes (Sitidgi, Husky). Ice types are delineated using the SAR segmentation program MAGIC (MAp Guided Ice Classification) using cross-polarized VH TerraSAR-X acquisitions as input. Based on output ice types produced by MAGIC, the relationship between active and passive microwave measurements is examined.

Identified ice classes corresponded well to those measured at coincident *in situ* sampling sites. Emission at 19 GHz H and cross-polarized X-band backscatter (9.65 GHz) exhibit an increase with ice types that presented correspondingly more scattering potential. Clear ice exhibits the lowest return, followed by grey ice which exhibits higher returns as a result of the inclusion of spherical air bubbles. The highest returns are noticed coincident to rafted ice, where there is potential for the presence of dihedral reflectors, and therefore increased scattering potential. Concurrently, transects of dual polarized 6.9 and 19 GHz PM Tbs exhibited a statistically significant positive relationship with cross-polarized active microwave backscatter (VH) over freshwater ice (Sitidgi Lake) with the highest R coefficient noticed in the H pol for 6.9 and 19 GHz emission (R = 0.64 and 0.46 respectively). In brackish water, 6.9 and 19 GHz PM Tbs exhibited a negative relationship as a result of a high concentration of bubbles at the ice/water interface, and the incorporation of lossy brine

pockets into the ice medium. This study identifies congruency between passive and active microwave measurements over lake ice for the purpose of improving SWE retrieval algorithms. Further quantification of passive microwave emission is needed for unique ice types, however it has been established that cross-polarized X-band backscatter can be utilized as *a priori* information for spaceborne PM algorithms, providing information on ice type, characteristics (floating, frozen to bed), and the concentration of bubbles near the ice/water interface.

4.1 Introduction

Seasonal snow in Arctic and sub-Arctic environments represents a significant amount of annual water storage within the hydrological cycle. Monitoring of snow properties, namely snow water equivalent (SWE) is important for both economic and scientific considerations. Economically, snow is a source of sustenance and electricity, providing drinking water to northern communities and fuelling hydroelectric dams, totalling a considerable economic benefit (Brown et al., 2000; Adams et al., 2004). Accurate snow extent and SWE datasets are important components in local and regional climate modeling, and are also a key indicator to be utilized in global climate assessment research (Marshall et al,. 1992; Kelly et al., 2003). An accurate observational SWE monitoring network in high latitudes is of critical importance in time series examinations, as polar regions have been identified as increasingly sensitive to changes in surface air temperature (Serreze and Francis, 2006).

Conventional SWE measurements in high latitude environments are obtained through *in situ* snow course surveys and are adequate to provide snow information locally, but the upscaling of observations to regional scales is biased by the extreme local variability of snow (order of hundreds of metres). Surveys are also generally restricted to populated regions and are intermittent at best, as the collection of snow information is logistically cumbersome in remote regions (Derksen et al., 2003). In Northern Canada, a lack of climate stations also restricts the spatial interpolation of snow information, requiring field campaigns to be conducted for detailed snow analysis in remote tundra or taiga environments (Brown et al., 2000).

Polar orbiting passive microwave (PM) remote sensing measurements are a viable solution to problems inherent with *in situ* data collection in Northern Canada, as it provides continuous daily measurements for large swaths and functions independently from solar radiation. SWE retrieval

algorithms are derived by exploiting the differences between a scattering and non-scattering frequency, commonly 37 and 19 GHz, respectively. Algorithms are based on the theory that microwave emission that propagates through a snowpack are scattered by snow grains that approximate the size of the incident wavelength (37 GHz), thereby producing lower brightness temperatures (Tbs). Longer wavelengths (19 GHz) do not interact with snow grains, and therefore the Tb remains constant (Hall et al., 1978). The frequency difference (i.e. 37 – 19 GHz) is related to the SWE content of a snowpack overlying ground, and is largely independent from the effects of atmospheric interference and physical temperature of the snowpack (Wang and Tedesco, 2007; Rees et al., 2010).

Algorithms have been applied hemispherically utilizing frequency differences (Chang et al., 1987; Kelly et al., 2003; Biancamaria et al., 2008) fare poorly when applied to lake-rich tundra regions, as the emission characteristics of a snowpack overlying lake ice is not explicitly understood. When regional algorithms developed for boreal and open prairie environments are applied to snow on lake ice, they are confounded by the unique emission characteristics exhibited by sub-snow lake ice and water mediums (Derksen et al., 2005; Rees et al., 2006). There are many possible scattering sources inherent in ice underlying snow, however previous studies pertaining to the effect of lake ice on SWE algorithm performance have treated lake-fraction as a homogeneous emitter (Gan, 1996). Studies examining passive microwave emission from Lake Erie, United States have noticed increases in emission with a C-band radiometer (5 GHz) coincident with pressure ridges and rubble fields, presumably caused by an increase in ice thickness. Hall et al. (1981) identified that bubbles within the ice volume can influence emission, dampening low frequency emission emanating from beneath the ice/water interface. Concurrently, increases in 19 GHz Tbs were noticed in areas where ice was frozen to the lake bed, as the emission is not subject to inclusions from radiometrically cold water (Toose, 2007). The influence of variable ice types (white, grey, rafted ice) at the ice/snow interface on Tbs has not yet been quantified because common spaceborne Tbs used in SWE mapping are scaled to the 25 x 25km Equal Area Scaleable Earth (EASE) Grid, and cannot resolve unique ice types on small tundra lakes (Hall et al., 1981; Duguay et al., 2005; Derksen et al., 2009, Derksen et al., 2010). The use of active microwave technology is required to obtain high resolution measurements to achieve *a priori* lake ice information to be utilized in SWE retrieval algorithms.

Synthetic aperture radar (SAR) backscatter measurements possess a much higher spatial resolution compared to spaceborne passive microwave Tbs, and has been demonstrated to interact with both snowpack (Ulaby and Stiles, 1980; Praks et al., 1998) and subsurface ice properties (Weeks et al., 1977, Swift et al., 1980; Duguay et al., 2002). Studies that examined SAR data for SWE retrieval established a positive relationship between backscatter returns at C- and X-band (5.6 and 9.65 GHz respectively) and SWE over terrestrial sites (Ulaby and Stiles, 1980; Praks et al., 1998). This relationship however, has not been reported over lakes, where the similar dielectric constant of the snow and ice medium permit transmission of the signal through the snow/ice interface at these and longer wavelengths. The signal is reflected away from the sensor at the ice/water interface due to the large contrast in dielectrics (ϵ^*~3 for ice / ϵ^*~*80* for water) producing an initial low backscatter for ice with no inclusions. However, if present, any of the following can contribute to volumetric scattering: air bubbles (columnar or spherical), deformation features (cracks, rafts), and sediment inclusions (Weeks et al., 1981; Duguay et al., 2002). SAR has also been used to classify lakes that have frozen to bottom, as the incident wavelength interacts with the soil instead of free water, producing backscatter similar to terrestrial sites (Weeks et al., 1981; Jeffries et al., 1994; Dugay and Lafleur, 2003).

With its high spatial resolution and comparable revisit time to spaceborne radiometers, the incorporation of lake ice information derived from SAR measurements could help quantify the effect of variable lake ice properties on emission characteristics of frequencies commonly utilized in SWE retrieval algorithms. In this study, we present the effects of differential ice types on microwave emission by comparing high resolution airborne passive microwave Tbs to spaceborne X-band SAR backscatter measurements. Ice types are delineated by the segmentation software MAGIC (MAp Guided Ice Classification System) that was originally conceived for sea ice segmentation, utilizing 8-bit SAR imagery as input (Clausi et al., 2010). Based on the output segmentation classes, we demonstrate the effectiveness of using cross-polarized VH SAR measurements for the delineation of ice types at the surface, and co-polarized VV measurements to identify volume scatter within the ice. The added ice property information provided by SAR imagery shows potential to be incorporated into tundra-specific SWE retrieval algorithms as *a priori* information to account for the influence of free-floating lake ice on low frequency (6.9, 19 GHz) Tbs.

4.2 Study Area

This study examines the interaction of both emitted and incident microwaves over two major lake systems (Sitidgi, Husky Lakes) adjacent to the Mackenzie River delta, approximately 45 km northeast of Inuvik Northwest Territories (NWT) (Figure 4-1). The surrounding land is classified as tundra, sparsely vegetated and located between boreal forest and shrub transition zone (Marsh et al., 2008). Climate normals for 1971 – 2000 were retrieved from the National Climate Data and Information Archive http://www.climate.weatheroffice.ec.gc.ca reported by the Inuvik weather station at Mike Zubko Airport. The regional climate normal indicates that average monthly air temperatures from October to May are sufficient for lake ice formation. Maximum snow depth and SWE measurements are reported from February to April by automated MSC weather stations. The Husky lakes exhibit low salinity concentrations ranging from 0.1-0.2% while Sitidgi lake is classified as fresh water (Hardwood and Sparling, 2008). According to bathymetry data provided by the Department of Fisheries and Oceans, the average depth of Husky and Sitidgi lakes were 27.8 and 6.75 metres respectively.

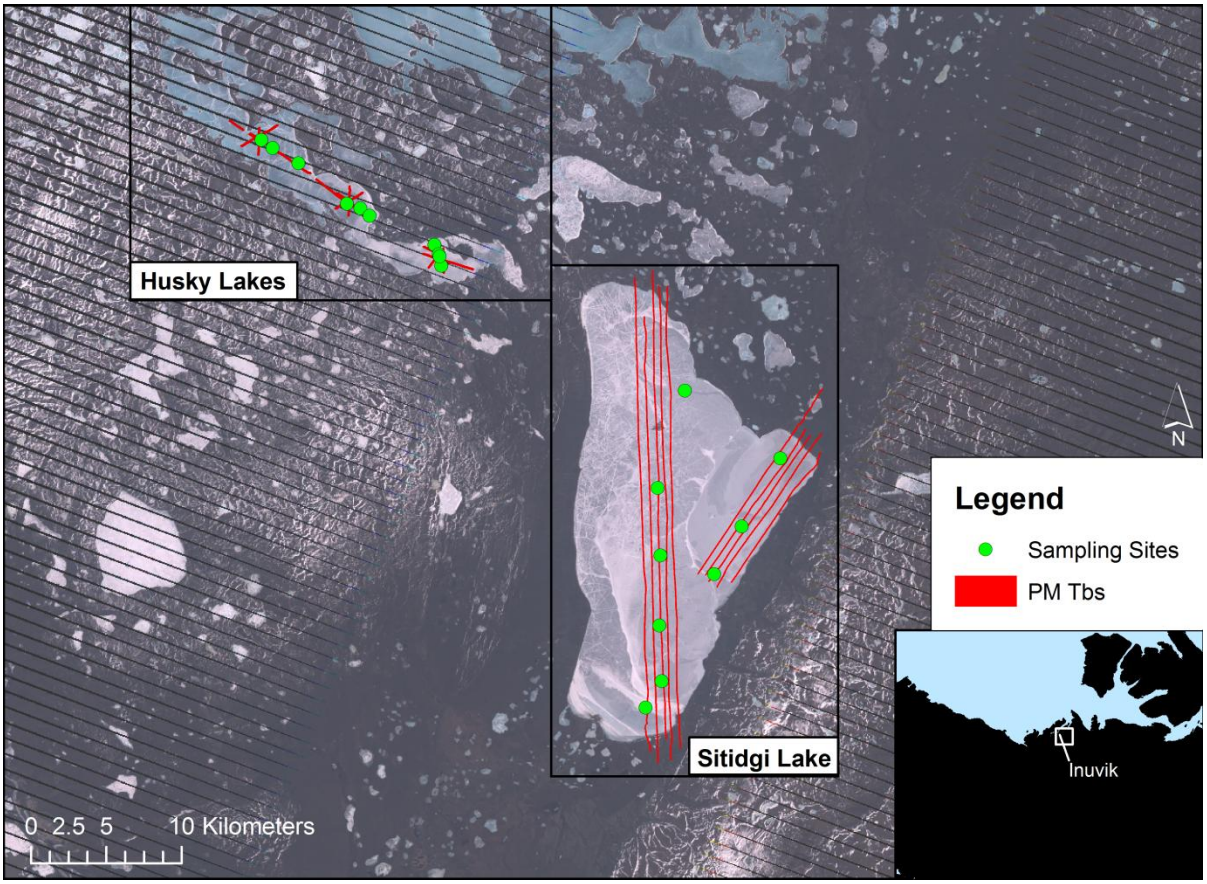

Figure 4-1: Study Site Northeast of Inuvik, NWT (Green circles denote sampling sites/Red transects denote areas of passive microwave airborne Tbs). Background image from Landsat 7 (SLC off), acquired May, 2008.

4.3 Data and Methods

Snow and Ice Cover Data

In situ snow and ice measurements were collected during the period of April 6th to 15th, 2008, with a total of nine sampling sites on Lake Sitidgi, and ten sites on Husky Lakes. At each sampling site a total of five ice type and thickness measurements were made by drilling an auger hole at a central point, and four others at 90° intervals in a 'cross' pattern. Surface ice types were classified as either clear, clear with bubbles, grey, white, or rough/rafted. Snowpack measurements consisting of snow depth, density, SWE, grain size and stratigraphy were conducted at each central point, with 30 extra snow depth measurements collected at random throughout the sampling site. Figure 4-2 and Figure 4-3 display the measured snow stratigraphy and surface ice type for each sampling site used in the

analysis. Snow measurements at each sampling site were collected to be used to examine the effects of variable snowpack properties on low frequency Tbs and backscatter that cannot otherwise be explained by lake ice parameters.

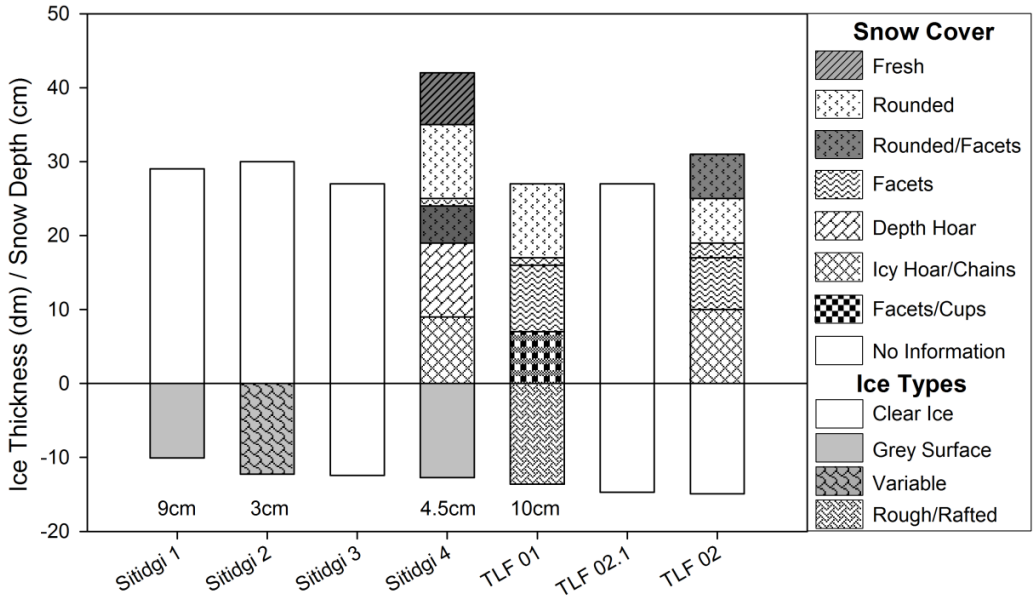

Figure 4-2: Snow stratigraphy and ice surface types for sampling sites on Lake Sitidgi. (Ice thickness measurements are in decimeters (10 dm = 1m)). Numbers above each site label indicate the thickness surface ice type layer.

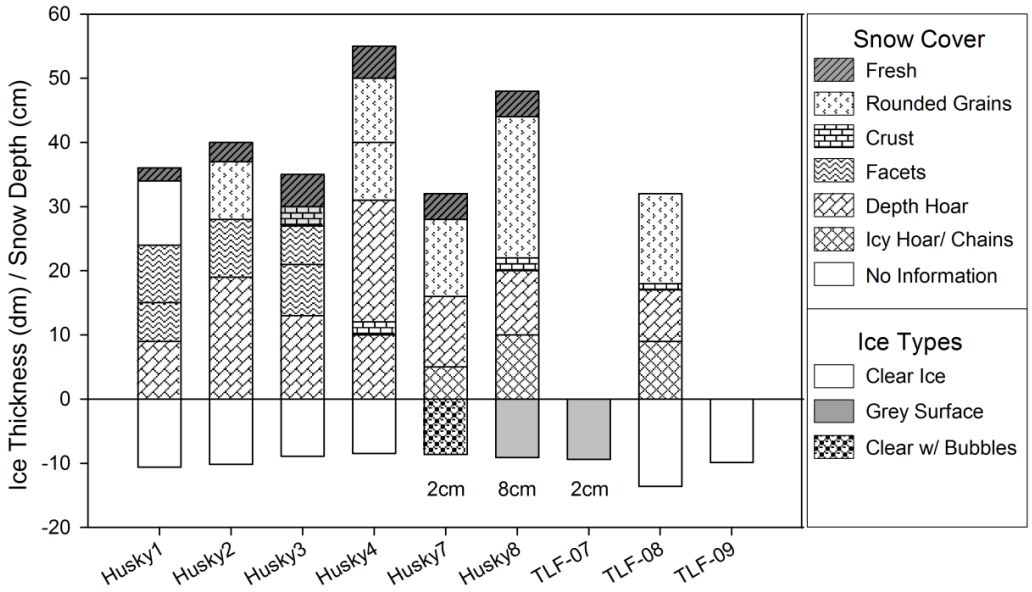

Figure 4-3: Snow stratigraphy and ice surface types for sampling sites on Husky Lakes (Ice thickness measurements in decimetres). Numbers above each site label indicate the thickness of the surface ice type layer.

Airborne Radiometer Data

Airborne passive microwave measurements at 6.9, 19, 37 and 89 GHz were collected using dual polarized radiometers (H,V polarizations) mounted onboard the National Research Council of Canada's Twin Otter aircraft. Tbs were collected on April 8th, 2008 at an altitude of 916 feet and an incidence angle of 53°, producing a high resolution passive microwave footprint of 80 x 100 metres. Calibration of the radiometers occurred pre and post flights using cold (liquid nitrogen) and warm (ambient temperature microwave absorber) targets. The calibration procedure aids in providing approximations of any receiver drift that was experienced during flight. In this dataset, the receiver drift was estimated to be +/- 2K at 19 and 37 GHz, and +/- 4K at 89 GHz. The 6.9 GHz channel receiver drift was higher (+/- 5K for 6.9 H and +/- 10K for 6.9 V) as a result of intermittent radio frequency interference due to radio communication at the Inuvik airport, and a reduced gain between the cold and warm calibration targets. Airborne Tbs were collected in transects over Sitidgi Lake, and in clover patterns on Husky Lakes where designated survey sites had not yet been sampled.

The bearing of each passive microwave Tb was calculated based on the geographic coordinates of the next footprint in each transect, providing the true approximation of the elliptical footprint. Radiometer footprints used to represent *in situ* snow and lake ice measurements are collected by selecting the closest Tb footprint to the sampling site, so long as the site was within 100 metres of the footprint. Any sampling site outside the 100 metre threshold is used as ancillary data, but is not referenced to any passive microwave Tbs. Two transects were extracted for both Husky and Sitidgi Lakes to illustrate Tb variability over lakes, and to quantify relationships present within the passive and active microwave measurements.

Spaceborne Active Microwave Data

Spaceborne X-band (9.6 GHz) active microwave SAR data consists of 2 dual-polarized scenes acquired by TerraSAR-X during the field season campaign, as shown in Table 4-1. Each image has been converted to sigma nought decibels (σ° dB) using a flat Earth assumption as the relief in the Inuvik region is not significant. Each acquisition consists of 2 bands: co-polarized vertical send/vertical return (VV), and cross polarized vertical send/horizontal return (VH). Both images were multi-looked at using a 7x7 window, reducing the spatial resolution of each pixel to 10x10 metres (Figure 4-4). The median of all X-band measurements within the 80 x 100 metre footprint of the

radiometers (n = 80) is appended in the attributes of the radiometer data to reduce the influence of SAR speckle while retaining the overall backscatter pattern present for each PM footprint. Assuming an inclusion-free freshwater ice cover, the penetration depth of an incident microwave is between 100 metres at 1 GHz and 10 metres at 10 GHz (Hallikainen and Winebrenner, 1992). With a maximum ice thickness of approximately 1.5 metres, incident X-band microwaves will interact with the ice/water interface, assuming no absorption occurs.

Table 4-1: TerraSAR-X Satellite Dataset

Lake	Imaging Mode	Date Acquired	Time of Day	Direction
Husky	StripMap	06/04/2008	02:17	Ascending
Sitidgi	StripMap	27/04/2008	15:30	Descending

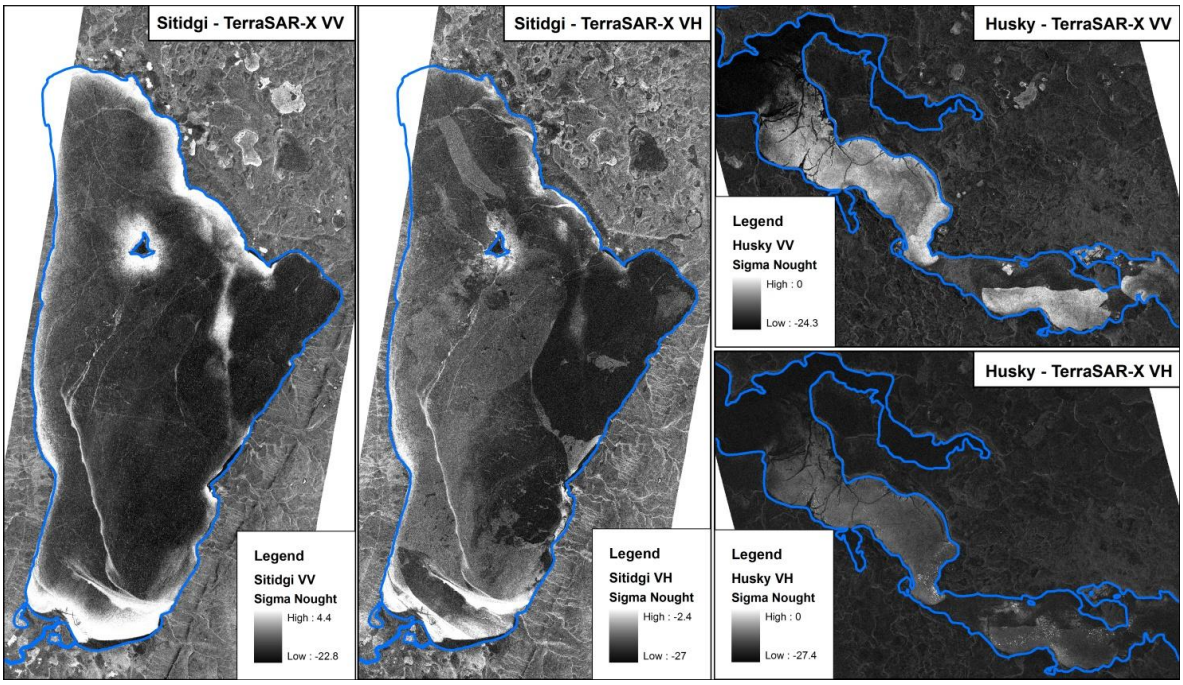

Figure 4-4: Radiometrically calibrated σ° TerraSAR-X images of Sitidgi and Husky Lakes.

4.4 Results

4.4.1 Brackish/Freshwater Site Delineation From Passive Microwave Tbs

As presented in previous studies, Tbs at low microwave frequencies (6.9, 19 GHz) are expected to correlate positively when compared to ice thickness measurements (Hall et al., 1981; Kang et al.,

2010), as less radiometrically cold water is included in emission from below the ice/water interface with continued ice growth. *In situ* measurements collected over Sitidgi and Husky lakes exhibit a negative association when lake ice thickness (averaged for each sampling site) is plotted relative to 6.9 GHz H Tbs. However, there are noticeable groupings within 6.9 GHz, displayed in Figure 4-5. The groups are spatially coherent, with measurements in Group 1 located in the Husky Lakes, and those in Group 2 located in Lake Sitidgi. Data provided by the Department of Fisheries and Oceans indicate that backflow of saline water from the Arctic Ocean infiltrates through Liverpool Bay at a concentration of ~2%, reducing in concentration to 0.1-0.2% in the Husky lakes and diminishing at the outflow of the river connecting Husky to Sitidgi lakes (Hardwood and Sparling, 2008). Based on Hewison and English (1999), the presence of brine inclusions raises the emissivity of the ice medium, thereby raising Tbs for Group 1.

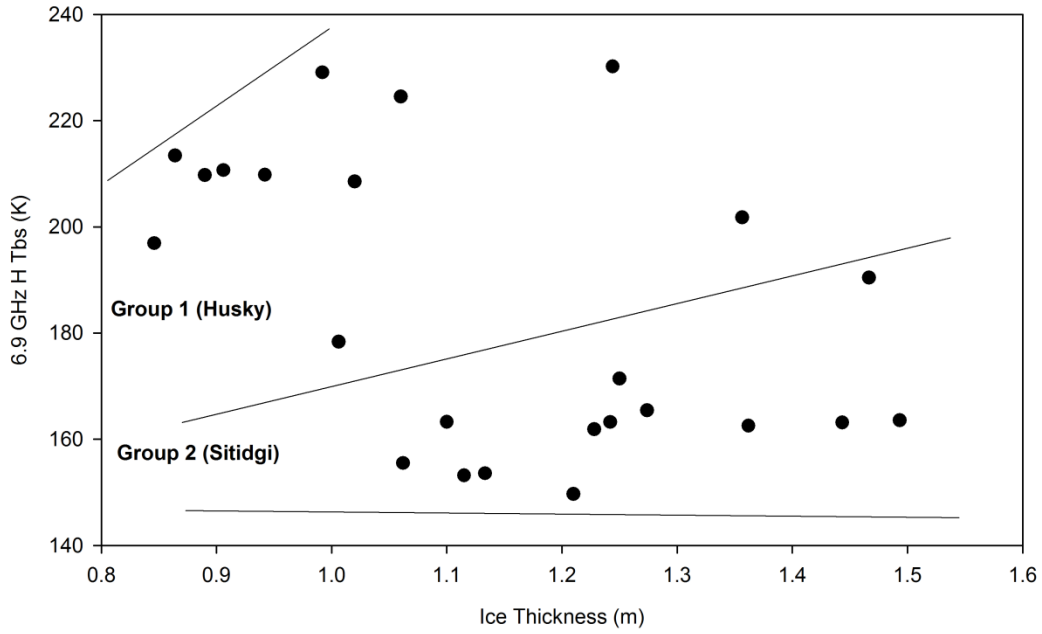

Figure 4-5: Delineation of brackish (Husky) and freshwater (Sitidgi) sites by grouping similar 6.9 GHz H Tb patterns.

Based on the apparent relationship between lake ice thickness and low frequency emission, the *in situ* measurements are examined to determine if there are any patterns between ice or snow properties that can also be explained by the presence of brackish water. Summaries of *in situ* measurements of snow and ice properties at each site is provided in Table 4-2. The depth, SWE and stratigraphy of the

snowpack in both groups appear to be independent of brackish or freshwater, and are consistent with the high slab-to-hoar and depth hoar fractions characterized by tundra snowpacks, as determined by Sturm and Liston (2003). Both brackish and freshwater groups exhibit the same sub-site ice type characteristics, with approximately 31% of sampling sites comprised of one ice type, 56% of sites with two ice types, and 12% with 3 or more. Unique microwave interaction characteristics are expected to be noticed at Site TLF-01 at the southern portion of Sitidgi Lake (Figure 4-1) where thicker than average ice is noticed, but may not contribute to higher Tbs because of the presence of rafted ice.

Table 4-2: Site Summaries of in situ measurements for Fresh and Brackish water groups

Freshwater

Site	Air Temp (C°)	Avg Snow Depth (cm)	Avg SWE (mm)	Avg Density (g/cm3)	Avg Grain Size (mm)	Avg Ice Thickness (m)	Dominant Ice Type
Sitidgi-1	-15.0	29	105	0.355	2.3	1.27	Grey Surface
Sitidgi-2	-15.0	30	93	0.310	2.3	1.24	Variable
Sitidgi-3	-15.0	27	77	0.281	2.3	1.23	Clear Ice
Sitidgi-4	-15.0	35	100	0.284	2.3	1.10	Grey Surface
TLF-01	-7.1	35	105	0.298	1.5	1.47	Rough-Rafted surface
TLF-02	-7.1	25	85	0.335	1.3	1.49	Clear Ice
TLF-02.1	-15.0	27	87	0.314	2.3	1.36	Clear Ice

Brackish Water

Site	Air Temp (C°)	Avg Snow Depth (cm)	Avg SWE (mm)	Avg Density (g/cm3)	Avg Grain Size (mm)	Avg Ice Thickness (m)	Dominant Ice Type
Husky-1	-11.0	30	79	0.252	1.5	1.06	Clear Ice
Husky-2	-11.0	37	103	0.271	2.4	1.02	Clear Ice
Husky-3	-11.0	40	117	0.286	3.2	0.89	Clear Ice
Husky-4	-11.0	36	84	0.232	2.7	0.85	Clear Ice
Husky-7	-11.0	36	80	0.225	3.1	0.86	Clear with Bubbles
Husky-8	-11.0	36	91	0.247	2.5	0.91	Grey Surface
Husky-9	-11.0	31	82	0.257	2.5	1.01	Clear Ice
TLF-07	-7.1	31	90	0.283	2.4	0.94	Grey Surface
TLF-08	-7.1	25	84	0.315	2.4	1.36	Clear Ice
TLF-09	-7.1	31	95	0.311	2.4	0.99	Clear Ice

4.4.2 Ice Type Delineation from Active Microwave Measurements

MAGIC Segmentation

Unique passive microwave emission is noticed in the presence of various ice types (Melloh et al., 1991; Eppler et al., 1992) but has not been quantified coincident with co- or cross-polarized SAR backscatter. Previous studies have utilized SAR measurements for the classification of sea-ice types and concentration. Therefore, the investigation of lake-ice types through the comparison of SAR and PM Tbs is of interest for ice type mapping. Ice types are delineated through the use of the segmentation program MAGIC (Map Guided Image Classification), originally conceived to classify sea ice concentration from egg code polygons provided by the Canadian Ice Service (CIS) (Clausi et al., 2010). The IRGS method (Iterative Region Growing with Semantics) utilized within MAGIC has been previously demonstrated as the state-of-the-art approach to provide unsupervised segmentation of ice types present in co-polarized C-band imagery (Clausi et al., 2010), and was selected to identify ice types present in the TerraSAR-X acquisitions used in this study. Inputs to MAGIC included co- and cross-polarized X-band σ° returns scaled to an 8 bit layer-stacked image (stored in band-interleaved (BIL) format), GCP points extracted from the input imagery, and a text file of polygon nodes to delineate the extent of the lake. The number of classes chosen for each image was based on the number of ice types collected in the *in situ* data. In this case, there were four input ice classes. Figure 4-6 displays the output produced by MAGIC for the cross-polarized image (VH) for Lake Sitidgi. The cross polarized imagery is determined to produce the best approximation of ice types based on the *in situ* measurements, as areas of unique (higher) backscatter on Lake Sitidgi correspond to grey and rafted ice, whereas areas of low backscatter correspond to clear ice (not shown). In the VV image, high backscatter is caused by either rafted ice, or by tubular bubbles near the ice/water interface (Weeks et al., 1977; Duguay et al., 2003). The spatial location of the high backscatter in the co-polarized VV image also indicates that the predominant source of scatter is caused by bubbles at the ice/water interface, as most high-backscatter regions are located close to the shoreline or the island in the centre of Lake Sitidgi, where bubble formation is most likely to occur (Duguay and Lafleur, 2003).

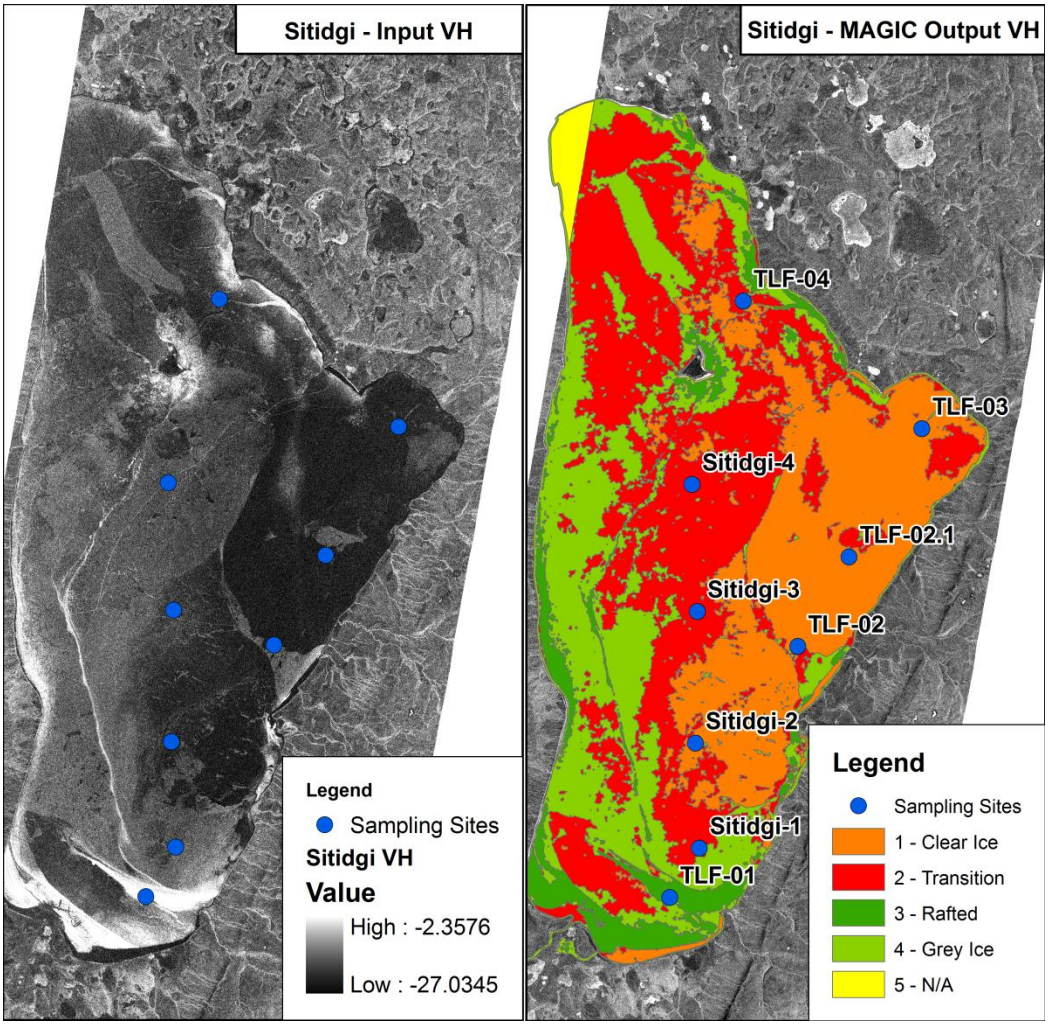

Figure 4-6: MAGIC input (X-band cross-pol VH) and output segmentation classes for Lake Sitidgi.

Lake Sitidgi

Due to the different salinity levels present in Sitidgi and Husky lakes, the agreement between the MAGIC segmentation output and X-band measurements are investigated for each lake individually. Based on the *in situ* data, the number of classes selected for segmentation was four. Each ice type class is categorized based on the *in situ* measurements, thereby creating 4 unique ice type classes on Lake Sitidgi: clear ice, a transition zone between clear and grey ice, grey ice, and rafted ice; each with unique backscatter properties Figure 4-7.

Kolmogorov-Smirnov (K-S) statistics are calculated to determine the probability of two distributions being from the same population, where a *p*- value of 0.00 at a significance level of 0.05 denotes that the null hypothesis (population 1 = population 2) is broken, and the distributions are statistically not the same (Pestman, 1998). The K-S test is applied to the distribution of σ° pixels within single PM footprints that are coincident with sampling sites (Table 4-3). Areas of unexpectedly low p-values exist when comparing Sitidgi-2 with other sites in the clear ice group. Also, unexpectedly high K-S values exist for Sitidgi 1, 3, and 4 when compared to sites in the clear ice group. These discrepancies can be explained by the situation of the sampling sites within ice classes. The variability of ice types within the 80 x 100 metre PM footprint does not capture the local ice conditions of the sampling site. All sites within the "clear ice" group are situated on boundary zones between MAGIC-defined ice type boundaries (Figure 4-6). The method used to classify ice types within MAGIC was the IRGS, where classification is based on the growth of like-valued regions. Therefore, sites at the boundary zones between these regions may have values that are less similar to that class' complete distribution, producing anomalous K-S statistics.

The K-S statistic was also used to test the distributions of the median of all σ° values for each ice type, the distributions of which are displayed in Figure 4-7. The application of the K-S test to each ice class produced *p=0.00* (at a significance of 0.05), indicating that the null hypothesis can be rejected and therefore, the distribution of σ° values for each ice classes are not from the same population.

Table 4-3: K-S Statistics for σ° distributions extracted from PM footprints coincident to sampling sites. The probability value (p-value) is bolded, with the point of occurrence in dB. (Sites are colour coded to match ice types in Figure 5).

	TLF02.1	TLF 02	Sitidgi 2	Sitidgi 1	Sitidgi 3	Sitidgi 4	TLF 01
TLF02.1	1	**0.59** (-22.8)	**0** (-20.1)	**0** (-20)	**0.49** (-20.7)	**0** (-19.7)	**0** N/A
TLF 02	**0.59** (-22.8)	1	**0** (-20)	**0** (-20)	**0.67** (-18.2)	**0** (-20)	**0** (N/A)
Sitidgi 2	**0** (-20.1)	**0** (-20)	1	**0.16** (-19.5)	**0** (-19.4)	**0.07** (-18.7)	**0** (N/A)
Sitidgi 1	**0** (-20)	**0** (-20)	**0.16** (-19.5)	1	**0** (-19.7)	**0.04** (-18.6)	**0** N/A
Sitidgi 3	**0.49** (-20.7)	**0.67** (-18.2)	**0** (-19.4)	**0** (-19.7)	1	**0** (-19.5)	**0** N/A
Sitidgi 4	**0** (-19.7)	**0** (-20)	**0.07** (-18.7)	**0.04** (-18.6)	**0** (-19.5)	1	**0** N/A
TLF 01	**0** N/A	**0** (N/A)	**0** (N/A)	**0** N/A	**0** N/A	**0** N/A	1

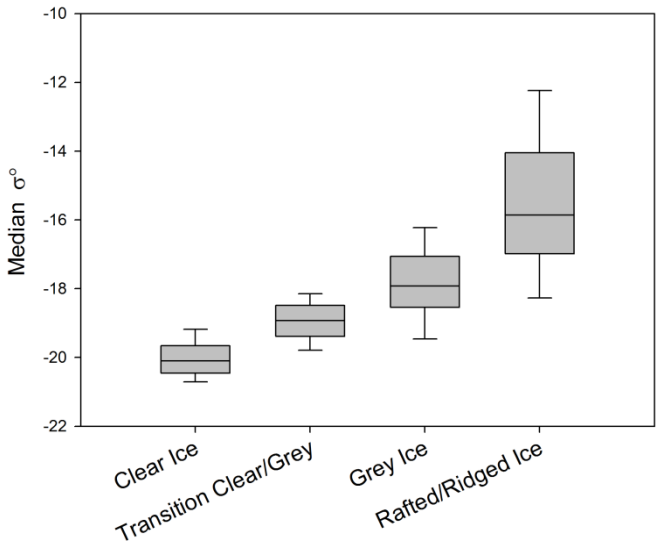

Figure 4-7: Median σ° extracted from all PM footprints relative to MAGIC-defined ice type

4.4.3 Lake Sitidgi – MAGIC Segmentation Analysis

Figure 4-8 displays the MAGIC segmentation output for various ice types in the northeast quadrant of Lake Sitidgi. Two sampling sites (TLF-01 and TLF-02.1) are present within the subset to be used as ground-truth data. Consistent with Figure 4-7, higher backscatter coincident with areas of grey and

rafted ice are classified as such, with areas of low backscatter classified as clear ice. Inherent in SAR images, speckle in areas of clear ice produce a range of values, with outliers sometimes consistent with the distributions of other classes. However, the *region growing* aspect of the IRGS algorithm utilized by MAGIC (Clausi et al., 2010) ensures that outliers are captured within like-groups, while markedly different backscatter caused by variable ice types such as TLF-01 in Figure 4-8 are still segmented accordingly. Output classes are observed to be both spatially (Figure 4-8) and statistically different (Figure 4-7), and have been segmented effectively by MAGIC.

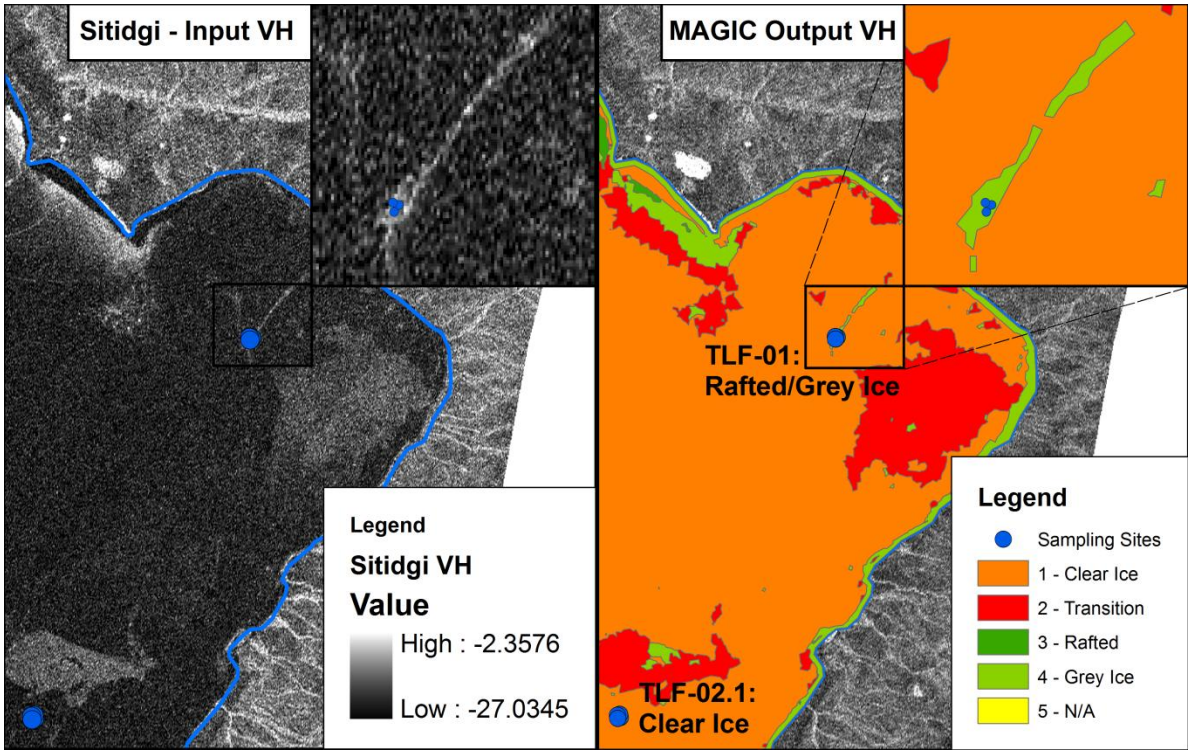

Figure 4-8: MAGIC segmentation for Lake Sitidgi: Areas of clear and rafted/grey ice is captured well by X-band VH measurements, also indicated by *in situ* measurements.

4.4.4 Husky Lakes – MAGIC Segmentation Analysis

Contrasting the straightforward case of lake Sitidgi, the physical characteristics of the ice and sub-ice water present in the Husky Lakes restrict the overall delineation of ice types. Whereas there were many ice types present in Sitidgi Lake and minimal scattering noticed at the ice/water interface, the ice/snow interface at sampling sites in the Husky Lakes is predominantly composed of clear ice, with the exception of sites Husky 8 and TLF-07, situated at the southeast portion of Husky Lakes.

However, the variability of σ° in the Husky Lakes in the cross-polarized (VH) channel is consistent with the co-polarized image (VV), specifically the high backscatter in the central and south half of the southern portion of the images. This indicates that the scattering mechanisms causing high σ° returns in the co-polarized image are also sufficient to cause multiple scattering events and depolarise incident microwaves, consistent with enhanced levels of volume scattering caused by bubbles at the ice/water interface (Woodhouse, 2006). Also, the high backscatter in both the co- and cross-polarized images indicates that even in the event that variable ice types are present in Husky Lakes the majority of the return would be from the bubbles near the ice/water interface, and any scattering caused by ice types may be subsequently lost.

Another interesting feature of the Husky Lakes is caused by the influence of the low-salinity gradient that continually infiltrates from the Arctic Ocean with concentrations of 2% in Liverpool Bay diminishing to 0.2% in Husky Lakes (Hardwood and Spaling, 2008). It is possible that brine inclusions are present within the ice or at the snow/ice interface as a result of slushing events, and can create a higher-loss medium similar in physical properties to first year sea ice. Areas of extremely low backscatter are present in both the northwest portion of Husky Lakes of the co- and cross-polarized acquisitions, indicative of either an inclusion-free ice cover and smooth ice/water interface, or absorption from a lossy medium (Onstott, 1992). It is important to recognize that the backflow of salinity has not been discretely quantified within the 2008 dataset, but generalized by Perrin (2007).

As a result of the confounding factors (high σ° returns due to bubbles at or near the ice/water interface, brine pockets), an accurate assessment of ice types in the Husky lakes is not possible. However, the unique physical characteristics of Husky Lakes provides a broader dataset for comparison with PM emission. Figure 4-9 displays the segmentation provided by MAGIC and proposed ice type classification based on image interpretation.

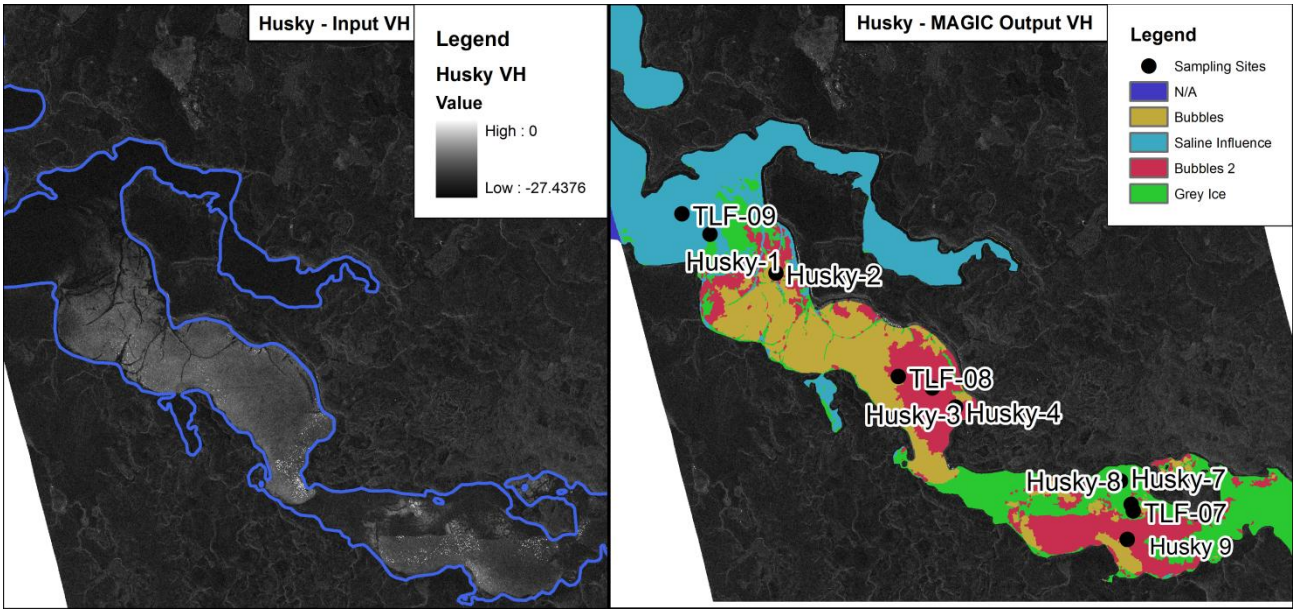

Figure 4-9: MAGIC input (X-band VH) and output segmentation with proposed classes for Husky Lakes.

4.5 Passive / Active Microwave Relationships

Previous work by Hall (1981) and more recently by Kang et al. (2010), demonstrate that low frequency (6.9, 19 GHz) PM emission is dependent on ice thickness, where thicker ice reduces the amount of radiometrically cold water included in the signal, thereby raising Tbs. Based on those results, a correlation analysis is conducted using ice thickness and coincident 6.9 and 19 GHz H/V Tbs. Anomalous emission at site TLF-01 is observed as a result of ice rafting, and therefore is not included in all reported correlation values. The *R* values for 19 GHz V and H when compared to ice thickness are $R = 0.67$ and -0.79, respectively (not shown). While the *R* value for 19 GHz V is consistent with Hall (1981) and Kang et al. (2010), the negative relationship between 19 GHz H and ice thickness is unexpected. It is unclear if variable snow depths or grain size contributed to signal scatter, since there were too few measurements on Lake Sitidgi. However, it is probable that the overlying snowpack is not the cause of reduced emission because 19 GHz V Tbs display the expected positive correlation with ice thickness. Rees et al., (2010) noticed drops in only horizontally polarized emission at various frequencies including 19 GHz when an ice lens is present at or near the top layer of a terrestrial snowpack, indicative that H pol is sensitive to surface characteristics. Snow pit profiles indicate that there are no ice lenses present in the dataset, only snow crusts on some sites in the Husky

lakes. Therefore, the reduced emission at 19 GHz H is tentatively attributed to be caused by the 0 – 15cm layer of variable ice types at the surface layer of the ice, and therefore should possess a relationship with the cross-polarized (VH) X-band measurements.

4.5.1 Sitidgi Lake – Active/Passive Transects

Single transects have been isolated from the PM dataset over Sitidgi Lake to assess the variability of PM emission relative to the lake ice types derived by MAGIC, and the footprints` corresponding radar returns. Figure 4-10 displays the spatial extent of Transect 1 and 2 within Sitidgi Lake, and the sequential emission/backscatter measurements from start point "A" to end point "B". Overall, 19 GHz H Tbs display a positive relationship with cross-polarized (VH) σ° returns. 19 GHz H Tbs also exhibit much more noise than the coincident VH σ° returns as a result of inherent smoothing within the backscatter measurements, as each σ° value is the median of 80 pixels within the passive microwave footprint. Positive associations with X-band σ° are also noticed with 19 GHz V, and both 6.9 GHz H and V polarisations (Table 4-4).

Table 4-4: Spearman Correlation (*R*) values for various frequencies relative to X-band VH σ°. * All are statistically significant at p = 0.01.

	Frequency (GHz)			
	6.9 V	6.9 H	19 V	19 H
Sitidgi Transect 1 (*n* = 468)	0.61*	0.64*	0.28*	0.46*
Sitidgi Transect 2 (*n* = 131)	0.23*	0.32*	0.01*	0.63*

When examining the correlation coefficients for frequencies that most commonly interact with the ice and water mediums, the ice types that are present in each transect is of importance. Figure 4-10 provides a delineation of the MAGIC produced ice types coincident with the passive microwave footprints. Transect 1 contains classes defined as clear ice, the transition zone between clear and grey ice, grey ice near the north end of the transect, and a considerable amount of rafting at the south end. Transect 1 also contains a considerable amount of footprints that exhibit bubbles near the ice/water interface, most noticeably around the island in the northern region of Sitidgi Lake. While footprints with land inclusions were filtered out of the transect, the shallow depths present around the island were sufficient to cause the formation of bubbles near the ice/water interface, producing significant

scatter and subsequent high σ° returns. Transect 2 contains classes defined as clear ice and the clear/grey ice transition zone. Therefore, there is a stark contrast between the high positive correlation coefficient in 6.9 GHz V/H and 19 GHz V noticed in Transect 1 and the low positive correlation in Transect 2. This contrast may be indicative that 6.9 GHz is sensitive to grey ice, rafted ice or bubble inclusions near the ice/water interface, but not extremely sensitive to changes in ice cover noticed in Transect 2 (clear to transition zone). However, 19 GHz H exhibits a moderately strong positive correlation coefficients regardless of Transect 1 or 2, indicating that ice type variability within the transition zone contributes to emission. Overall, 19 GHz H displays the best relationship with freshwater ice types.

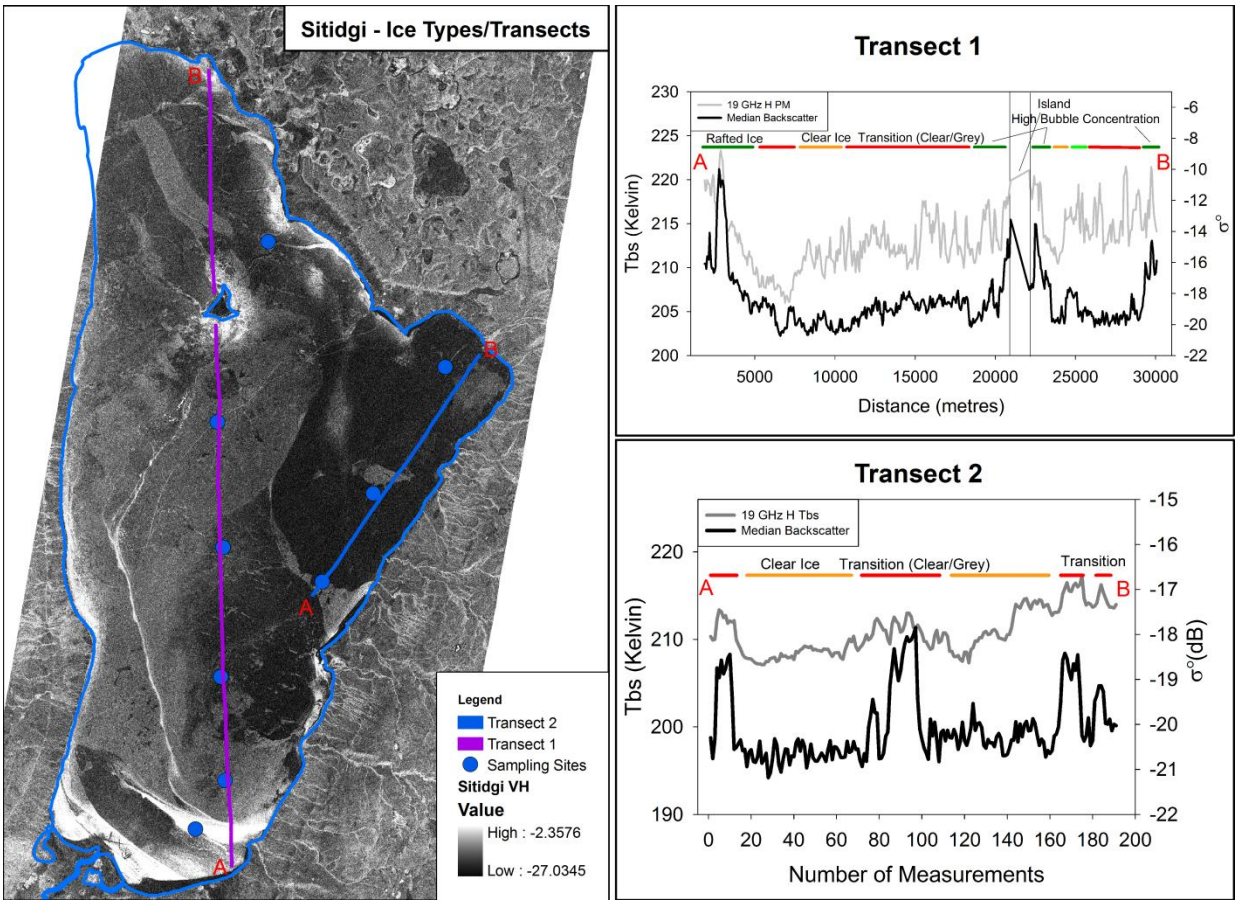

Figure 4-10: Transects of 19 GHz H and X-band backscatter relative to ice types, Sitidgi Lake, NWT.

Ice Type Thresholds

Based on the agreement between 19 GHz H and ice types produced by MAGIC using X-band SAR data as input, the following thresholds were observed for variable ice types (Table 4-5). A great deal of overlap exists between emission of all ice groups; for instance, the Clear/Grey ice transition zone and both the upper limits of the Clear ice group and the lower limits of the Grey Ice group. This overlap is caused by the *region growing* aspect of MAGIC during image segmentation where outlier values are included into spatially exclusive classes, reducing the amount of small isolated classes in the image. However, median Tbs for horizontally polarized frequencies increase together with X-band backscatter, identifying that it is possible to establish thresholds for PM Tbs and σ^{O} returns based on *in situ* ice types.

Table 4-5: Emission statistics for unique ice types based on MAGIC-derived thresholds using X-band σ° as input. Quartiles are defined at 25 and 75% (Percentage of samples when sorted according to emission magnitude).

		6.9 GHz V (K)	6.9 GHz H (K)	19 GHz V (K)	19 GHz H (K)	X-band (dB)
Clear Ice	Quartile (25%)	199.51	167.47	236.46	209.44	-20.46
	Median	**200.58**	**168.81**	**238.59**	**211.38**	**-20.10**
	Quartile (75%)	201.87	170.43	240.29	213.72	-19.66
Transition Clear/Grey	Quartile (25%)	199.29	167.60	235.00	211.00	-19.39
	Median	**200.23**	**168.85**	**236.90**	**212.79**	**-18.92**
	Quartile (75%)	201.14	170.33	238.84	214.97	-18.49
Grey Ice	Quartile (25%)	200.22	169.32	235.64	212.30	-18.53
	Median	**201.68**	**171.49**	**238.67**	**214.36**	**-17.93**
	Quartile (75%)	203.95	174.90	241.14	217.54	-17.06
Rough/ Rafted Ice	Quartile (25%)	202.16	171.39	237.85	214.13	-16.94
	Median	**204.14**	**174.80**	**239.95**	**216.76**	**-15.85**
	Quartile (75%)	210.21	182.51	241.76	219.30	-14.07

4.5.2 Husky Lakes - Active/Passive Transects

Transects extracted from the PM dataset over Husky lakes exhibit different emission and backscatter characteristics compared to Sitidgi Lakes, caused by spatial variations in the physical properties of the ice. Areas of high backscatter are coincident with sampling sites that are classified as “clear ice”, and

areas of low backscatter (such as the north extent of transect 2 (Figure 4-11)) are coincident with "grey ice" classifications. According to patterns present in VH returns over Sitidgi Lake, this indicates that another physical mechanism is controlling backscatter returns from the Husky Lakes. It has previously been identified that a high concentration of elongated bubbles near the ice/water interface can cause scatter of both emitted microwaves (Hall et al., 1981; Eppler et al., 1992) and incident microwaves (Weeks et al., 1978; Weeks et al., 1981; Duguay et al., 2002). Therefore in areas of high bubble concentration a negative association would be expected, whereby increases in backscatter would be coincident with low microwave emission. Table 4-6 indicates that negative correlation coefficients are indeed produced when comparing PM emission to backscatter, and are strongest in 6.9 GHz H/V and 19 GHz V. 19 GHz V is displayed in Figure 4-11 to illustrate PM emission characteristics relative to *in situ* ice properties.

Table 4-6: Spearman Correlation (*R*) values for various frequencies relative to X-band VH σ° over Husky Lake Transects. *Denotes statistical significance at p = 0.01.

	Frequency (GHz)			
	6.9 V	6.9 H	19 V	19 H
Husky Transect 1 (*n* = 157)	-0.56*	-0.73*	-0.56*	-0.56*
Husky Transect 2 (*n* = 41)	-0.84*	-0.82*	-0.54*	-0.34*

Transect 1 covers the spatial extent from the eastern point of the main Husky Lakes channel to the outlet of a larger, more saline lake that connects to Liverpool Bay. *In situ* sampling sites Husky-3, Husky-4 and TLF-08 at the start of Transect 1 are all classified as areas of completely clear ice. High backscatter returns and low PM emission is consistent with the presence of elongated bubbles near the ice/water interface. In the middle of the transect where there are apparent large cracks (Figure 4-11), it is unclear what physical property is controlling the variability in the microwave measurements. The sub-site variability of ice types at Husky-2 (classified as clear ice) contains 3 clear ice, 1 clear ice with bubbles at the surface, and 1 grey ice measurements. When examined closely, the grey ice sampling site is coincident with low backscatter/high PM emission areas, and the clear ice sites are located over areas of high backscatter/low PM emission (not shown). This indicates that possible cracks or leads in the ice could have flooded the area, creating locally variable ice types. In the western-most portion of the transect, it is apparent that the salinity concentrations in the water is sufficient to be included into the ice as small pockets of brine, emulating first year sea ice. The

inclusion of brine pockets into the ice have reciprocal effects on emission and backscatter, as it raises the emissivity of the medium as a whole (and in turn, 19 GHz V Tbs) (Eppler et al., 1992; Hewison and English 1999), but also increases the dielectric loss potential, absorbing incident microwaves and subsequently lowering backscatter returns (Onstott, 1992). Absolute differences as a result of brine inclusions generally increase in PM emission of about 8K, while backscatter returns dropped by approximately 4dB.

Transect 2 also exhibits a clear negative relationship between PM Tbs and σ° returns. However, it does not appear to be the result of brine inclusions. Whereas sampling sites in areas of both high and low backscatter were classified as clear ice in Transect 1, sites in areas of high backscatter in Transect 2 are only classified as clear ice, while those in areas of low backscatter are classified as grey ice. However, ice type classification is still restricted by the higher magnitude of backscatter caused by bubbles near the ice/water interface.

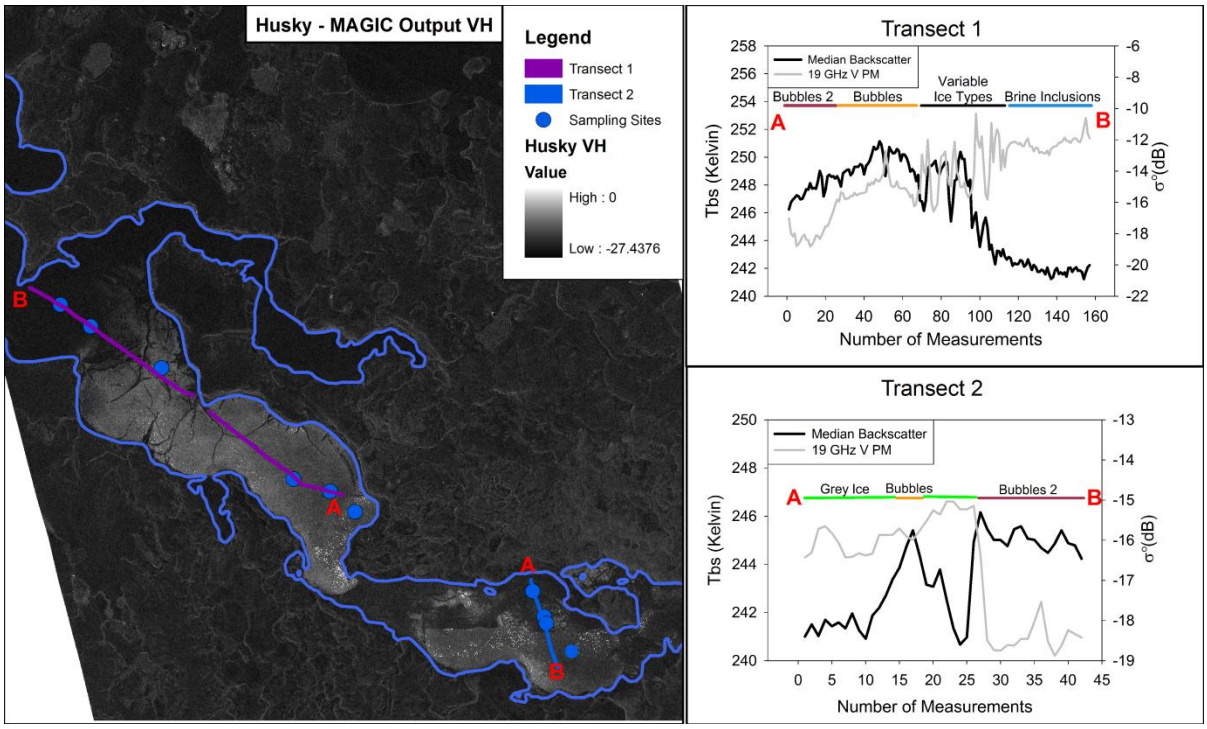

Figure 4-11: Transects of 19 GHz V and X-band backscatter relative to ice properties, Husky Lakes, NWT.

4.5.3 Implications for SWE Retrievals

Classic SWE retrieval algorithms have faltered in tundra environments due to the emission properties of small ponds and lakes that dot the landscape (Derksen et al., 2005; Rees et al., 2006). Free water beneath the ice is radiometrically cold, and therefore reduces emission when the signal begins propagating from a depth below the ice/water interface. In this study, *in situ* ice thickness measurements indicate that the measured 19 GHz H/V includes a portion of emission emanating from below the ice/water interface. The maximum 19 GHz H Tb identified from measurements on the lake was 227.06K, while land produced a maximum of 242.19K. Late winter (April 2008) SWE concentrations are calculated using the Meteorological Service of Canada's "open environment" SWE retrieval algorithm which utilizes 19 and 37 GHZ V (Derksen et al., 2005), and the Chang`s hemispherical SWE algorithm (Chang et al., 1987), which utilizes 18 and 37 GHz H. Both algorithms severely underestimate SWE, with negative values reported for many PM footprints. For example, Sitidgi-3 has the lowest measured SWE (averaged by site for local variability), with 77mm. The MSC-Open environment algorithm had 100% of estimates below 77mm, with only 62% above 0mm. The algorithm provided by Chang et al., (1987) produced higher estimates, with 83% below 77mm, and 94% above 0mm.

The predominant reason for SWE underestimation over lakes is the drop in the non-scattering 19 GHz frequency, affecting the 37/19 GHz frequency difference utilized by both the MSC and Chang algorithms. 19 GHz emission exhibits a positive association with X-band σ° (Table 4-4& Table 4-5). If 19 GHz emission increases, the background frequency in both algorithms rises and becomes more similar to those on land, thereby producing realistic SWE estimates. Table 4-7 displays the rise in SWE estimates for the proposed ice classes, which are consistent with the 19 GHz rises in Table 4-5**.**

Table 4-7: Application of SWE algorithms to late winter airborne PM Tbs relative to ice type classes derived by MAGIC segmentation.

	MSC				Chang			
	Clear (*n*=1705)	Transition (*n* =1834)	Grey (*n*=844)	Raft (n=324)	Clear (*n*=1705)	Transition (*n* =1834)	Grey (*n*=844)	Raft (n=324)
Min	-69.49	-69.49	-46.13	-38.65	-91.73	-91.73	-48.43	-34.56
Mean	**0.05**	**10.32**	**12.82**	**14.67**	**37.16**	**53.11**	**60.83**	**64.25**
Max	93.11	79.64	93.11	69.38	209.62	184.66	209.62	165.65
St. Dev	16.14	15.24	24.72	21.02	29.92	31.68	45.81	38.96

Husky lakes exhibit differential backscatter patterns than lake Sitidgi, caused by a high amount of bubble inclusions near the ice/water interface. Transect 2 in the Husky lakes (Figure 4-11) provides a rough quantification of the effect of bubbles on 19 GHz emission, and illustrate the reason for the sharp Tb fluctuation noticed by other studies when examining microwave emission over lake ice (Hall et al., 1981, Eppler et al., 1992). In Transect 2, 19 GHz V emission coincident with grey ice are approximately 246K, and exhibit a drop of about 6K when coincident with bubbles. The influence of brackish water is evident in the northwest portion of the Husky lakes, causing the divergence of PM Tbs and σ^o from average measurements made over freshwater lake ice. Unfortunately, the increasing level of salinity noticed in Transect 1 and the high concentration of bubbles near the ice water interface in both Transects 1 and 2 perturbs the quantification of the influence of ice types on PM emission. Therefore, the further application of SWE algorithms to PM Tbs over Husky Lakes would not be appropriate, as any divergence or variability is not representative of ice types at the ice surface.

4.6 Conclusion

This study examined the effect of the physical characteristics of lake ice on coincident passive and active microwave measurements to assess the potential of developing operational *a priori* information to be used as input to tundra-specific SWE retrieval algorithms. Results suggest that the segmentation program MAGIC can be used operationally to derive classes based on like-values within regions, while incorporating the consideration of radar artifacts and speckle. MAGIC requires *in situ* measurements pertaining to the amount of ice types present, but does not differentiate between surface and volume scatter. MAGIC outputs for Sitidgi lake provided ouput ice types consistent with the spatial extent of ice types present within the *in situ* samples. The segmentation provided by MAGIC over the Husky Lakes was hindered only because of the similar backscatter noticed in the co- and cross-polarized channels caused by bubbles near the ice/water interface.

Sites on Lake Sitidgi were found to exhibit a positive relationship between ice thickness and 6.9 H/V and 19 GHz V consistent with previous studies (Hall et al., 1981; Kang et al., 2010). 19 GHz H Tbs exhibit a negative relationship with ice thickness, consistent with previous observations that horizontally polarized emission is more sensitive to roughness and deformations at the surface (Rees et al., 2010).

X-band measurements over Sitidgi and Husky Lakes provided contrasting relationships with passive microwave Tbs. For the background frequency most suitable for operational SWE monitoring (19 GHz), X-band measurements exhibit the highest correlation with 19 GHz H over Sitidgi Lake (Transect 1: 0.58, Transect 2: 0.56), and 19 GHz V over Husky lake (Transect 1: – 0.37, Transect 2: -0.63). The contrasting relationships are the result of the variable physical characteristics of the ice at a) ice/snow interface b)ice/water interface and c) sub-ice mediums. According to *in situ* measurements the ice/snow interface in Lake Sitidgi consisted of multiple ice types, while the majority of Husky Lake was classified as clear ice. Fluctuations in both backscatter and Tbs for Husky Lake are likely to be the result of bubble inclusions near the ice/water interface, providing a dominant source of scatter in even the cross-polarized measurements. Increasing salinity concentrations in the northwest Husky Lakes appear to be causing decreases in backscatter and increases in Tbs.

Extremely low and negative estimated SWE values were obtained when using Chang's algorithm and MSC's open environment algorithm, respectively. However, when the algorithm is applied to the MAGIC ice type classes over Lake Sitidgi, incremental increases in SWE are noticed to be coincident with increases in 19 GHz H. Offsets to emission cannot be applied to 19 GHz H to account for the inclusion of free water into the signal because its effect cannot be determined based on one time observations. The evolution of 19 GHz H Tbs coincident with variable ice types must be examined to quantify their effects on microwave emission. Other required inputs should be measurements pertaining to the snow stratigraphy overlying the ice, variability in ice thickness and bubble concentration at the ice/water interface. Future ice type analysis studies should also most likely be conducted in the mid-winter months, before the ice thickness is such that air bubbles are included as potential scatterers.

This study identified relationships between high resolution spaceborne active microwave X-band SAR measurements and high resolution 19 GHz airborne passive microwave measurements when examining ice types over lake ice consisting of multiple ice types. Increases in 19 GHz Tbs are noticed coincident with increases in X-band returns, and with increasing surface interactions (transition zones, grey ice, rafted ice). Understanding the emission characteristics of 19 GHz over

lake ice is of paramount importance to automated SWE retrieval, as low frequency Tb fluctuations are the source of error in common algorithms that utilize the differences in 18/19 and 37 GHz.

4.7 Acknowledgements

This research was supported by a Government of Canada IPY grant (Variability and change in the Canadian Cryosphere, Anne Walker, PI) and an NSERC Discovery Grant to C. Duguay. Thanks to Ken Asmus and Walter Strapp (Environment Canada) for support with radiometer measurements and processing, and Arvids Silis and Erin Thompson (Environment Canada) for contributing field measurements. Our thanks is also extended to Professor Clausi for providing the use of MAGIC for this study and to Shuhrat Ochilov at the University of Waterloo for providing technical support.

Chapter 5
General Conclusions

5.1 Summary

Previous studies investigating the influence of small ponds and lakes on passive microwave SWE retrieval algorithms have been carried out by (Derksen et al., 2003; Derksen et al., 2005; Duguay et al., 2005; Rees et al., 2005; Derksen et al., 2007; Toose, 2007; Derksen et al., 2009), concluding that they faltered due to a combination of factors including the presence of a) variable ice thicknesses, b) bubbles near the ice/water interface, and c) areas of ice frozen to bed. However, their influence on bulk emissivity have not been quantified. Advancements in SWE algorithms are restricted by the large ground-resolution footprint of common spaceborne radiometers, indicating the need for high-resolution data. Active microwave SAR obtains measurements with a small ground footprint, sufficient for inferring ice thickness (Duguay and Lafleur, 2003) and monitoring variable ice characteristics, such as bubble concentration, surface roughness variability (ice type, rafting) and ice frozen to bed (Weeks et al., 1978; Weeks et al., 1981; Swift et al., 1980; Leconte and Klassen, 1991; Kozlenko and Jeffries, 2000; Duguay et al., 2002; Kouraev et al., 2007). This study focused on variable methodologies of assessing the influence of variable ice properties on microwave interaction (emitted from/incident to the medium) through the use of microwave emission models and passive/active microwave observations over Husky and Sitidgi Lakes near Inuvik, NWT. The main objectives in this study as discussed in Section 1.2. were to a) evaluate the efficacy of the HUT snow emission model that was modified to simulate emission from multiple layers (lake ice) [Paper 1, Chapter 3] and b) to evaluate the effect of ice types on microwave emission using the spatial distribution of ice classes derived by the software MAGIC using X-band data as *a priori* information [Paper 2, Chapter 4].

Chapter 3 provided the results of an evaluation of a HUT snow emission model that was modified to include multiple emission and scattering considerations for multiple layers and their corresponding interfaces. As stated in Section 2.1.1., the accurate simulation of PM Tbs is paramount in the formulation of SWE retrieval algorithms, as measured Tbs over lakes are considerably more variable than those on land as a result of inclusions within the ice or variable surface characteristics at the snow/ice interface. Outputs from the HUT model were compared to two ice groups that exhibited unique emission characteristics (brackish and freshwater). The combination of experimental

treatments for physical characteristics of the mediums that produced the best results was the use of a modeled effective grain size (based on *in situ* measurements) and a 1mm RMS surface roughness at the ice/water interface. The best RMSE values were attained using those input parameters for all frequencies, emulating the general magnitude of emission, however did not simulate the pattern of emission well for the 6.9 and 19 GHz H/V frequency channels. Low correlation coefficients indicated that emission patterns for frequencies that are emanated from beneath the ice/water interface were either being modeled incorrectly or there are physical characteristics of the ice that are either dampening or increasing emission. However, simulations at 19 GHz exhibited a high positive correlation when compared to ice thickness ($R = 0.92$) which is consistent with previous studies (Hall et al., 1981), but contradictory to the moderate negative 19 GHz correlation observed at sampling sites. It was therefore assessed that multiple scatter effects caused by the presence of bubble inclusions near the ice/water interface or variable ice types at the surface were the most likely cause of the poor correlation coefficients noticed in the 6.9 and 19 GHz data. Unfortunately, the sub-site variability of ice types (approximately 70% of sites with 2 or more ice types) and the lack of ice cores present in the *in situ* dataset hindered any chance of ruling out either potential source of error. Therefore the effect of lakes on passive microwave emission at 6.9 and 19 GHz cannot be explicitly quantified.

Chapter 4 examined the radiometric effect of variability in the physical characteristics of a lake ice surface, most notably bubble inclusions and ice types. The purpose of the study was to develop a theoretical construct for the production of zones of unique SAR backscatter and passive microwave brightness temperatures that correspond to measured ice types. Providing that X-band backscatter possesses a relationship with 19 GHz passive microwave Tbs, the zones can be used as *a priori* information for the spatial extent of ice type variability over single or multiple lakes. With knowledge of the microwave properties of the lakes within each footprint, fractional considerations can potentially be included into the background frequency (19 GHz) of SWE retrieval algorithms.

X-band backscatter presents contrasting relationships with passive microwave Tbs. X-band exhibits a positive relationship with 19 GHz H over freshwater, and a negative relationship over brackish water. It is noticed that even with low salinity concentrations that brine pockets form in ice; absorbing incident radiation (lowering backscatter) and emitting at a higher magnitude (raising Tbs). A similar inverse relationship is also noticed coincident with a high concentration of bubbles near the ice/water

interface; whereby co- and cross-polarized X-band returns increase and 19 GHz Tbs decrease as both are scattered. Positive relationships between cross-polarized X-band returns and 19 GHz are noticed in areas where there are variable ice types at the surface and few bubbles or inclusions near the ice/water interface.

The spatial extent of ice types based on X-band cross-polarized backscatter correlated well with measured airborne Tbs. The best correlation coefficient existed between ice types and horizontally polarized Tbs, consistent with Grody et al., (1998) and more recently Rees et al., (2010) who noticed that horizontally polarized emission was affected the most by surface characteristics of a snowpack (ice lenses), while the vertically polarized emission was unaffected. Overall, increases in both emission and backscatter were noticed over changes in the following ice types (from low to high): clear ice, transition zone between clear and grey ice, grey ice and finally rafted ice. Previous studies have noticed higher emission coincident with areas of rafted ice or rubble fields (Melloh et al., 1991; Eppler et al., 1992) but have not mentioned grey ice.

5.2 Limitations

There were some limitations for this study, particularly within the *in situ* measurement dataset. Sampling sites and methods were originally designed with the assumption that measurements conducted over Sitidgi and Husky lake could be used in tandem as a distinct sample of snow on lake ice in a tundra environment. However, the unique emission properties of the ice caused by the backflow of salinity, divided the entire sample in two. As a result, the sample size in which all ice thickness, snow depth, stratigraphy, etc, were correlated against radiometric measurements were quite small, and not completely representative of the entire lake. Although from the data available, it appears that all ice types present on the lakes were captured by the *in situ* measurements.

Another limitation present in the *in situ* measurements was the absence of measurements at the ice/water interface, namely salinity and ice core data. According to Perrin (2006), the inflow of salinity into the Husky lakes is continual, and therefore should be monitored as SAR acquisitions over Husky lakes indicate that even low salinity concentrations can affect backscatter return considerably. The absence of ice cores hindered the characterization of the amount of bubble inclusions near the ice/water interface.

Traditionally, lake ice classification has been conducted using a time series of images, whereby the evolution of σ° is tracked, aiding in delineating areas of high bubble concentration or areas that are frozen to bed (Duguay and Lafleur, 2003; Weber et al., 2003; Gauthier et al., 2006). In this study, SAR acquisitions were only available at one time stamp, restricting analysis to a single backscatter range and thereby reducing the confidence in proposing thresholds for variable ice characteristics (inclusion of bubbles, brine pockets, etc). It is also apparent that the robustness of ice type classifications using cross-polarized X-band SAR backscatter may increase when done at the beginning or middle portion of the winter season, as the ice thickness in deeper portions of the lake would not be sufficient for the incorporation of air bubbles.

5.3 Recommendations for Future Work

There is a great potential for future research concerning SWE retrieval over lake ice in tundra environments. There are three main avenues for research that would greatly benefit in the accurate assessment of ice types on microwave interaction, for the purpose of estimating SWE. First, it would be beneficial for a study of this magnitude to take place earlier in the winter season, before the formation of air bubbles within the ice volume as a result of gas-saturated water that would be present late in the season. It is apparent that scattering of microwaves in both active and passive measurements as a result of ice types are muted by the intense amount of scatter caused by bubble inclusions near the ice/water interface. Second, it is necessary to further isolate the scattering mechanisms within the ice and snow mediums at a local scale. Airborne passive microwave measurements acquire Tbs at high resolution 80x100 metre footprints without land inclusions, but still generalize 800m^2 with one Tb. For future studies, it is recommended that a time series of *in situ* measurements of snow and ice properties be coupled with sled-borne radiometer and scatterometer measurements to reduce the spatial footprint of each acquisition. *In situ* and radiometric measurements should encompass the spatial extent of a lake with a structured sampling method designed so that any spatial interpolation applied to the data would be representative at regional scales. Therefore all Tb and σ° measurements would be coincident with snow and ice samples both spatially and temporally. Lastly, the continuation of research focused on the simulation of variability in passive microwave emission from lake ice is important for SWE monitoring, as it provides a scientific basis for the physical relationships utilized in SWE retrieval algorithms. It is recommended

that research into the effect of ice types on microwave emission be investigated through modifications to the multi-layered HUT snow emission model. Improvements in simulated emission will aid in isolating the physical mechanisms controlling emission from a snowpack over lake ice, further improving SWE retrieval algorithms.

Improvements in SWE algorithms applied to tundra environments resulting from this research can be applied to the near 35 year record of passive microwave observations, providing important knowledge as to the past, present and future variations in climate states present in remote northern locations where few continuous observations exist.

References

Adams, W.P., (1976). Diversity of lake cover and its implications, *Musk-Ox Journal*, 18: 86-98.

Adams, W.P., & Roulet, N.T., (1980). Illustration of the roles of snow in the evolution of the winter cover of a lake. *Arctic*, 33(1): 100-116.

Adams, R.M., Houston, L.L, & Weiher, R.F. (2004). The value of snow and snow information services. Report prepared for NOAA's Office of Program, Planning and Integration under contract DG1330-03-SE-1097.

Armstrong R. L., Chang, A., Rango, A., & Josberger, E., (1993). Snow depths and grain-size relationships with relevance for passive microwave studies. *Annals of Glaciology*, 17: 171-176.

Biancamaria, S., Mognard, N., Boone, A., Grippa, M., & Josberger, E. G. (2008). A satellite snow depth multi-year average derived from SSM/I for the high latitude regions. *Remote Sensing of Environment*, 112: 2557-2568

Bengtsson, L., (1986). Spatial variability of lake ice covers, *Geographiska Annaler*, 68A**(**1-2): 113-121.

Brown, R., Walker, A. E., & Goodison, B. (2000). Seasonal snow cover monitoring in Canada: An assessment of Canadian contributions for global climate modeling. *Proceedings, 57th Eastern Snow Conference, Syracuse, New York. 17 – 19 May, 2000.* 131 – 141.

Brown, R., Derksen, C., & Wang, L. (2007). Assessment of spring snow cover duration and variability over northern Canada from satellite datasets. *Remote Sensing of Environment, 111*, 367-381.

Butt, M. J., & Kelly, R. E. J. (2008). Estimation of snow depth in the UK using the HUT snow emission model. *International Journal of Remote Sensing*, 29:14 4249 – 14 4267.

Canadian Centre for Remote Sensing (CCRS) (2008). Tutorial: Fundamentals of remote sensing - microwave remote sensing. <http://www.ccrs.nrcan.gc.ca >.

Chang, A., Foster, J., & Hall, D. K. (1987). Nimbus-7 SMMR derived global snow cover parameters. *Annals of Glaciology*. 9: 39-44.

Chang, A., Foster, J., Hall, D. K., Goodison, B., Walker, A., Metcalfe, J., & Harby. A. (1997). Snow parameters derived from microwave measurements during the BOREAS winter field campaign. *Journal of Geophysical Research*, 102(D24): 29663-29671.

Choudhury, B. J., Schmugge, T. J., Newton, R. W., & Chang, A. (1979). Effect of surface roughness on the microwave emission from soils. *Journal of. Geophysical. Research*., 84: 5699-5706.

Clausi, D.A., Qin, K., Chowdhury, M.S., Yu, P. & Maillard, P. (2010) MAGIC: MAp-Guided Ice Classification, *Canadian Journal of Remote Sensing*, 36(S1): S13-S25.

Cohen, J., & Entekhabi, D. (1999). Eurasian snow cover variability and northern hemisphere climate variability. *Geophysical Research Letters*, 26(3): 345-348.

Colbeck, S. (1991). The layered character of snow covers. *Reviews of Geophysics*, 29(1): 81-96.

Derksen C., Walker A., & Goodison, B. (2003). A comparison of 18 winter seasons of in situ and passive microwave-derived snow water equivalent estimates in Western Canada. *Remote Sensing of Environment*, 88: 271-282.

Derksen C., & Walker, A. (2004). Evaluating spaceborne passive microwave snow water equivalent retrievals across the canadian northern boreal – tundra ecotone. *Transactions on Geoscience and Remote Sensing, 3*: 1641-1644.

Derksen, C., Walker, A., & Goodison, B. (2005). Evaluation of passive microwave snow water equivalent retrievals across the boreal forest/tundra transition of western Canada. *Remote Sensing of Environment*, 96(3/4): 315-327.

Derksen, C., Silis, A., Sturm, M., Holmgren, J., Liston, G. E., Huntington, H., & Solie, D. (2009). Northwest Territories and Nunavut snow characteristics from a subarctic traverse: implications for passive microwave remote sensing. *Journal of Hydrometeorology*, 10(2): 448-463.

Derksen, C., Toose, P., Rees, A., Wang, L., English, M, Walker, A., & Sturm, M. (2010) Development of a tundra-specific snow water equivalent retrieval algorithm for satellite passive microwave data. *Remote Sensing of Environment*, 114(8): 1699 – 1709.

Duguay, C.R., Pultz, T., Lafleur, P.M., & Drai, D. (2002). RADARSAT backscatter characteristics of ice growing on shallow sub-Arctic lakes, Churchill, Manitoba, Canada. *Hydrological Processes*, 16: 1631-1644

Duguay, C.R., & Lafleur, P. M. (2003). Determining depth and ice thickness of shallow sub-Arctic lakes using space-borne optical and SAR data. *International Journal of Remote Sensing*, 24(3): 475-489.

Duguay, C., Green, J., Derksen, C., English, M., Rees, A., Sturm, M., & Walker, A. (2005). preliminary assessment of the impact of lakes on passive microwave snow retrieval

algorithms in the Arctic. *62nd Eastern Snow Conference Proceedings*, Waterloo Ontario Canada

Edgerton, A. T., Stogryn, A., & Poe, G. (1971) Microwave radiometric investigations of snowpacks. *Final Rep. 1285R-4*: *Aeroject Gen Corp., E1 Monte, California:* 49pp.

Eppler, D. T., Anderson, M.R., Cavalieri, D.J., Comiso, J., Farmer, L.D., Garrity, C., Gloersen, P., Grenfell, T.C., Hallikainen, M., Lohanick, A.W., Mätzler, C., Melloh, R.A., Rubinstein, I., & Swift, C.T. (1992). Passive microwave signatures of sea ice, *Chapter 4 in Microwave Remote Sensing of Sea Ice*, Carsey, F., ed., Geophysical Monograph Series 68: 73-104.

Gan, T. Y. (1996). Passive microwave snow research in the Canadian high Arctic, *Canadian Journal of Remote Sensing.* 22(1): 36-44.

Forster, R. R., Long, D. G., Jezek, K. C., Drobot, S. D., & Anderson, M. R. (2001). The onset of Arctic sea-ice snowmelt as detected with passive- and active-microwave remote sensing. *Annals of Glaciology*, 33: 85 – 93.

Goodison B. E., & Walker, A. E. (1994). Canadian development and use of snow cover information from passive microwave satellite data in *Passive Microwave Remote Sensing of Land-Atmosphere Interactions.* Edited by B. J. Choudhury et al., pp. 2450262, VSP, Utrecht, The Netherlands.

Goodison B. E., Brown R. D., Crane R. G., Alley R., Bales R., Barber D., Barry R., Bentley C., Carrol T., Cline D., Duguay C. R., Flato G. M., Hall D. K., Harrington R., Kieffer H., Munro S., Parkinson C., Raup B., Rothrock A., & Sharp M. (1999). Cryospheric systems. *In National Aeronautics and Space Agency, EOS Science Plan*; 261–307.

Goita, K., Walker, A., & Goodison, B. (2003). Algorithm development for the estimation of snow water equivalent in the boreal forest using passive microwave data. *International Journal of Remote Sensing*, 24(5): 1097-1102.

Grody, N., Rosenfeld, S., & Basist, A. (1998). Relationship between SSM/I measurements and snow conditions. *In CD-ROM Proceedings, International Geoscience and Remote Sensing Symposium, 1998.*

Guissard, A., & P. Sobieski (1987). An approximate model for the microwave brightness temperature of the sea. *International Journal of Remote Sensing*, 8, 1607-1627.

Hall, D.K., Foster, J.L, Rango, A. & Chang. A.T.C. (1978). Passive microwave studies of frozen lakes. *Proceedings of the American Society of Photogrammetry: Fall Technical Meeting:* 195-207.

Hall, D. K., Foster, J. L., Chang, A. T. C., & Rango, A. (1981). Freshwater ice thickness observations using passive microwave sensors, *IEEE Transactions on Geoscience and Remote Sensing*. GE-19(4): 189-193.

Hall., D., Chang, A., & Foster. J. (1986). Detection of the depth-hoar layer in the snow-pack of the Arctic coastal plain of Alaska, U.S.A., using satellite data. *Journal of Glaciology*. 32(10): 87-94.

Hall, D. K., Sturm, M., Benson, C. S., Chang, A.T.C., Foster, J. L., Garbeil H., & Chacho, E. (1991). Passive microwave remote and *in situ* measurements of Arctic and Subarctic snow covers in Alaska. *Remote Sensing of Environment,* 38: 161-172.

Hall, D. K., & Riggs, G. A. (2007). Accuracy assessment of the MODIS snow products. *Hydrological Processes*, 21: 1534-1547.

Hallikainen, M. T., Ulaby, F. T., & Abdelrazik, M. (1986). Dielectric properties of snow in the 3 to 37 GHz range. *IEEE Transactions on Geoscience and Remote Sensing,* 11(AP-34). 1329-1340.

Hallikainen, M. T., Ulaby, F. & Deventer, T. (1987). Extinction behavior of dry snow in the 18- to 90-GHz range. *IEEE Transactions on Geoscience and Remote Sensing, GE-25,* 737–745.

Hallikainen, M. T., Halme, P., Takala, M., & Pulliainen, J. (2003). Combined active and passive microwave remote sensing of snow in Finland. *Geoscience and Remote Sensing Symposium, IGARSS 2003, Proceedings,* 2: 830 – 832.

Hallikainen, M., Halme, P., Lahtinen, P., & Pulliainen, J. (2004). Retrieval of snow characteristics from spaceborne scatterometer data. *International Geoscience and Remote Sensing Symposium*, 7: 1849 – 1852.

Harwood, L.A., & Sparling, P. (2008). Lake trout distribution and salinity: an assessment of the relative abundance and distribution of lake trout throughout Husky Lakes, 2001-2004. InL Mills, K.H., Dyck, M., and Hardwood, L.A. (2008). Proceedings of the Second north American Lake Trout Symposium 2005, Yellowknife, Northwest Territories. Canadian Technical Report of Fisheries and Aquatic Sciences, 2778. 247p.

Helfrich, S.R., McNamara, D., Ramsay, B.H., Baldwin, T., & Kasheta, T. (2007). Enhancements to, and forthcoming developments in the Interactive Multisensor Snow and Ice Mapping System (IMS). *Hydrological Processes*, 21(12): 1576-1586.

Hewison, T. J., & English, S. J. (1999). Airborne retrievals of snow and ice surface emissivity at millimeter wavelengths. *IEEE Transations on Geoscience and Remote Sensing*, 37(4):1871-1879.

Jeffries, M. O., Morris, K., Weeks, W. F., & Wakabayashi, H. (1994). Structural and stratigraphic features and ERS-1 synthetic aperture radar backscatter characteristics of ice growing on shallow lakes in NW Alaska, winter 1991-1992. *Journal of Geophysical Research*, 99(C11): 22459 – 22472.

Jeffries, M.O., Morris, K., & Duguay, C.R. (2005). Lake ice growth and decay in central Alaska, USA: observations and computer simulations compared. *Annals of Glaciology*, 40: 195-199.

Jin, Y. Q. (1989). The radiative transfer equation for strongly-fluctuation continuous random media. *Journal of Quantitative Spectroscopy and Radiative Transfer*, 42(6): 529 – 537.

Kang, K. K., Duguay, C.R., Howell, S.E.L., Derksen, C. P., & Kelly, R.E.J. (2010) Sensitivity of AMSR-E brightness temperatures to the seasonal evolution of lake ice thickness. *IEEE Geosciene and Remote Sensing Letters*, 7(4): 751-755.

Kazumori, M., Liu, Q., Treadon, R., & Derber, J. C. (2008). Impact study of AMSR-E radiances in the NCEP global data assimilation system. *Monthly Weather Review*, 136 (2): 541 – 559. DOI: 10.1175/2007MWR147.1

Kelly, R. E., Chang, . T., Tsang, L., & Foster, J. L. (2003). A prototype AMSR-E global snow area and snow depth algorithm. *IEEE Transactions on Geoscience and Remote Sensing, 41(2)*: 230-242.

Kelly, R. (2009). The AMSR-E snow depth algorithm: description and initial results. *Journal of the Remote Sensing Society of Japan*, 29(1): 307-317.

Klein, L. A., & Swift, C. T. (1977). An improved model for the dielectric constant of sea water at microwave frequencies. *IEEE Transactions Antennas and Propagagation*, AP-25, 104-111.

Kontu, A., Pulliainen, J., Heikkinen, P., Suokanerva, H., & Takala, M. (2007). Validation of microwave emission models by simulating AMSR-E brightness temperature data from ground-based observations. *Geoscience and Remote Sensing Symposium, IGARSS*, 1440 – 1443.

Kontu, A., Kemppainen, S., Lemmetyinen, J., & Pulliainen, J. (2008a). Determination of snow emission on lake ice from airborne passive microwave measurements. *Geoscience and Remote Sensing Symposium, 2008, IGARSS 2008. IEEE International, 4(4*): 1046-1049. Poster.

Kontu, A., Kemppainen, S., Lemmetyinen, J., Pulliainen, J., & Hallikainen, M. (2008b). Determination of snow emission on lake ice from airborne passive microwave measurements. *Geoscience and Remote Sensing Symposium, 2008, IGARSS 2008. IEEE International, 4(4*) 1046-1049. Paper.

Kontu, A., & Pulliainen, J. (2010). Simulation of spaceborne microwave radiometer measurements of snow cover using in situ data and brightness temperature modeling. *Transactions on Geoscience and Remote Sensing, 48(3)*: 1031-1044-40.

Kouraev, A.V., Semovski, V., Shimaraev, M. N., Mognard, N. M., Legresy, B., & Remy, F. (2007). The ice regime of Lake Baikal from historical and satellite data: Relationship to air temperature, dynamical and other factors. *Limnology and Oceanography,* 52(3): 1268-1286.

Kouraev, A. V., Shimaraev, M. N., Buharizin, P. I., Naumenko, M. A., Crétaux, J. F., Mognard, N., Legresy, B., & Rémy, F. (2008). Ice and snow cover of continental water bodies from simulations radar altimetry and radiometry observations. *Surveys in Geophysics*, 29: 271 – 295.

Kozlenko, N., & Jeffries, M. O. (2000). Bathymetric mapping of shallow water in thaw lakes on the North Slope of Alaska with spaceborne imaging radar. *Arctic*, 53(3): 306-316.

Krieger, G., Fiedler, H., Hajnsek, I., Eineder, M., Werner, A., & Moreira A. (2005). TanDEMX-Mission concept and performance analysis. *IGARSS 2005, Seoul Korea.*

Kuga, Y., Ulaby, F, T., Haddock, T. F., & DeRoo, R. (1991). Millimeter-wave scattering from snow. 1. Radiative transfer model. *Radio Science*, 26(2): 329 – 341.

Lemmetyinen, J., Derksen, C., Pulliainen, J., Strapp, W., Toose, P., Walker, A., Tauriainen, S., Pihlflyckt, J., Kärnä, J., & Hallikainen. M. T. (2008a). A Comparison of airborne microwave brightness temperatures and snowpack properties across the boreal forests of Finland and Western Canada. *IEEE Transactions on Geoscience and Remote Sensing,* 47(3): 965-978.

Lemmetyinen, J., Kontu, A., Qiu, Y., Pulliainen, J., & Hallikainen, M. (2008b). Experimental validation activities of HUT snow emission model. *IEEE International Geoscience and Remote Sensing Symposium Proceedings, Boston, MA.*

Lemmetyinen, J., Kontu, A., Qiu, Y., Pulliainen, J., & Hallikainen, M. (2009). Experimental validation activities of HUT snow emission model. *2009 IEEE International Geoscience and Remote Sensing Symposium*, TU3.010.5.

Lemmetyinen, J., Pulliainen, J., Rees, A., Kontu, A., Qiu, Y. & Derksen, C. (2010). Multiple layer adaptation of HUT snow emission model: comparison with experimental data. *Transactions on Geoscience and Remote Sensing*, 48(7): 2781 – 2794.

Lenormand, F., Duguay, C.R., & Gauthier, R. (2002). Developlemt of a historical ice database for the study of climate change in Canada. *Hydrological Processes*, 16(18): 3707-3722.

Liston, G.E., & Hall, D.K. (1995). An energy-balance model of lake-ice evolution. *Journal of Glaciology*, 41(138): 373-382.

Liston, G. L., & Sturm, M. (1995). A snow-transport model for complex terrain. *Journal of Glaciology*, 44(148): 498 – 516.

Marsh, P., Pomeroy, J., Pohl, S., Quinton, W., Onclin, C., Russell. M., Neumann, N., Pietroniro, A., Davison, B., & McCartney, S. (2008). Snowmelt processes and runoff at the arctic treeline: ten years of MAGS research. In *Cold Region Atmospheric and Hydrologic Studies*, Edited by Woo, M. Springer, Berlin Heidelberg, 97-123.

Marshall, S., Glatzmaier, G., & Roads, J. O. (1992). Snow hydrology, in *Climate Change and Energy Policy*, Edited by Rosen, L., and Glasser, R., American Institute of Physics. New York.

Mätzler, C., E. Schanda, & W. Good. (1982). Towards the definition of optimum sensor specifications for microwave remote sensing of snow. *IEEE Transactions on Geoscience and Remote Sensing*. GE-20: 57-66.

McCandless, S. W., & Jackson, C. R. (2004) Chapter 1. Principles of synthetic aperture radar. *Synthetic Aperture Radar Marine User's Manual, NOAA* <http://www.sarusersmanual.com/>.

Melloh, R. A., Eppler, D.T., Farmer, L.D., Gatto, L.W., & Chacho, E. F. (1991). Interpretation of passive microwave imagery of surface snow and ice, Harding Lake, Alaska. *CRREL Report 91-11*, Cold Regions Research and Engineering Laboratory, Hanover, New Hampshire.

Morris, K., Jeffries, M.O., & Weeks W.F. (1995). Ice processes and growth history on Arctic and sub-Arctic lakes using ERS-1 SAR data. *Polar Record*, 3(177): 115-128.

Mullen, P.C., & Warren, S.G. (1988). Theory of the optical properties of lake cce, *Journal of Geophysical Research*, 93(D7): 8403-8414.

Nghiem, S. V., & Tsai, W. (2001). Global snow cover monitoring with spaceborne Ku-band scatterometer. *IEEE Transactions on Geoscience and Remote Sensing*, 39(10): 2118 – 2134.

Nghiem S. V., & Leshkevich, G. A. (2007). Satellite SAR remote sensing of Great Lake ice cover, Part 1. Ice backscatter signatures at C-band. *Journal of Great Lakes Research,* 33(4): 722 - 735

Onstott, R. G. (1992). SAR and scatterometer signatures of sea ice, *Chapter 5 in Microwave Remote Sensing of Sea Ice*, Carsey, F., ed., Geophysical Monograph Series 68: 73-104.

Perrin, C. J. (2007). *Fish species distribution and associated water chemistry attributes in the Husky Lake and Sitidgi Lake system, NT*. Limnotek Research and Development Inc, Vancouver, BC.

Pestman, W. R. (1998). Mathematical Statistics: an introduction. *Walter de Gruyter GmbH & Co.* Berlin.

Pomeroy, J. W., Marsh, P., & Gray, D. M. (1997). Application of a distributed blowing snow model to the arctic. *Hydrological Processes,* 2: 1451 – 1464.

Praks, J., Koskinen, J., Arslan, A.N., Kruopis, N., Alasalmi, H., & Hallikainen, M. (1998). Cloude's target decomposition theorems applied to EMISAR data acquired during EMAC'95 snow campaign. *Geoscience and Remote Sensing Symposium, IGARSS'98 Proceedings*, 3: 1538 – 1540.

Pulliainen, J., Grandell, J., & Hallikainen, M. (1999). Hut snow emission model and its applicability to snow water equivalent retrieval. *IEEE Transactions on Geoscience and Remote Sensing,* 37(3): 1378 – 1390.

Ramage, J.M., Apgar, J.D., McKenney, R.A., & Hanna, W. (2007). Spatial variability of snowmelt timing from AMSR-E and SSM/I passive microwave sensors, Pelly River, Yukon Territory, Canada. *Hydrological Processes,* 21(12): 1548-1560

Rees, A., Derksen, C., English, M., Walker, A., & Duguay, C. (2006). Uncertainty in snow mass retrievals from satellite passive microwave data in lake-rich high-latitude environments. *Hydrological Processes,* 20: 1019-1022.

Rees, A., Lemmetyinen, J., Derksen, C., Pulliainen, J., & English, M. (2010). Observed and modelled effects of ice lens formation on passive microwave brightness temperatures over snow covered tundra. *Remote Sensing of Environment*, 114: 116-126.

Roulet, N.T., & Adams, W.P. (1986). Spectral distribution of light under a subarctic winter cover, *Hydrobiologia*, 134: 89-95.

Rott, H., & Aschbacher, J. (1989). On the use of satellite microwave radiometers for large-scale hydrology. *Remote Sensing and Large-Scale Global Processes*. Proceedings of the IAHS 3rd International Assembly, Baltimore, MD, IAHS Pub no. 186.

Rott, H., Nagler, T., & Scheiber, R. (2004) Snow mass retrieval by means of SAR interferometry. *ESA SP-550* 46*_rott*.

Roy, V., Goita, K., Royer, A., Walker, A. E., & Goodison, B. E. (2004). Snow water equivalent retrieval in a Canadian Boreal environment from microwave measurements using the HUT snow emission model. *IEEE Transactions on Geoscience and Remote Sensing,* 42(9): 1850-1859.

Sadiku, M. N. O. (1985). Refractive index of snow at microwave frequencies. *Applied Optics*, 24(4): 572 – 575.

Serreze, M. C., & Francis, J. A. (2006). The Arctic amplification debate. *Climate Change,* 76: 241 – 264.

Shi, J., & Dozier, J. (2000). Estimation of snow water equivalence using SIR-C/X-SAR, Part 2: inferring snow depth and particle size. IEEE Transactions on Geoscience and Remote Sensing, 38: 2475 – 2488.

Shi, J. (2004). Estimation of snow water equivalence with two Ku-Band dual polarization radar. International Geoscience and Remote Sensing Symposium, 7: 1649 – 1652.

Sommerfeld, R.A., & LaChappele, E. (1970). The classification of snow metamorphishm. *Journal of Glaciology,* 9(53): 3-17.

Stogryn, A. (1971). Equations for calculating the dielectric constant of saline water. *IEEE Trans. Microwave Theory Tech.*, 19, 733-736, 1971.

Stogryn, A. (1986). A study of the microwave brightness temperature of snow from the point of view of strong fluctuation theory. *IEEE Transactions on Geoscience and Remote Sensing, GE-24, (2),* 220-231

Sturm, M., Grenfell, T. C., & Perovich, D. K. (1993). Passive microwave measurements of tundra and taiga snow covers in Alaska, U.S.A. *Annals of Glaciology, 17:* 125 – 130.

Sturm, M., J. Holmgren, & Liston, G. (1995). A seasonal snow cover classification system for local to global applications. *Journal of Climate,* 8: 1261-1283.

Sturm, M., & Liston, G. E. (2003). The snow cover on lakes of the Arctic Coastal Plain of Alaska., U.S.A.. *Journal of Glaciology,* 49(11): 370-380.

Surdyk, S. (2002). Using microwave brightness temperature to detect short-term surface air temperature changes in Antarctica: An analytical approach. *Remote Sensing of Environment*, 80: 256- 271.

Swift, C. T., Jones, W. L.; Harrington, R. F.; Fedors, J. C. & Couch, R. H.(1980). Microwave radar and radiometric remote sensing measurements of lake ice. *Geophysical Research Letters*, 7(4): 243-246.

Tang, Q., Gao, H., Lu, H., & Lettenmaier D. P. (2009). Remote sensing: Hydrology. *Progress in Physical Geography*, 33(4): 490 – 509.

Tedesco, M., Pulliainen, J., Takala, M., Hallikainen, M., & Pampaloni, P. (2004). Artificial neural network-based techniques for the retrieval of SWE and snow depth from SSM/I data. *Remote Sensing of the Environment*, 90(1): 76 – 85.

Tedesco M., & Miller, J. (2007). Observations and statistical analysis of combined active-passive microwave space-borne data and snow depth at large spatial scales. *Remote Sensing of Environment*, 111: 382-397.

Toose, P. (2007). The influence of snow cover variability and Tundra lakes on passive microwave remote sensing of late winter snow water equivalent in the Hudson Bay Lowlands. *Master's Thesis at the University of Waterloo*, Waterloo, Ontario, Canada.

Tsang, L., Kong, J. A., & Shin, R. T. (1985). Theory of microwave remote sensing. Wiley Series in Remote Sensing, Kong, J, A., (ed.), New York.

Tsang, L. (1987). Passive remote sensing of dense nontenuous media. *Journal of Electromagnetic Waves and Applications*, 1: 159 – 173.

Tsang, L., Chen, C., Chang, A.T.C., Guo, J., & Ding, K.H. (2000). Dense media radiative transfer theory based on quasicrystalline approximation with applications to passive microwave remote sensing of snow. *Radio Science*, 35(3): 731 – 749.

Ulaby, F. T., & Stiles, H. (1980). The active and passive microwave response to snow parameters 2. water equivalent of dry snow. Journal of Geophysical Research, 85(C2): 1045-1049.

Ulaby, F. T., Moore, R. K., & Fung, A. K. (1982). *Microwave Remote Sensing: Active and Passive,vol 2*. Addison-Wesley/Benjamin-Cummings, Dedham, MA.

University of Waterloo. (2010). The snowtweets project. http://snowcore.uwaterloo.ca/snowtweets/. Accessed 12.5.2010.

Walker A. E., & Goodison B. E. (2000). Challenges in determining snow water equivalent over Canada using microwave radiometry. *IEEE Transactions on Geoscience and Remote Sensing*, 4: 1551-1554.

Walker A. E., & Silis, A. (2002). Snow-cover variations over the Mackenzie River basin, Canada, derived from SSM/I passive microwave satellite data, *Annals of Glaciology*. 34(1): 8-14.

Wang, J. R., & Tedesco, M. (2007). Identification of atmospheric interferences on the estimation of snow water equivalent from AMSR-E measurements. *Remote Sensing of Environment*, 111: 398 – 408.

Weeks, W.F., Sellmann, P.V., & Campbell, W.J. (1977). Interesting features of radar imagery of ice-covered North Slope lakes. *Journal of Glaciology* 18(78):129 – 136.

Weeks, W.F., Sellmann, P.V., & Campbell, W.J. (1981) Ground-truth observations of ice-covered North Slope lakes imaged by radar. *Research Report 81-19*. Hanover, New Hampshire: Cold Regions Research and Engineering Laboratory.

Wegműller U., & Mätzler C. (1999). Rough bare soil reflectivity model. *IEEE Transactions on Geoscience and Remote Sensing*. 37:1391-1395.

Werninghaus. R., Balzer, W., Buckreuss, S., Mittermayer, J., & Muhlbauer, P. (2003). The TerraSAR-X Mission. *Proceedings of SPIE,* SPIE-5236: 9 – 16.

Wiesmann A., & Mäztler, C. (1999a). Microwave emission model of layered snowpacks. *Remote Sensing of Environment*, 70: 308-317.

Wiesmann A., & Mäztler, C., (1999b). Extension of the microwave emission model of layered snowpacks to coarse-grained snow. *Remote Sensing of Environment*, 70(3): 317-325.

Woo, M., & Heron, R. (1989). Freeze-up and break-up of ice cover on small Arctic lakes. *Journal of Northern Lakes and Rivers*, W.C. Mackay, 56-62.

Woodhouse, I. H. (2006) Introduction to Remote Sensing. *Taylor and Francis.* Boca Raton, Florida.

Yueh, S. H., Dinardo, S. J., Akgiray, A., West, R., Cline, D. W., & Elder, K. (2009). airborne Ku-Band polarimetric radar remote rensing of Terrestrial snow cover. Transactions on Geoscience and Remote Sensing, 47(10): 3347 – 3364.